universe

MDPI

Review

Key Space and Ground Facilities in GRB Science

Anastasia Tsvetkova [1,2,*], Dmitry Svinkin [1], Sergey Karpov [3,4,5] and Dmitry Frederiks [1]

[1] Ioffe Institute, Politekhnicheskaya 26, 194021 St. Petersburg, Russia; svinkin@mail.ioffe.ru (D.S.); fred@mail.ioffe.ru (D.F.)
[2] Dipartimento di Fisica, Università degli Studi di Cagliari, SP Monserrato-Sestu, km 0.7, I-09042 Monserrato, Italy
[3] CEICO, Institute of Physics, Czech Academy of Sciences, 182 21 Prague, Czech Republic; karpov@fzu.cz
[4] Special Astrophysical Observatory, Russian Academy of Sciences, 369167 Nizhniy Arkhyz, Russia
[5] Institute of Physics, Kazan Federal University, 420008 Kazan, Russia
* Correspondence: tsvetkova@mail.ioffe.ru or tsvetkova.lea@gmail.com

Abstract: Gamma-ray bursts (GRBs) are short and intense flashes of γ-rays coming from deep space. GRBs were discovered more than a half century ago and now are observed across the whole electromagnetic spectrum from radio to very-high-energy gamma rays. They carry information about the powerful energy release during the final stage of stellar evolution, as well as properties of matter on the way to the observer. At present, space-based observatories detect on average approximately one GRB per day. In this review, we summarize key space and ground facilities that contribute to the GRB studies.

Keywords: gamma-ray bursts; instrumentation; detectors

check for updates

Citation: Tsvetkova, A.; Svinkin, D.; Karpov, S.; Frederiks, D. Key Space and Ground Facilities in GRB Science. *Universe* **2022**, *8*, 373. https://doi.org/10.3390/universe8070373

Academic Editor: Fridolin Weber

Received: 24 May 2022
Accepted: 1 July 2022
Published: 6 July 2022

Publisher's Note: MDPI stays neutral with regard to jurisdictional claims in published maps and institutional affiliations.

1. Introduction

Gamma-ray bursts (GRBs) are the most powerful and luminous transient phenomena in the Universe. Their high luminosity, up to 5×10^{54} erg s^{-1} [1], makes them detectable out to the edge of the visible spectrum, up to $z \sim 9.4$ [2]. The GRBs prompt emission, bursts of gamma-rays lasting from shorter than one second to thousands of seconds, most probably originated from the relativistic ejecta from the central engine: a newborn black hole or magnetar. The following multiwavelength afterglow is produced by the interaction of the ejecta with the interstellar medium.

As of now, two "physical" classes of GRBs are distinguished (see, e.g., [3]): merger-origin GRBs (Type I) [4–8], which are usually short (with a duration of less than 2 s [9,10]) and spectrally hard (SGRBs); and collapsar-origin GRBs (Type II) [11–14], typically long bursts (LGRBs).

GRBs give us a unique opportunity to probe the properties of high-redshift Universe: they can shed light on the cosmic expansion and dark energy, help study the intergalactic medium properties and the nature of first stars, help examine the reionization epoch, and help probe the metal evolution of the intergalactic medium. LGRBs may be used to estimate the star formation rate, which cannot be examined by current observations, i.e., GRBs can help study early in a redshift range, which is almost out of the reach of other cosmological probes [15]. In addition, one can test Einstein's equivalence principle and constrain Lorentz invariance violation using the GRB high-energy photons.

Several major milestones have marked GRB research. GRBs were discovered in the late 1960's by the U.S. military satellites Vela, designed to monitor nuclear explosions forbidden by the Nuclear Test Ban Treaty [16]. In 1979–1983, from about 150 GRB detections in the Konus experiments on board the Venera 11–14 missions, the main observational characteristics of GRB time profiles and their energy spectra were for the first time determined, and it was established that the burst sources are randomly distributed over the celestial sphere, without the concentration on the Galactic plane [9,17]. In 1992, the results obtained from the

Burst and Transient Source Experiment (BATSE) on board the Compton γ-ray observatory proved that GRBs do not originate from a thick disk of neutron stars in our own galaxy, the Milky Way, suggesting the cosmological origin of GRBs [18]. In 1997, the cosmological scale of distances to LGRBs was unambiguously determined by BeppoSAX [19], providing indirect evidence of the connection of LGRBs with the deaths of massive stars (see, e.g., [20]). In 2003, the insights made by the High Energy Explorer Satellite 2 (HETE-2) [21] securely confirmed the GRB–supernova (SN) connection and the LGRB association with Type Ic core-collapse SNe. Launched in 2004, the Neil Gehrels Swift Observatory revolutionized the follow-up observations of GRBs, providing quick and precise GRB localizations and, thus, enabling optical telescopes to acquire GRB afterglows in a timely manner. This led to a significant increase of the number of measured GRB redshifts. At present, space-based observatories detect approximately one GRB per day with flux above $\sim$1 photons cm^2 s^{-1} (in the typical energy range of 10 keV–10 MeV). Finally, the detection in 2017 of a short gamma-ray burst (GRB 170817A) in coincidence with the gravitational wave event (GW 170817) from a binary neutron star merger [22] inaugurated a new era of multimessenger astrophysics.

In this paper, we review the key GRB-dedicated missions focused on revealing GRB emission mechanisms, hosts, and progenitor properties. We do not pursue the goal of reviewing all instruments and missions detecting GRBs and focus only on some of them, providing examples of modern (presently or recently active) instrumentation for GRB studies and a brief description of the main scientific achievements of each mission/observatory up to now. The selection of the referenced projects was subjective. The paper is organized as follows. First, we describe the detectors of soft γ-emission including crucial missions that revolutionized GRB science and have already been decommissioned. Second, we present current key X-ray detectors contributing to the GRB research. Then, we give an idea about the diversity of facilities operating in optics, giving examples of robotic telescopes, devices for spectroscopy and photometry, and surveys. Lastly, we briefly review GRB observations in the radio and very-high-energy (VHE) ranges and conclude the paper.

2. Gamma-Ray Facilities

All GRB detectors may be divided by the number of design concepts: (1) nearly omnidirectional γ-ray spectrometers (e.g., Konus-Wind, Fermi-GBM, AGILE-MCAL, HETE-2/FREGATE); (2) imaging telescopes (e.g., Swift-BAT, INTEGRAL-IBIS/SPI); and (3) promising Compton polarimeters, which allow measuring photon polarization, spectrum, and source position (e.g., POLAR, AstroSAT). The instruments of specified class are mentioned in parenthesis and will be discussed below. In particular, the most prolific ones ($\gtrsim$100 GRBs yr^{-1}) recording GRB time profiles and spectral data in wide energy ranges are, in order of launch, Konus-Wind, Swift-BAT, and Fermi-GBM. Table 1 provides a comparison of their key properties.

In this section, we briefly review the design and main goals of decommissioned and current instruments that detect GRB prompt emission. The section is concluded with Figure 1, which illustrates the timeline of GRB missions; Figure 2, which presents a comparison of effective areas of different GRB detectors giving an overview of instrument energy ranges (detectors with a large effective area collect more photons, providing higher sensitivity); Figure 3, which gives an idea about the GRB detection timeline; and Table 2, which summarizes the key parameters of the aforementioned GRB missions. The instruments are listed below in the order of their launch, which does not reflect their priority nor importance for GRB studies.

Table 1. Comparison of Konus-Wind, Swift-BAT, and Fermi-GBM properties.

	KW	**BAT**	**GBM**
Crystal	NaI(Tl)	CdZnTe	NaI(Tl)/BGO
Number of detectors	2	– [a]	12/2
Diameter (cm)	12.7	–	12.7/12.7
Thickness(cm)	7.5	–	1.27/12.7
Approx. max. eff. area (cm^2)	160	5200	120/110
Energy range	20 keV–20 MeV [b]	14–150 keV [c]	8 keV–40 MeV
Approx. sensitivity (erg cm^{-2} s^{-1})	5×10^{-7}	1×10^{-8}	5×10^{-8}
FoV (sr)	4π	1.4 [d]	> 8
Operation time (yrs)	27	17	13
SGRB-to-LGRB rate	1:5	1:9	1:5

[a]: BAT is an assembly of 32,768 planar CdZnTe detectors (4×4 mm^2 large, 2 mm thick) to form a 1.2 m $\times$ 0.6 m sensitive area; [b]: Drifts with time; [c]: For coded FoV and up to 350 keV with no position information; [d]: For >50% coded FoV; ∼2.2 sr for >10% coded FoV.

Table 2. Past, present, and future space-based GRB detectors.

Mission	**Operation Period**	**Instrument**	**Energy Range**	**Localization Accuracy**
Venera 11–14	1979–1983	Konus	20 keV–2 MeV	$\gtrsim 10^\circ$
CGRO	1991–2000	BATSE EGRET	20 keV–2 MeV 20 MeV–30 GeV	$\gtrsim$few deg
Wind	1994–present	Konus-Wind	20 keV–20 MeV	
BeppoSAX	1996–2002	GRBM WFC NFIs	40–700 keV 2–26 keV 0.1–300 keV	1–$3'$
CXO	1999–present	ACIS	0.5–8 keV	$\lesssim 1''$
XMM-Newton	1999–present	EPIC	0.1–15 keV	$\lesssim 2''$
HETE-2	2000–2006	FREGATE WXM SXC	6–400 keV 2–25 keV 0.5–10 keV	3–15″
INTEGRAL	2002–present	SPI/ACS IBIS	20 keV–8 MeV 15 keV–10 MeV	10–$20'$ $<1'$
Swift	2004–present	BAT XRT UVOT	15–150 keV 0.2–10 keV 170–650 nm	1–$3'$ $3''$ $0.3''$
Suzaku	2005–2015	WAM	50-5000 keV	5°–10°
AGILE	2007–present	GRID SA	30 MeV–50 GeV 15–45 keV	5–$20'$ 1–$3'$
Fermi	2008–present	LAT GBM	20 MeV– $\gtrsim$300 GeV 8 keV–40 MeV	0.2–0.5° $\gtrsim$few deg
MAXI	2009–present	GSC SSC	2–30 keV 0.5–10 keV	$<6'$ $<6'$
IKAROS	2010–2015	GAP	50–300 keV	
NuSTAR	2012–present		3–79 keV	
AstroSAT	2015–present	SZTI	10–100 keV	
CALET	2015–present	CGBM	7 keV–20 MeV	

Table 2. *Cont.*

Mission	Operation Period	Instrument	Energy Range	Localization Accuracy
Lomonosov	2016–2019	BDRG SHOK UBAT SMT	10–3000 keV 330–820 nm 5–200 keV 200–650 nm	$\gtrsim$few deg 0.5″
Polar	2016–2017		50–500 keV	
Insight-HXMT	2017–present	HE	40 keV–3 MeV	
ASIM	2018–present	MXGS	20 keV– >20 MeV	
GECAM	2020–present		6 keV–5 MeV	$\gtrsim$few deg
SVOM	2023	ECLAIRs GRM MXT VT	4–250 keV 15 keV–5 MeV 0.2–10 keV 450–1000 nm	>12′ 1′ <1″
Einstein Probe	2023	WXT FXT	0.5–4.0 keV 0.5–4.0 keV	< 1′ <10″

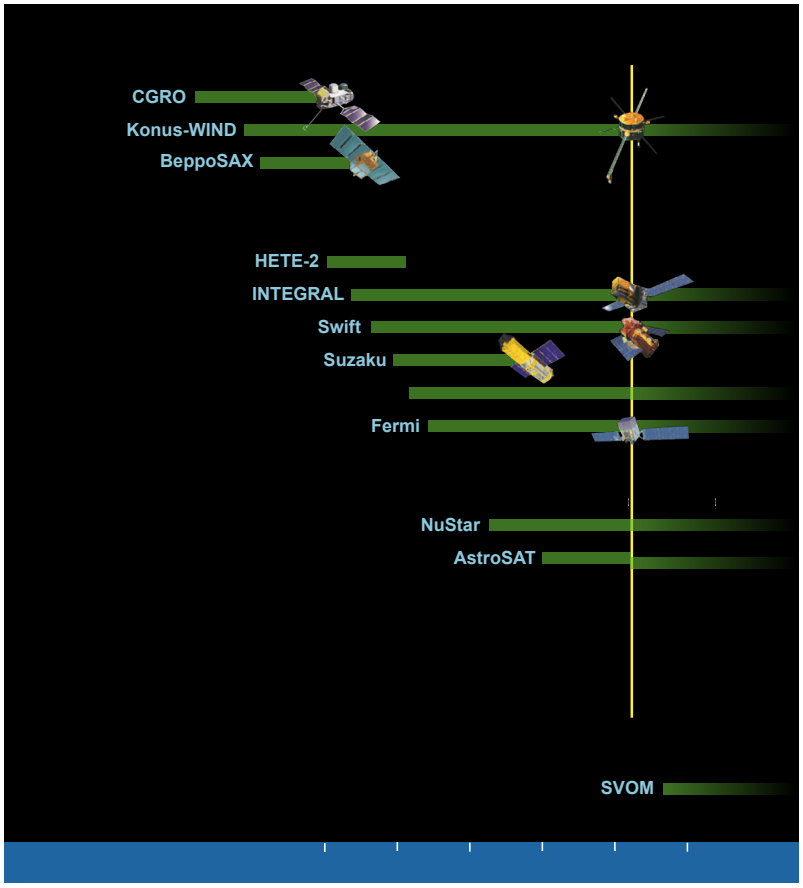

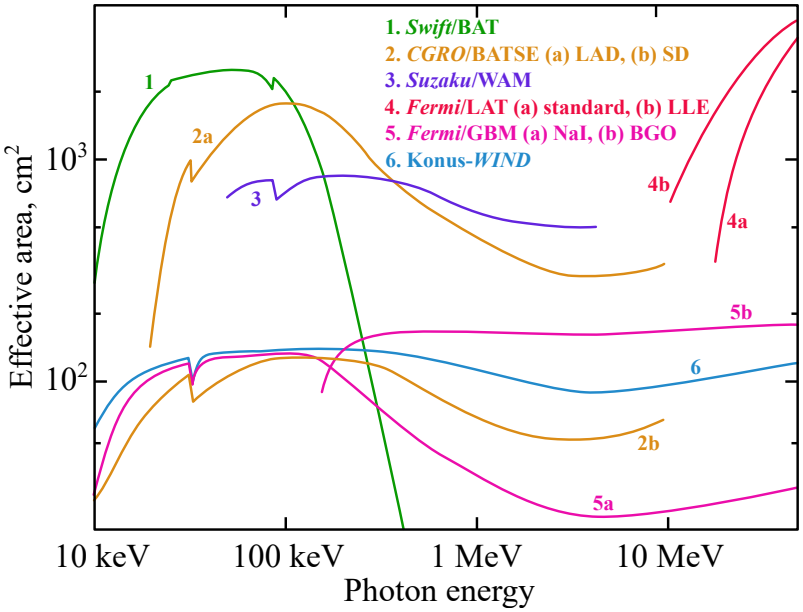

Figure 2. Comparison of the on-axis effective area of gamma-ray instruments with wide fields of view adapted from [24].

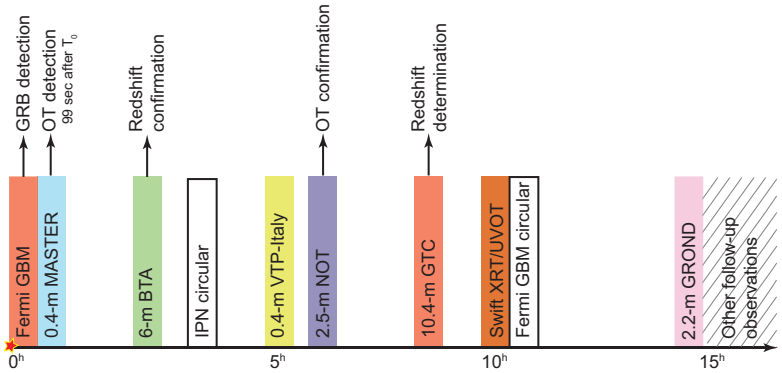

Figure 3. Sample GRB observation timeline. The figure shows the approximate time of observations obtained for GRB 140801A by the different facilities. For IPN and Fermi GBM, the time of GCN circular publication is shown. Adopted from Figure 2 in [25].

2.1. Past Missions

2.1.1. Konus (Venera 11–14)

Cosmic gamma-ray bursts (GRBs) were discovered in 1967–1973 by the U.S. Vela military satellites equipped with small (10 cm^3) CsI detectors [16]. By the beginning of the 1970s, the Vela satellites had observed several dozen gamma-ray events of an unknown nature. Directions to the sources, roughly estimated by analyzing arrival times of the bursts as detected by different satellites, eliminated terrestrial or solar origin of the events. One of the first independent confirmations of the discovery of cosmic GRBs came from the Kosmos-461 satellite [26].

The early GRB studies showed clearly that progress in obtaining new information on this unusual astrophysical phenomenon can be achieved only by employing specially designed instrumentation, which would be able not only to detect GRBs, but also to measure with adequate resolution the time profile and spectral composition of the radiation, as well as to determine the direction to the source.

The first comprehensive studies of the GRB phenomenon were performed in the Konus experiments on board the Soviet Venera 11–14 interplanetary missions in 1979–1983. Each spacecraft was equipped with an omnidirectional array of six NaI(Tl) scintillation

detectors, 80 mm in diameter and 30 mm thick, with anisotropic angular sensitivity. The instruments operated in the 20 keV–2 MeV energy range and recorded GRB light curves with time resolution starting from 1/64 s and measured 16-channel energy spectra in eight successive intervals of 4 s each. The detectors were placed along the positive and negative directions of the Cartesian coordinate system of the spacecraft, thus enabling autonomous GRB localization. In addition, the Venera spacecraft were separated by distances of several million kilometers, which enabled a high-precision localization of GRBs by the triangulation method and provided an independent determination of their coordinates.

From about 150 GRB detections in the Konus-Venera experiments, the main observational characteristics of GRB time profiles and their energy spectra were for the first time determined [9,17], including the existence of a separate class of short-duration GRBs and the presence of hardness-intensity correlation in GRB pulses. It was established that the burst sources are randomly distributed over the celestial sphere, without the concentration on the Galactic plane. About ten years later, the key results of the Konus experiments were confirmed with larger statistics of events by the next major GRB mission, the BATSE experiment on board the NASA Compton Gamma-Ray Observatory.

2.1.2. CGRO-BATSE

The Compton Gamma-Ray Observatory (CGRO) was launched to low-Earth orbit ($\sim$400 km) on 5 April 1991 and deorbited on 4 June 2000. The Burst and Transient Source Experiment (BATSE) was one of four experiments on board the satellite. Being the first large detector system dedicated to GRB studies, it consisted of eight modules operating in the $\sim$10 keV–8 MeV energy range and installed in each of eight corners of the satellite, allowing the maximum field of view (FoV) $\approx 2.6\pi$ sr for a low-Earth orbit spacecraft. Each module comprised two NaI(Tl) scintillators, a large area detector (LAD), a NaI crystal $\sim$51 cm in diameter and $\sim$1.3 cm thick, which recorded the data with high temporal resolution, and a spectroscopy detector (SD), which collected the data with high-energy resolution. The instrument was able to estimate GRB localization comparing the relative count rates in the detectors (usually, three or four) that observed the burst [27].

The ultimate catalog, 5B [28], comprises 2145 GRBs detected with BATSE during its entire period of operation (1991–2000). BATSE enabled several breakthroughs in the field: observation of the sky distribution and intensity distribution of numerous GRBs provided strong evidence for the cosmological distances to GRBs [18]; definitive separation between the short/hard and the long/soft classes of GRBs [10]; evidence that many GRB spectra are nicely fit by a function of two power laws, continuous and smoothly joined (so-called Band function) [29]; and the "hard-to-soft" evolution of GRB spectra [30].

The other three experiments on CGRO were the Oriented Scintillation Spectrometer Experiment (OSSE), Compton Telescope (COMPTEL), and Energetic Gamma Ray Experiment (EGRET), covering the energy ranges 100 keV–10 MeV, 1 MeV–30 MeV, and 20 MeV–30 GeV, respectively.

2.1.3. BeppoSAX

The X-ray astronomy satellite Satellite per Astronomia X, "Beppo" (BeppoSAX, in honor of Giuseppe Occhialini [31]), was a project of the Italian Space Agency with the participation of the Netherlands Agency for Aerospace Programs. The mission was launched on 30 April 1996, and deactivated on 30 April 2002. The main scientific characteristic of the BeppoSAX mission was the wide spectral coverage, ranging from 0.1 keV to over 200 keV. The BeppoSAX payload comprised five instruments: Low Energy Concentrator Spectrometer (LECS); Medium Energy Concentrator Spectrometer (MECS); High Pressure Gas Scintillation Proportional Counter (HPGSPC); Phoswich Detector System (PDS); and Wide Field Camera (WFC).

The Wide Field Cameras (WFCs) onboard BeppoSAX consisted of two coded aperture cameras, pointing 180° away from each other, perpendicular to the Sun vector and to the other instruments, each with a FoV of 40° × 40° (full width at zero response) and an angular

resolution of 5′. They operated in normal mode with 31 energy channels in 2–28 keV and 0.5 ms time resolution [32].

The main scientific highlights of the mission are: (1) the first rapid arc-minute localization and first X-ray follow-up observations of GRB 970228 [19,33]; (2) enabling the first direct redshift measurements of the optical afterglow of GRB 970508 with ground-based telescopes [34,35]. The detection of the first GRB afterglow (GRB 970228) and its association with a distant (z = 0.695) host galaxy allowed unveiling the 30-year mystery of GRB origin and further measurements of GRB redshifts [36]. Among other discoveries made possible by BeppoSAX are the GRB/SN connection [37] and the existence of a hardness–intensity correlation of GRB prompt emission in the rest frame (the "Amati" relation [38]).

2.1.4. HETE-2

The High Energy Transient Explorer (HETE-2) mission was devoted to the study of GRBs using soft X-ray, medium X-ray, and γ-ray instruments mounted on a compact spacecraft. The HETE-2 satellite was launched into equatorial low-Earth orbit on 9 October 2000, and deactivated on March 2008 [39]. The satellite payload included three instruments. The French Gamma Telescope (FREGATE) was a set of omnidirectional γ-ray spectrometers designed to detect and conduct spectroscopy on GRBs. The instrument covered an energy range from 6 to 400 keV with a spectral resolution of $\sim$25% at 20 keV and $\sim$9% at 662 keV. The field of view was 3 sr, and the time resolution was 10 µs. The Wide Field X-Ray Monitor (WXM) consisted of two orthogonal one-dimensional X-ray detectors covering an energy range from 2 to 25 keV with the spectral resolution $\sim$22% at 8 keV and 90% at 5 keV. The instrument had 1.6 sr FoV and the 1 ms time resolution. The Soft X-Ray Camera (SXC), as well as WXM, was designed to detect GRBs and to measure the intensities, time variation, and spectra of X-ray bursts and black hole X-ray transients. The SXC consisted of two orthogonal sets of one-dimensional coded aperture X-ray imagers. The imagers covered a range from 0.5 to 14 keV with a spectral resolution of 46 eV at 525 eV and 129 eV at 5.9 keV. The instrument had 0.91 sr FoV and 1.2 s time resolution. The goal of the mission was to continuously scan the sky and detect GRBs, establish precise locations, and transmit coordinates in near-real time ($\lesssim$10 s).

The HETE-2 mission observed more than 250 GRBs, localizing 25–30 GRBs per year. HETE-2 placed severe constraints on any X-ray or optical afterglow of a short GRB, leading to a firm establishment of the cosmological origin of this subclass of GRBs. It made it possible to explore the previously unknown behavior of optical afterglows at very early times and opened up the era of high-resolution spectroscopy of GRB optical afterglows. A new subclass of GRBs, the less-energetic X-ray flashes (XRFs), and their first optical counterparts were discovered. It also solved the mystery of "optically dark" GRBs and revealed the nature of XRFs ([40] and the references therein).

2.1.5. Suzaku-WAM

The Wide-band All-sky Monitor (WAM; [41]) on board the Japan–US Suzaku satellite [42] launched on 10 July 2005, and deactivated on 30 May 2015, was a large and thick BGO (bismuth germanate: $Bi_4Ge_3O_{12}$) active lateral shield for the Suzaku Hard X-ray Detector (HXD), used mainly for rejecting its detector background, but it also worked as an all-sky monitor for soft gamma-ray transients. The WAM consisted of four perpendicular walls, each with a geometrical area of $\sim$800 cm^2. The instrument operated in a wide nominal energy range of $\sim$50–5000 keV, which depended on the gain of the photo-multipliers; in a wide, about half of the sky, field of view. The WAM detected more than 1400 GRBs and 300 bursts from SGRs, observing GRBs at a rate of 140 events per year including both triggered and untriggered events, and this detection number was comparable to that of other GRB-specific instruments. The coincident rate with the Konus-Wind and the Swift-BAT triggers was $\sim$70 and $\sim$14 per year, respectively. The GRB localization capability was $\gtrsim$5°–10° using the WAM alone.

2.1.6. IKAROS-GAP

The first polarimeter dedicated to the GRB polarization measurements, the Gamma-Ray Burst Polarimeter (GAP) aboard the Interplanetary Kite-craft Accelerated by Radiation Of the Sun (IKAROS) solar sail, was launched in 21 May 2010, by JAXA [43]. Contact with the spacecraft was lost on 20 May 2015. Being a moderate-size detector of 3.8 kg weight and 17 cm size operating in the 50–300 keV band, it comprised two coaxial detectors: a plastic scintillator and CsI crystals. The instrument measured γ-ray polarization based on the anisotropy of the Compton scattering: the Compton-scattering angle, expected to be angular-dependent if polarization is present, can be obtained from the coincidence between the central plastic medium and CsI detectors surrounding the plastic Compton-scattering medium. The scientific highlights from GAP include the observation of GRB 100826A in the 70–300 keV band and fitting its modulation curve with a Monte Carlo model of the experiment [44], as well as a marginal (2.9σ) observation of a time variable polarized signal and a measurement of polarization of GRB 110301A and GRB 110721A.

2.1.7. Lomonosov

The Lomonosov satellite operated by Moscow State University was launched to the heliosynchronous orbit on 28 April 2016, and deactivated on 14 January 2019. The mission allowed the simultaneous observation of GRBs in γ-ray, X-ray, and optical bands with three onboard payloads: directed in three axes GRB monitors (BDRG [45]); SHOK wide-field optical cameras; and the Ultra-Fast Flash Observatory (UFFO) payload [46,47].

The monitor BDRG was designed to obtain temporal and spectral information about GRBs in the 10–3000 keV energy range, as well as to provide GRB triggers for the SHOK and UFFO instruments. The GRB localization technique used by BDRG was based on the same concept as Veneras 11–14 (Konus), CGRO (BATSE), and Fermi (GBM), utilizing the ratio of count rates from all three detectors to determine burst location. The three-detector configuration of BDRG provided a field of view equivalent to at least a half of the entire celestial sphere. The main advantages of the instrument were a high time resolution ($\sim$15 ms) and the use of phoswich NaI(Tl)/CsI(Tl) detectors, which provided active shielding against the γ-ray background and the ability to distinguish GRB signals from electron precipitation and other geophysical phenomena occurring in near-Earth space. The BDRG instrument operated in two main observational modes: the monitor, or continuous observation, and event modes. The optical and γ-ray GRB light curves were recorded simultaneously, allowing detection of prompt GRB emission, as well as GRB precursors in the optical band [48]. The UFFO payload included the wide-field coded mask X-ray Burst Alert and Trigger Telescope (UBAT) and the optical/UV telescope. The UBAT had an $\sim$190 cm^2 effective area, $90.2^\circ \times 90.2^\circ$ FoV, and 15–150 keV energy band.

BDRG detected 20 GRBs; no GRB was in the SHOK FoV during the time when the instrument was operating. The joint observations of BDRG and MASTER (see Section 4.1.10) of robotic telescopes allowed for comparing optical and γ-ray light curves of two long-duration and the most powerful bursts, GRB 160625B and GRB 161017A, at different phases of their activity. These observations allowed clarifying the details of the birth of rapidly rotating black holes of stellar mass [49].

2.1.8. Polar

The POLAR was a dedicated GRB polarimeter developed by a Swiss/Chinese/Polish collaboration. The instrument was launched on board the second Chinese Space Lab, the Tiangong-2, in September 2016 after which it took 6 months of scientific data [50]. Composed of 1600 plastic scintillators, the Compton telescope operated in the 50–500 keV band and covered a wide ($\gtrsim$35% of the sky) FoV with good polarimetric capability.

The instrument recorded light curves of 55 GRBs, including five events bright enough to conduct studies of polarization, which showed a low polarization fraction $\sim$10%. However, the time-resolved analysis of the brighter bursts revealed a 28% polarization, which

may indicate that the polarization degree decreases due to the polarization angle change during the burst [51].

2.2. Current Missions

2.2.1. Konus-Wind

Launched on 1 November 1994, Wind is a spin-stabilized spacecraft placed in a Lissajous orbit around the L1 Lagrange point of the Earth–Sun system. Konus-Wind (KW [52]) is a γ-ray spectrometer onboard Wind aimed at studies of temporal and spectral parameters of GRBs, solar flares (SFs), soft gamma repeaters (SGRs), and other transients. Comprising two identical NaI(Tl) detectors with a 7.5 cm thickness, 12.7 cm diameter, and $\sim$80–160 cm^2 effective area, the instrument continuously covers all-sky over a wide energy range ($\sim$20 keV–15 MeV) in stable background conditions.

The instrument operates in two modes: waiting and triggered. In both modes, the event light curves in three energy windows: G1 ($\sim$20–80 keV), G2 ($\sim$80–300 keV), and G3 ($\sim$300–1200 keV), are recorded with a fine (2–256 ms, triggered mode) or coarse (2.944 s, waiting mode) time resolution. In the triggered mode, the instrument also measures 64 energy spectra over 63 pseudo-logarithmic channels in each of two overlapping energy intervals, PHA1 ($\sim$20–1200 keV) and PHA2 ($\sim$400 keV–15 MeV). The detector energy scale is calibrated in flight using the 1460 keV line of ^{40}K and the 511 keV e^+e^- annihilation line. A more detailed discussion of the KW instrument can be found in [53–55].

As of 2022 May, KW has triggered $\sim$5200 times on different transients, including $\sim$3450 GRBs, providing the trigger rate of $\sim$130 GRBs per year. Moreover, a search in the KW waiting mode data revealed $\sim$2500 untriggered GRBs detected simultaneously by CGRO, BeppoSAX, Swift, and Fermi [56]. Various KW catalogs and databases, including those of short bursts along with their IPN localization maps, GRBs with known redshifts, SGR flares, and SFs, can be found at the KW web page[1]. There were several instruments similar to Konus-Wind operating in 1995–2009: Konus-A [57] on board the Cosmos 2326 spacecraft (1995–1997); Konus-A2 (Cosmos 2367, 1999–2001); HELICON (KORONAS-F, 2001–2005); Konus-A3 (Cosmos 2421, 2006–2008); Konus-RF (the Coronas-Photon solar observatory, 2009).

2.2.2. INTEGRAL

The INTErnational Gamma-Ray Astrophysics Laboratory (INTEGRAL) was launched by ESA on 17 October 2002 to a highly elliptical orbit. INTEGRAL was designed to perform observations in the hard X-ray/soft γ-ray energy range over a $\sim 30^\circ \times 30^\circ$ FoV with two main instruments: Imager on Board the INTEGRAL Satellite (IBIS), optimized for high angular resolution [58], and SPectrometer aboard INTEGRAL (SPI), which provides a high spectral resolution [59]. Even though INTEGRAL was not developed as a GRB-dedicated mission, its main instruments detect bursts every 1–2 months, while the Anticoincidence Shield of the SPI instrument (SPI-ACS; 512 kg BGO crystals) detects approximately one GRB per every two days, nevertheless not providing spatial or spectral information on the events [60].

The IBIS instrument can localize GRBs in its imaging FoV of $\sim 30^\circ \times 30^\circ$ with arcmin accuracy, and the IBAS localizes GRBs using the imaging data from the IBIS/ISGRI detector, while the large collecting area of the SPI-ACS allows recording GRB light curves from almost any position of the sky. Both INTEGRAL main telescopes can work as polarimeters. Polarization measurements are based on the detection of multiple events (when a photon deposits energy in several detectors) in the range above $\sim$100 keV and further Monte Carlo simulations of the SPI response to polarized emissions in GEANT 4. The two position-sensitive detectors of IBIS, ISGRI (made of CdTe crystals and sensitive in the 15–1000 keV range) and PICsIT (made of CsI bars and sensitive in the 200 keV–10 MeV band), allowed using the telescope as a Compton polarimeter as well. See [61] for further details on the polarization measurements.

The main highlights for INTEGRAL include the localization and spectrum measurements for an off-axis GRB 030406 using the Compton scattering between ISGRI and PICsIT [62]; the detection of 127 GRBs in the IBIS FoV (as for July 2019) [63]; the sampling of the population of the faintest GRBs (down to the peak fluxes below $\sim$0.1 photons cm^{-2} s^{-1}) thanks to the high sensitivity of IBIS; the detection of six SGRBs [63]; the SPI-ACS detection of about 300 GRBs per year outside the FoV of the main instruments [64].

2.2.3. Swift-BAT

The Neil Gehrels Swift Observatory, dedicated to GRB studies, was launched on 20 November 2004 [65], to a low-Earth orbit. The Swift payload comprises three instruments working together to provide rapid (within a few hundred seconds after the trigger) GRB identification and multiwavelength follow-up: the Burst Alert Telescope (BAT; [66]), the X-ray Telescope (XRT [67,68]; see Section 3.3), and the UV-Optical Telescope (UVOT [69]; see Section 4.1.19). Once a GRB has triggered BAT, the spacecraft slews to the GRB position and starts observations of the GRB counterpart with the XRT and the UVOT telescopes, which can further refine the localization to $\lesssim 1''$. Comprising a detector plane with 32,768 CdZnTe (CZT) detectors and a coded-aperture mask with $\sim$52,000 lead tiles, BAT is a highly sensitive, large-FoV (1.4 sr for $>$50% coded FoV and 2.2 sr for $>$10% coded FoV) telescope that operates in the 14–150 keV[2] energy range. Further details on the instrument, including the in-orbit calibrations, can be found in [66] and the BAT GRB catalogs [70–72].

The precise and quick GRB localization allows multiwavelength follow-ups and estimation of GRB redshifts, which are necessary to use GRBs as cosmological tools. As of May 2022, the instrument has detected $\sim$1500 GRBs, of which $\sim$410 events have redshift measurements[3], ranging from $z = 0.03$ to $z = 9.38$ [72]. The Swift data products are publicly available at the mission web page[4].

2.2.4. AGILE-MCAL

The Astrorivelatore Gamma ad Immagini LEggero (AGILE) is an Italian space mission dedicated to high-energy astrophysics launched in low-Earth orbit on 23 April 2007 [73]. The AGILE payload comprises three instruments able to conduct broad-band (20 keV–50 GeV) observations of Galactic and extragalactic objects: a tungsten-silicon tracker (ST) with imaging capability, operating in the 30 MeV–50 GeV band; a coded mask hard X-ray imager SuperAGILE (SA), acquiring data in the 18–60 keV band; and a CsI(Tl) all-sky MiniCALorimeter (MCAL), working in the 0.4–100 MeV energy range. ST and MCAL together form the Gamma-Ray Imaging Detector (GRID). AGILE has an anti-coincidence (AC) system and plastic scintillation detectors surrounding the main detectors, sensitive to the γ-rays in the $\sim$50–200 keV band. Due to a failure of the onboard reaction wheel after two years since the launch, AGILE lost its capability to point at a certain position in the sky. It also started to spin around its Sun-pointing axis, which can affect spectral analysis, as the incident angle varies in time, which requires correction of the DRM for the events lasting more than several tens of seconds or minutes. Only a few very long-lasting GRBs have been detected in the "spinning period" and required a special approach [74].

A non-imaging γ-ray scintillator, MCAL [75] comprises 30 CsI(Tl) scintillator bars ($15 \times 23 \times 375$ mm^3 each) with a total on-axis geometrical area of $\sim$1400 cm^2 and operates in the 400 keV–100 MeV energy band. MCAL cannot localize GRBs and can only provide a rough (>30°) reconstruction of the incident photon direction for some angles. However, the AGILE-MCAL is part of the IPN. The incoming photons can be discriminated from the high-energy particles using the tracks in the detector bars produced by the incident photons. Unlike GRID or SuperAGILE, MCAL observes all-sky, only constrained by Earth occultations. MCAL can operate in one of two modes (or in both simultaneously): in the GRID mode, MCAL acts as a secondary instrument lead by ST; in the BURST mode, MCAL works as an independent self-triggering detector and is able to collect the data down to an $\sim$300 μs timescale, providing studies of very fast transients, e.g., submillisecond TGFs [76,77].

As of November 2020, MCAL detected 503 GRBs (394 recorded with high time resolution), 44% of which are SGRBs and the rest are LGRBs. Moreover, 109 bursts triggered partial MCAL onboard data acquisitions, allowing further joint analyses or triangulations. AGILE Scientific RateMeters (RMs) detected $>$ 90% of these GRBs, allowing simultaneous observations in the 20 keV–100 MeV range [74].

2.2.5. Fermi-GBM

The Fermi Gamma-ray Space Telescope, dedicated to studying transient γ-ray sources, was launched in June 2008 to a low-Earth orbit. It harbors two scientific instruments: the Gamma-ray Burst Monitor (GBM [78]) and the Large Area Telescope (LAT [79]). The LAT is sensitive in the energy range from 30 MeV to 300 GeV, while the GBM, whose direct experimental objective was to identify and study GRBs, covers the energy range from 8 keV to 40 MeV, extending the energy range over which bursts are observed downward to the hard X-ray range. The GBM observes the whole sky that is not occulted by the Earth ($>$8 sr).

GBM is composed of twelve NaI(Tl) detectors and two bismuth germanate (BGO) scintillation detectors. With a thickness of 1.27 cm and a diameter of 12.7 cm, the NaI crystals cover an energy range of 8 keV–1 MeV. They are oriented around the spacecraft, three at each of the four corners in a way that the position of the GRB can be determined from the relative count rates seen in the individual detectors. The uncertainty of the GBM localization of bright GRBs is about several degrees in radius [80]. The two BGO crystals have a diameter and thickness of 12.7 cm, covering an energy range of 200 keV–40 MeV, and are located on opposite sides of the spacecraft so that at least one is always illuminated from any direction.

A detailed detector response model has been developed based on Geant4 simulations and confirmed by extensive ground testing, which included the calibration with radioactive sources (from 14.4 keV to 4.4 MeV), the low-energy calibration of the NaI detectors performed at the synchrotron radiation facility BESSY, and the high-energy calibration of the BGO detectors carried out at the SLAC National Accelerator Laboratory, in order to determine the response as a function of orientation [81,82]. In flight, fits to background lines (e.g., 511 keV) over time show a stable gain and energy resolution in all the GBM detectors and electronics, with lines typically within 1% of their expected position [83]. The GBM detectors and their calibration are described in more detail in [78,82,84].

During a 10-year time period up to 2018 July 11, GBM triggered almost twice a day on transient events, 2356 of which we identified as cosmic GRBs. Additional trigger events were due to SF events, magnetar burst activities, and terrestrial gamma-ray flashes (TGFs) [85]. The data on the GRBs detected by GBM are available at the Fermi GBM Burst Catalog (FERMIGBRST) web page[5].

2.2.6. AstroSAT-SZTI

Astrosat, the first Indian satellite mission dedicated to astronomical studies, was launched on 28 September 2015. The Cadmium Zinc Telluride (CZT) Imager, one of four X-ray instruments onboard the satellite, covers the the energy range of 10–100 keV and has a large detection area of $\approx$976 cm^2. The instrument energy response is calibrated using radioactive sources. CZTI is the first modern instrument able to constrain any intrinsic polarization greater than $\sim$40% for bright X-ray sources (>500 mCrab) within a short exposure of $\sim$100 ks with a 3σ confidence level [86,87]. The GRB polarization measurement is based on the principle of Compton scattering and may be taken using the azimuthal distribution of simultaneous events in two adjacent pixels of the pixelated detector plane. Having the experimentally verified polarization measurement capability in the 100–300 keV band, the instrument gives a unique opportunity for spectro-polarimetric studies of GRBs. As of now, SZTI has detected $\lesssim$500 GRBs[6]. Seven GRBs were found to have significant polarization [88,89].

2.2.7. CALET-CGBM

The CALorimetric Electron Telescope (CALET) space experiment, developed by Japan in collaboration with Italy and the United States, is a high-energy astroparticle physics mission installed on the International Space Station (ISS) [90]. The Gamma-ray Burst Monitor (CGBM) is the secondary scientific instrument of the CALET mission that has been monitoring X-ray and γ-ray sky since October 2015. The main observational target of the CGBM is GRBs and SGRs. The CGBM can measure GRB light curves and spectra in the energy range from 7 keV to 20 MeV thanks to two kinds of scintillation detectors, which are the Hard X-ray Monitor (HXM), which comprises two $LaBr_3$(Ce) (7 keV–1 MeV, ⌀66 mm, 12.7 mm thick, effective area of 68 cm^2, 3% energy resolution at 662 keV), and the Soft Gamma-ray Monitor (SGM), which is a BGO crystal (100 keV–20 MeV, ⌀102 mm, 76 mm thick, effective area of 82 cm^2, 15% energy resolution at 662 keV), each read by a single photomultiplier [91,92]. Being partially blocked by the ISS structures, CGBM observes about half of the sky. As of the end of June 2019, CGBM had detected 161 GRBs.

2.2.8. Insight-HXMT

The Hard X-ray Modulation Telescope (Insight-HXMT) launched on 15 June 2017, is China's first X-ray astronomy satellite devoted to the observations in the 1–250 keV energy range. The facility comprises three collimator-based telescopes: the High Energy X-ray Telescope (HE [93]), the Medium Energy X-ray Telescope (ME [94]), and the Low Energy X-ray Telescope (LE [95]). The main detector plane of Insight-HXMT/HE constitutes an array of 18 NaI(Tl)/CsI(Na) phoswich detectors with a total geometric area of about 5100 cm^2 and a combined FoV of $\sim 5.7^\circ \times 5.7^\circ$ (FWHM). The CsI(Na) detector can be used as an all-sky γ-ray monitor in the 0.2–3 MeV band. The measured energy band is ∼40–800 keV in the normal-gain (NG) mode and ∼200 keV–3 MeV in the low-gain (LG) mode. Switching between the modes is carried out by adjusting the high voltage of the PMTs, which readout the phoswich detectors.

In the absence of an on-board GRB trigger algorithm, nor prompt data telemetry for Insight-HXMT, GRBs are identified on-ground using two pipelines: the blind search on all data acquired by the InsightHXMT/HE CsI(Na) detector; and the targeted search for the GRBs reported via GCN in the CsI(Na) data. During the first four years of operation, the facility detected 660 events: 322 GRBs, 245 TGFs, four SFs, 33 charged particle events, and 56 unclassified events.

2.2.9. ASIM-MXGS

The Atmosphere-Space Interactions Monitor (ASIM) is an instrument suite on the ISS for measurements of lightning, transient luminous events (TLEs), and TGFs operating since 2 April 2018 [96]. The Modular X- and Gamma-ray Sensor (MXGS) is an imaging and spectral X- and γ-ray instrument mounted on the starboard side of the Columbus module on the ISS [97]. As a byproduct of its work, MXGS can detect GRBs and giant magnetar flares, e.g., GRB 200415A—a giant flare in NGC 253 [98]. MXGS consists of a low-energy detector (LED) and a high-energy detector (HED). The LED detector plane is composed of the pixelated cadmium-zinc-telluride (CZT) crystals measuring photons in the 20–400 keV energy range. A hopper-shaped collimator defines the $80^\circ \times 80^\circ$ fully coded FoV of the LED. The HED consists of 12 bismuth-germanium-oxide (BGO) detector bars, each coupled to a PMT. The HED is sensitive to photons with energies from 200 keV to >20 MeV.

2.2.10. GECAM

The Gravitational wave high-energy Electromagnetic Counterpart All-sky Monitor (GECAM) is a Chinese space-based observatory launched on 9 December 2020. Its main scientific goal is to monitor various types of GRBs originating from the merger of binary compact stars, which can also produce gravitational waves, and from the collapse of massive stars.

GECAM was planned to consist of two low-orbit microsatellites (GECAM-A and GECAM-B, but currently, only GECAM-B is in operation) in conjugate constellation layout on opposite sides of the orbit, each of which detects and localizes GRBs using 25 compact and novel gamma-ray detectors (GRDs) in the 6 keV–5 MeV energy range. Each GRD module is comprised of a $LaBr_3$(Ce) scintillator joined with a silicon photo-multiplier (SiPM) array and preamplifier. The designed sensitivity of GECAM is about 2×10^{-8} erg cm^{-2} s^{-1}, and the localization accuracy is about 1° for medium-bright GRBs (10^{-6} erg cm^{-2} s^{-1}, 10 s). A large dynamic range of the GRD is achieved by the high-gain and low-gain channels of the preamplifier. The energy response of the GRD prototype was evaluated using radioactive sources in the range of 5.9–1332.5 keV. An energy resolution of 5.3% at 662 keV was determined from the ^{137}Cs pulse height spectra. As of now, GECAM has detected ∼60 GRBs according to the GCN Circulars Archive[7].

2.3. The Interplanetary Network

The currently active instruments with accurate (of order of a few arcmin) GRB localization capability, Swift and INTEGRAL, localize less that 25% of the GRBs detected by all instruments with GRB detection capability [99]. The current optical surveys such as ZTF (see Section 4.2.2) and MASTER (see Section 4.1.10) add a few independent discoveries of GRB afterglows per year.

A number of the active instruments with GRB detection capability taken together form an all-sky, full-time high-energy transient phenomena monitor called the Interplanetary Network (IPN). The IPN provides GRB localizations with accuracy down to a few arc-minutes using propagation time delay analysis (triangulation). In addition to the GRB-specific missions, the IPN includes non-GRB-specific instruments such as planetary geochemistry probes: Mars-Odyssey, which was launched in 2001 April and reached an orbit around Mars on October 2001 [100], equipped with the Gamma-Ray Spectrometer (GRS), which includes two detectors with GRB detection capabilities, the Gamma Sensor Head (GSH) and the High Energy Neutron Detector (HEND) [101,102]); and the Mercury exploration mission BepiColombo [103], launched on 20 October 2018 and equipped with the Mercury Gamma-ray and Neutron Spectrometer (MGNS) [104,105]. Earlier, the IPN included the Mercury Surface, Space Environment, Geochemistry, and Ranging mission (MESSENGER) carrying the Gamma-Ray and Neutron Spectrometer (GRNS) [106], in Mercury orbit from March 2011 to 2015 [107,108]; and the Sun-observing Ramaty High Energy Solar Spectroscopic Imager (RHESSI) [109,110].

The IPN detects about 300 GRBs per year. Localizations for about a few dozen of the brightest GRBs per year are published in GCN circulars[8]. Recently, rapid IPN localizations have facilitated significant discoveries in the GRB field, e.g., the localization of the short GRB 170817A, the counterpart of the gravitational wave event GW170817 from a binary neutron star merger [22], the detection of the extragalactic magnetar giant flare in NGC 253 [111], the discovery and confirmation of the shortest GRB from a collapsar [112], and the association of a number of GRBs with fast optical transients [113].

2.4. CubeSat Constellations

Any single spacecraft in a low-Earth orbit cannot provide all-sky coverage, due to duty cycle, Earth-blocking, field of view considerations, or all three. On average, 50% sky coverage is a rough estimate of what can be achieved by a mission such as, e.g., Fermi. Although the current IPN GRB detectors are functioning well and their spacecrafts are not scheduled for decommissioning, they are nevertheless old, and new interplanetary opportunities do not arise frequently.

A network of small, identical GRB-dedicated satellites in near-Earth orbits, with a simple instrumentation, can achieve sensitivity comparable to large GRB missions, providing entire-sky coverage; see, e.g., [114]. Presently, there are numerous alternative concepts and pathfinders for all-sky monitoring using multiple Earth-orbiting satellites involving a variety of localization techniques, such as: BurstCube [115,116], Gamma-Ray

Integrated Detectors (GRID) [117], CubeSats Applied for MEasuring and LOcalising Transients (CAMELOT) [118], HERMES [119,120], Interconnected Multi-hop Array of CubeSats for transients (IMPACT) [121], GRBAlpha [122], and its successor VZLUSAT-2 launched on 13 January 2022 [123], and EIRSAT-1 [124]. For example, the High Energy Rapid Modular Ensemble of Satellites (HERMES) Technological and Scientific pathfinder is a space-borne mission based on an LEO constellation of nano-satellites [120,125–128]. The instrument will be able to study and quickly localize high-energy transients with sub-microsecond time resolution in a wide energy band, spanning from a few keV up to 2 MeV. It will have a peak effective area of about 50 cm^2, 3.2 sr FWHM FoV, and energy resolution of $\leq$800 eV FWHM (at 6 keV in the soft X-ray X-mode) and $\leq$5 keV FWHM (at 60 keV in the hard X-ray and γ-ray S-mode).

3. X-ray Observations

It is believed that the main contribution to the GRB afterglow emission is synchrotron radiation from electrons accelerated in the presence of a magnetic field in the "external" shock produced as the blast wave from the explosion collides with and sweeps up material in the circumburst medium [129–131]. The afterglow emission spectrum from X-ray to radio is expected to appear as a sequence of smoothly connected power laws $f_\nu \propto \nu^\beta$, where the energy spectral index β is determined by the index of the electron energy distribution p and the frequency in relation to the evolving breaks in the spectrum (e.g., [132]). These break frequencies are the cooling frequency ν_c, the characteristic synchrotron frequency ν_m, and the self-absorption frequency ν_a.

Canonical X-ray afterglow light curve may be represented as the following sequence of smoothly connected power law segments $f_\nu \propto t^{-\alpha}$, where α is the temporal index. The steep decay ($\alpha \sim 3$) is generally attributed to high latitude emission. The plateau phase ($\alpha \sim 0.5$) may be explained by a continuous energy injection from the central engine. The normal afterglow decay ($\alpha \sim 1.2$) produced by jet propagation through the ISM. When the radiation beaming angle becomes similar to the jet opening angle, an achromatic steepening of the light curve, known as a jet break, is expected to appear [133–135]. The post-jet break decay typically has $\alpha \sim 2$. X-ray light curve may also show multiple flares with widely varying strengths which can occur during any phase.

Thus, afterglows are extremely important for obtaining a complete picture of the GRB emission mechanisms and constraining theoretical models. The instruments are listed below in the order of launch, which does not reflect their priority or importance for GRB studies.

3.1. CXO (Chandra)

Launched into elliptical high-Earth orbit (HEO) beyond the outer Van Allen Belt on 23 July 1999, the Chandra X-ray Observatory (CXO; named after Subrahmanyan Chandrasekhar), formerly known as the Advanced X-ray Astrophysics Facility (AXAF), is one of NASA's "Great Observatories". The telescope system comprises four pairs of mirrors providing reflection at grazing incidence angles, necessary to focus X-ray photons [136–138].

The High Resolution Mirror Assembly (HRMA) has exceptional capabilities for subarcsecond imaging: 0.5″ resolution in contrast to the ∼5″ imaging for previous X-ray missions. The exquisite imaging capability allows CXO to resolve formerly "point" sources, studying jets and outflows in QSOs and active galaxies, and the structure and interactions within clusters of galaxies. CXO also detects point sources with fluxes 100-times fainter than previously due to the reduction of the detector area, which accumulates background. The Science Instrument Module (SIM) comprises the two focal plane instruments: the Advanced CCD Imaging Spectrometer (ACIS) and the High Resolution Camera (HRC), which record the photon number, position, energy, and time of arrival. Two additional science instruments, the Low Energy Transmission Grating (LETG) and High Energy Transmission Grating (HETG) spectrometers, provide high-resolution spectroscopy in the

0.08–2 keV (15–0.6 nm) and 0.4–8 keV (MEG: 0.4–4 keV, 3–0.3 nm, and HEG: 0.8–8 keV, 1.5–0.15 nm) bands, respectively.

With excellent spatial and spectral imaging, high-resolution dispersive spectroscopy, along with a duty cycle of >70% and up to two days of continuous observations possible, CXO provides a great opportunity to explore the X-ray spectrum. Chandra science highlights include observations of GW 170817, studies of pulsar wind nebulae, cooling flows in clusters of galaxies, X-ray jets in QSOs, along with the observations of SN remnants, supermassive BHs, GRBs, and brown dwarfs.

3.2. XMM-Newton

Launched into elliptical HEO in 10 December 1999, the XMM-Newton observatory, also known as the High Throughput X-ray Spectroscopy Mission and the X-ray Multi-Mirror Mission, is one of the ESA's Horizon 2020 flagship missions. Each of the three X-ray telescopes on board XMM-Newton consists of 58 gold-coated nested mirrors, providing a large collecting area over a wide energy band (see [139] and the reference therein).

The science payload comprises three devices: the European Photon Imaging Camera (EPIC), the primary instrument, the Reflection Grating Spectrometers (RGSs), which is a secondary instrument, and the Optical Monitor (OM). Installed at the prime focus of each of the telescopes, three EPICs are equipped with silicon chips able to register extremely weak X-ray radiation and advanced CCDs with a scale of $1.1''$/pixel, capable of detecting rapid variations in intensity, down to a thousandth of a second and less. The EPIC CCDs are designed to cover the full design range of the X-ray mirrors, 0.1–15 keV with an energy resolution of $E/dE \sim 50$ at 6.5 keV and positional resolution sufficient to resolve the mirror performance of $6''$ FWHM. Aimed at the complementary analysis of the spectrum, RGSs are installed on two of the three XMM-Newton X-ray telescopes. RGSs provide high-resolution ($E/dE =$ 200–800) X-ray spectroscopy over the 0.35–2.5 keV band, thus yielding more detailed information on the condition of individual elements (e.g., oxygen and iron) than EPIC. OM is a highly sensitive (equivalent to a 4 m ground-based telescope) 30 cm Ritchey–Chretien telescope able to observe objects in the UV and the blue region in optics simultaneously with the X-ray telescopes. OM has a spatial pixel size of $1''$ and a limiting sensitivity of B = 24 in unfiltered light and is equipped with broad- and narrow-band filters and two grisms, which provide spectral resolution.

The science highlights of the observatory include studies of galaxy clusters, supermassive BHs, stars, neutron stars, TDEs, SNe, GRBs, GWs, supergiant fast X-ray transients, exoplanets, and Solar System bodies and tests of cosmology and dark matter scenarios.

3.3. Swift/XRT

The X-ray Telescope (XRT [67,68]) on board the Swift observatory enables it to localize GRBs with a few arcsecond accuracy within 100 s of the burst onset. The XRT is a sensitive (down to 2×10^{-14} erg cm^{-2} s^{-1} in 10^4 s) broad-band (0.2–10 keV) X-ray imager with an effective area of >120 cm^2 at 1.5 keV, FoV of $23.6' \times 23.6'$, and angular resolution of $18''$ (HPD). Its CCD comprises an 600×602-pixel image area and a storage region of 600×602 pixels. XRT can also estimate the GRB redshifts based on the Fe line emission or other spectral features.

Scientific implications of the Swift XRT data include collecting the GRB afterglow statistics, studies of X-ray flares, GRB rapid decay, and plateau phases [140] and contributing to the research on the closure relations, used to identify potential jet breaks with diverse characteristics [141,142]. The XRT science highlights include studies of GRBs, the follow-up of GW triggers in the Second Advanced LIGO/Virgo Observing Run [143,144], studies of TDEs, dust halos in V404 Cyg, nearby active galaxies, SNe and their shock breakouts, large amplitude variability in nova X-ray light-curves, and magnetars[9].

3.4. MAXI/GSC

The Monitor of All-sky X-ray Image (MAXI) Gas Slit Camera (GSC), mounted on the ISS, detects GRBs and XRFs. The GSC consists of 12 one-dimensional position-sensitive proportional counters operating in the 2–30 keV energy range [145]. Pointing in directions orthogonal to each other, GSC-H (horizontal camera) and GSC-Z (zenithal camera) achieve an instantaneous FoV of $3° \times 160°$, allowing 70% coverage of the whole sky every orbit (i.e., every 92 min) with a typical transit time on a point source of ∼40–100 s, depending on the incident angle [146]. With a modest (and varying during a scan) ∼10 cm^2 effective area for a point (in the 4–10 keV band), GSC usually cannot perform spectral analysis of short events and estimate exactly the intrinsic variation of a source flux [145]. Since the commissioning of MAXI operation on 8 August 2009, GSC observed $\gtrsim$140 GRBs[10]. MAXI/GSC also observes XRFs, which are a subclass of GRBs having significantly softer spectra than those of classical GRBs, at a high rate [145].

3.5. NuSTAR

The Nuclear Spectroscopic Telescope Array (NuSTAR) mission, launched on 13 June 2012, into a 600 km, near-circular, 6° inclination orbit, is the first focusing high-energy X-ray telescope in orbit. Operating in the 3–79 keV energy range, it significantly extended the sensitivity of focusing compared to the previous X-ray satellites, which were limited by the ∼10 keV high-energy cutoff. It comprises two co-aligned grazing-incidence X-ray telescopes pointed at targets by the spacecraft and benefits from the inherently low background, allowing the telescope to probe the hard X-ray sky with a significantly (100-fold) improved sensitivity compared to the collimated or coded mask instruments with the same bandpass.

With its unprecedented combination of sensitivity (2×10^{-15} erg cm^{-2} s^{-1} in the 6–10 keV range and 1×10^{-14} erg cm^{-2} s^{-1} in the 10–30 keV range) and spatial (18″ FWHM), spectral (400 eV at 10 keV, 900 eV at 68 keV FWHM), and temporal (2 μs) resolution, NuSTAR pursues following core scientific goals: (1) studies of obscured AGN activity out to the peak epoch of galaxy assembly in the Universe; (2) probing the population Galactic compact objects; (3) investigating the non-thermal radiation in young SN remnants; (4) constraining the structure of AGN jets; and (5) constraining the SN explosion models [147]. Its science highlights include the first measurement of black hole spin with high precision, untangling the mystery of how stars explode, the discovery of a shockingly bright dead star, staring deep into the hidden lairs of black holes, and a contribution to the first picture of a black hole[11].

4. Optical Facilities

Optical and NIR observations of GRB afterglows and host galaxies give a unique opportunity to measure GRB redshifts, jet opening angles, and local environment properties, which are the key parameters necessary to estimate the GRB rest-frame energetics and other properties.

Generally, GRB prompt emission detectors yield a large ($\gtrsim$1°) localization error. However, a small localization box is needed to find the host galaxy in surveys or to point an optical telescope with a relatively narrow FoV to observe the GRB afterglow. Indeed, some γ-ray imaging facilities, such as Swift/BAT, can localize GRBs with an uncertainty of several arcminutes; however, the fraction of GRBs with coarse localizations is relatively high. In the latter case, the rapid optical follow-up with robotic telescopes can provide a localization box narrow enough for the observations with large optical telescopes or search in the galaxy surveys.

Another way of observing poorly localized GRBs in optics is by means of wide-field monitoring cameras that continuously monitor large regions of the sky simultaneously with gamma-ray facilities. This way, one may expect to obtain the optical light curve covering the very first moments of the event, which is otherwise unattainable using a follow-up observing strategy. However, due to the obvious hardware limitations of wide-field

cameras, only the brightest events, such as GRB 080319B [148,149] or GRB 160625B [150], are observable with them.

Since polarization measurements give important information on the nature of radiation sources, magnetic fields, the geometry of the emitting regions, and the spatial distribution of matter around sources, polarimetry is also a valuable source of data, especially for the transient or fast variable objects such as SNe or GRBs.

4.1. Global Networks of Robotic Telescopes/Rapid Follow-Up

Since a typical GRB afterglow rapidly fades by about 2–3 mag within 5–10 min after its onset and by another 3 mag in the following 50 min [151], quick GRB follow-ups are extremely important. The low latency and cost and high reliability and efficiency of the observations with robotic telescopes are provided by computer-controlled low-level behavior, ensuring the absence of manual control by humans. Running under the control of a scheduler, which selects observational targets, robotic telescopes can operate in remote and extreme environments such as mountain tops, deserts, and even Antarctica. One of main goals of such telescopes and their networks is the rapid observation of transient events within seconds or minutes after they are detected by space-borne facilities. In this section, we briefly review the robotic telescopes aimed at GRB follow-ups in the optical and NIR ranges. As the number of such instruments is huge (Literally hundreds of different optical facilities observed GRBs over the last twenty years!), we do not pursue the goal of reviewing all the robotic telescopes or their networks. The selection of the referenced projects is thus inevitably subjective. The telescopes are listed below in alphabetical order, which does not reflect their priority or importance for GRB studies.

4.1.1. BOOTES

The Burst Optical Observer and Transient Exploring System (BOOTES) [152,153], a worldwide robotic telescope network, had first light in 1998. Depending on the error box size, it uses wide-field cameras (WFC), ultra-wide-field cameras (UWFC), and narrow-field cameras (NFC) attached to small robotic telescopes, or the telescopes themselves. The BOOTES network consists of five stations, four in the Northern Hemisphere and one (and two more in the near future) in the Southern Hemisphere, which will ensure that there will always be telescopes that can cover any source either in the northern or in the southern night sky. Presently, the BOOTES observatories are located in Huelva and Málaga (Spain), Otago (New Zealand), Lijiang (China), and the "Javier Gorosabel Telescope" ("JGT") in Baja California (México), and two more observatories are planned to be deployed in South Africa and Chile. The BOOTES telescopes reaction time is of the order of 10–20 s, and any part of the sky is accessible in less than 8 s.

Equipped with the same 0.6 m Ritchey–Chretien telescopes with the $f/8$ focal ratio, the stations in Málaga (Spain), New Zealand, China, and México have EMCCD covering $10' \times 10'$ FoV with clear, Sloan g; r' i', and WFCAM/VISTA Z and Y filters. The station in Málaga is also equipped with the COLORES imaging spectrograph. The station in Huelva comprises two domes, one of which is equipped with a wide-field CCD camera (4096×4096 pix) attached to a 400-mm $f/2.8$ lens, which covers a $5° \times 5°$ FoV. and the other is a 0.3 m-diameter Schmidt–Cassegrain reflector telescope mounted on a Paramount mount, which provides a $15' \times 15'$ FoV. Moreover, an all-sky camera, Compact All-Sky Automated Network Developed for Research in Astronomy (CASANDRA), which is a 4096×4096 pixel^2 CCD attached to a 16 mm $f/2.8$ lens covering a 180° FoV, is installed in each station. The images showing the sky conditions (clouds, etc.) and stars brighter than 10 mag are recorded every minute.

BOOTES's scientific goals include: (1) observations of GRB optical counterparts important to study the burst central engine; (2) monitoring of astrophysical optical transients of cosmic origin, which could be related to FRBs, neutrino sources, GWs, QSOs, AGN, TDEs, etc.; (3) ground-based support for space-borne high-energy missions, such as INTEGRAL,

Swift, and Lomonosov/UFFO; (4) monitoring of astronomical galactic objects, including asteroids, meteors, comets, variable stars and novae, etc. [154].

4.1.2. COATLI

COATLI (stands for "Corrector de Óptica Áctiva y de Tilts al Límite de dIfracción" or "active optics and tilts corrector at the diffraction limit"; coatli also means "twin" in the indigenous Mexican Nahuatl language) is a robotic 50 cm Ritchey–Chretien telescope on a fast equatorial mount installed at the Observatorio Astronómico Nacional in Mexico. COATLI is currently operating with the HUITZI $f/8$ instrument, an EMCCD with a $11.9' \times 11.9'$ FoV with griz broad-band filters and 470/10, 640/10, and 656/3 narrow-band filter. However, a medium-term aim is to install a fast-guiding imager, which will provide $0.35''$ FWHM images over a field of at least $4'$ and coverage of a large fraction of the sky [155]. COATLI will provide 0.3" FWHM images from 550 to 900 nm over a large fraction of the sky. The instrument operates in two channels: a red channel (from 550–920 nm; $4.1'$ FoV) and a blue channel (from 400–500 nm; $4.9'$ FoV). The interim instrument is a simple CCD imager with a $12.8' \times 8.7'$ FoV with the long axis roughly N-S equipped with BVRI filters and a clear w filter.

Apart from the GRB follow-up, the scientific goals of the instrument include observations of HII regions in nearby galaxies, eclipsing binaries in the Trapezium, sub-stellar companions in the Solar neighborhood, galactic star clusters, multiplicity in young clusters, and planetary nebulae in the bulge.

4.1.3. DDOTI

Installed at the Observatorio Astronómico Nacional in Mexico, the Deca-Degree Optical Transient Imager (DDOTI) is a wide-field robotic imager comprising six 28 cm telescopes with prime focus CCDs on a common equatorial mount. These telescopes, having a 12 $\deg^2$ FoV with 2" pixels each, provide an instantaneous FoV of about 72 $\deg^2$ when observing jointly [156]. The DDOTI 10σ limiting magnitudes in 60 s (4×60 s exposures) are $r \approx 18.7$ (18.8) and $r \approx 18.0$ (19.5) in dark and bright time, respectively. The Celestron Rowe-Ackermann Schmidt Astrograph (RASA), installed on the telescopes, is a prime-focus Schmidt astrograph with a 279 mm aperture, a 620 mm focal length, a $\varnothing$70 mm focal plane developed for the observations in the 400–700 nm range, and a final focal ratio of $f/2.22$.

The key science goals of DDOTI are the localization of the optical transients with 100 $\deg^2$ positional uncertainties and requiring a wide-field imager, e.g., GRBs detected by Fermi/GBM and GW events detected by LIGO and Virgo.

4.1.4. FRAM

FRAM (short for the F/(Ph)otometric Robotic Atmospheric Monitor [157]) is a part of the atmospheric monitoring system of the Pierre Auger Observatory, located near Malargue, Argentina. It has been operational in different configurations since 2006 and currently consists of a 10Microns GM2000 mount with Orion UK 12-inch "Optimised Dall-Kirkham" telescope with an ASA three-inch focuser and Moravian Instruments G4-16000 CCD [158]. It also contains a wide-field Nikkor 300/2.8 lens equipped with the G4-16000 CCD, yielding a 7×7-degree field of view. The telescope is primarily used for real-time measurements of vertical aerosol optical depth over the observatory, but it also robotically reacts to GCN triggers and performs the GRB follow-up. A similar setup, called FRAM-ORM, has also been installed since 2018 on the future north Cherenkov Telescope Array site on La Palma, Canary Islands, and has also been following GRBs since then.

4.1.5. GIT

The GROWTH India Telescope (GIT) is a 70 cm fully robotic telescope on an altitude–azimuth mount located at the Indian Astronomical Observatory (Hanle)[12]. It has a $0.7° \times 0.7°$ FoV, an $f/6.5$ focal ratio, and a back-illuminated CCD camera with 4096×4108 pixels with a scale of $0.7''$ per pixel. GIT's scientific goals include studies of fast transients

(electromagnetic counterparts to GW sources, GRBs, FRBs, fast blue optical transients, etc.); SNe and novae; and Solar System objects (near-Earth asteroids, active asteroids, outbursting comets, etc.).

4.1.6. GRANDMA

The Global Rapid Advanced Network Devoted to the Multi-messenger Addicts (GRANDMA) is an international project, which currently coordinates 25 telescopes with both photometric and spectroscopic facilities [159,160], including the TAROT and FRAM described above, purposed to provide coordinated observations of transients in large regions of the sky. Being primarily aimed at GW alert follow-ups, GRANDMA can follow-up any transient alerts, even with poor spatial localization.

4.1.7. IKI GRB-FuN

The IKI Gamma-Ray Burst Follow-up Network (IKI GRB-FuN [161]) is another project on joining existing telescopes to a dedicated network for GRB rapid follow-up observations. Currently, IKI GRB-FuN conducts TOOs at a number of medium/large optical telescopes: AZT-22 (Maidanak), AZT-20 (Assy), AZT-33IK (Mondy), Zeiss-1000 (TShAO), and Zeiss-1000 (Koshka). Besides that, IKI GRB-FuN initiates GRB follow-ups at the International Scientific Optical Network (ISON [162,163]) of several dozen automated and robotized small aperture telescopes worldwide aimed at space debris, comet, and asteroid observations. IKI GRB-FuN's performance can be illustrated by the statistics of observations in 2021: the network performed 49 GRB follow-ups; detected 32 GRB afterglows; discovered four optical transients, two GRB host galaxies, and two accompanying SNe.

4.1.8. KAIT

The Katzman Automatic Imaging Telescope (KAIT), named after the Sylvia and Jim Katzman Foundation, whose donation made possible the completion of the telescope, is a fully robotic instrument operated at Lick Observatory in California, USA [164,165]. The telescope control system checks the weather, opens the dome, points to the desired objects, acquires guide stars (in the case of long exposures), exposes the CCD ($6.7' \times 6.7'$ FoV), stores the data, and manipulates the data automatically. Regarding its main features, KAIT has a 0.76 m-diameter primary with a Ritchey–Chretien mirror set with the focal ratio $f/8.2$, reaches a limit of R $\sim$ 20 mag (4σ) in a 5 min exposure, and can take close to 100 images per hour and observe about 1000 galaxies a night.

KAIT is programmed to conduct multi-filter (VRIz) observations of GRB afterglows, with the V-band capability present as a consistency check with the Swift UVOT [166]. Apart from GRB follow-ups, KAIT discovered comets and contributed to the SN Search and the Lick AGN Monitoring Projects at the Lick observatory.

4.1.9. Liverpool Telescope

The Liverpool Telescope (LT) is located in La Palma (Canary Islands, Spain) and operates in fully robotic mode. It has a 2 m-diameter primary mirror, an altitude–azimuth design, and a final focal ratio of $f/10$. Following an automatic GRB follow-up program started in 2005, upon receiving an automatic GRB alert from a GRB detector on board Swift, INTEGRAL, HETE-2, or from IPN, the LT initiates a special override mode that conducts GRB follow-up. Due to the fully opening enclosure and the fast slew rate of $2^\circ/s$, the observation starts within 1–3 minutes of the GRB onset [167]. LT comprises five instrument ports (four folded and one straight-through), selected by a deployable rotating mirror in the acquisition and guidance box within 30 s. The telescope is equipped with the RATCam optical CCD camera and the SupIRCam 1–2.5 mm camera.

LT aims to observe time-variable sources over a wide range of timescales from targets of opportunity (e.g., novae, SNe, and anomalies in gravitational lenses) to long-term monitoring (e.g., AGNs, variable stars).

4.1.10. MASTER

The Mobile Astronomical System of TElescope Robots project (MASTER) was run in 2002 [168]. All MASTER telescopes can be guided by alerts and observe prompt optical emission from GRBs synchronously in several filters and in several polarization planes (see, e.g., [169] for the MASTER observations of GRB polarization). Master has ten stations including the sites in the Russian Far East, Ural, Siberia, Europe, South Africa, Spain, Argentina, and México. The MASTER-Net project is mainly aimed at conducting fast sky survey with all-sky observed over a single night down to 19–20 mag, which will enable the search for exoplanets, microlensing effects, and dark energy via the discovery and photometry of SNe and monitoring of Solar System objects, including space junk.

Each MASTER II telescope contains an aperture system comprising two tubes with polarizers having polarization directions perpendicular to each other. Every telescope is equipped with a 4000 pixel $\times$ 4000 pixel CCD camera with a 1.85″/pixel scale, a photometer with B, V, R, and I filters (Johnson–Cousins system), and polarizing filters and has a total FoV of 8 deg^2, providing a survey speed of 128 deg^2 per hour with a 20^m limit on dark moonless nights [170]. Observations with different orientation of the polarizers, relevant for the transients with significant intrinsic polarization, can be carried out using several telescopes [171].

In general, MASTER is close to the American ROTSE-III network (see Section 4.1.16) in many aspects with a difference in the larger FoV and several telescopes mounted on a single axis, allowing images to be taken at several different wavelengths simultaneously [172].

4.1.11. PAIRITEL

The Peters Automated Infrared Imaging Telescope (PAIRITEL), named after the late telescope operator Jim Peters, is the first meter-class telescope operating as a fully robotic IR imaging system [173]. Located in Arizona, USA, PAIRITEL began regular observations in mid-December 2004. The 1.3 m telescope and simultaneous J,H,Ks camera were formerly used in the 2MASS project, which ended data taking operations in 2001. PAIRITEL was designed for automated, queue-based observing, with the ability to rapidly respond to ToOs such as GRB alerts from space-based satellites. The best response was 90 seconds from a GRB trigger to the beginning of the first observation.

4.1.12. Pi of the Sky

A wide-field camera developed in order to continuously observe the night sky in the search for optical transients, and in particular, for the untriggered search of GRBs, the Pi of the Sky (after envisioned simultaneously covered sky solid angle $> \pi$ sr) consists of observing modules of custom design, each having four 85 mm objectives and CCDs with 2000 $\times$ 2000 pixels 15 $\times$ 15 μm^2 each [174]. When operated with 10 s exposures, each module allows the detection of transients with 12–13 magnitudes in a 33 $\times$ 33° FoV. The prototype with two cameras has been installed at Las Campanas (Chile) and was operational since July 2004 and till 2009. Since 2014, the full system consisting of four observing modules (16 objectives in total) has been active at INTA El Arenosillo test center in Mazagon, Huelva, Spain [175].

The scientific goals of the project include the search for optical flashes accompanying GRBs and a contribution to the multiwavelength observations of transients, the investigation of fast variable stars, and observations of blazars and other AGNs.

4.1.13. RAPTOR

The first robotic optical facility for the real-time follow-up of optical transients is a spatially distributed system of autonomous telescopes, RAPid Telescopes for Optical Response (RAPTOR), located in New Mexico (USA) [176,177]. The scientific goals of the RAPTOR experiment include the studies of optical transients (e.g., GRBs), near-Earth objects (NEOs) and killer asteroids, flares on Solar-type stars, exoplanets, mapping the Galaxy in 3D (e.g., the RR Lyrae stars investigation), nearby SNe, and cosmology.

The basic system observes a 1500 deg^2 FoV with a wide-field imaging array and a central 4 deg^2 FoV with a more sensitive narrow-field "fovea" camera, which uses different filters to image a transient, providing color information. Comprising two telescope arrays, separated by 38 kilometers, the system provides a stereoscopical view of an object and is complemented by a rapidly slewing telescope with a low-resolution spectrograph.

4.1.14. RATIR

Installed on the $f/13$ secondary of the 1.5 m Harold Johnson telescope of the Observatorio Astronómico Nacional on the Sierra de San Pedro Mártir, Baja California, Mexico, the Reionization And Transients Infra-Red (RATIR) camera comprises two optical and two IR arms, with a two-color split filter, allowing for simultaneous imaging in six colors (two optical and four NIR) [178,179]. RATIR has been built for rapid GRB follow-up and provides simultaneous optical and infrared photometric detections with H = 20.3 and J = 20.9 (AB mags) detectability limits within 10 min of a GRB [180].

4.1.15. REM

Rapid Eye Mount (REM) is a 60 cm-diameter fast-reacting telescope installed in the La Silla premises of the ESO Chilean Observatory at a 2400 m altitude on the edge of the Atacama Desert in Chile in June 2003 [181]. Hosting two instruments: a visible imager and slitless spectrograph ROSS and an infrared imaging camera REMIR, REM is able to observe using both cameras simultaneously the same $10' \times 10'$ FoV thanks to a dichroic placed before the telescope focus. The [z', J, H, K'] filters and frames are used on REMIR to reach H = 15 in IR (1–2.3 μm) in 5 s exposure. The standard [V, R, I] filters and a slitless Amici prism, which can divide the 0.45–0.9 μm range into 30 bins, are installed on ROSS to reach R = 16 in a 1 s exposure. A typical time delay from receiving alert to start of observations is ∼30 s. The telescope also hosts the TORTORA camera. REM has been acquiring data since June 2003. The telescope is aimed to catch the optical and NIR afterglows of GRBs. REM is triggered by a signal from a high-energy satellite and rapidly points to the detected location in the sky.

4.1.16. ROTSE III

ROTSE is a Robotic Optical Transient Search Experiment aimed to search for fast optical transients, including GRB follow-up [182]. The telescope is a modified 450.0 mm-diameter Cassegrain with 2.64°FoV, $f/1.9$ primary mirror with an 850.0 mm focal length. There are four equatorial-mount ROTSE-III telescope systems: in Coonabarabran (Australia), Mount Gamsberg (Namibia), Bakirlitepe (Turkey), and Fort Davis (Texas, USA).

4.1.17. SARA

The Southeastern Association for Research in Astronomy (SARA) operates remotely three telescopes, namely a 0.96 m telescope at Kitt Peak, Arizona; a 0.6 m telescope on Cerro Tololo, Chile; and a 1 m Jacobus Kapteyn Telescope at the Roque de los Muchachos, Spain [183]. The telescope in the U.S. (SARA-KP) has $UBV\,RI$, zero-redshift Hα, Hβ and [O III], redshift-stepped Hα with 75-Å FWHM, and medium-band continuum including one at 5100 Å, also usable for redshifted [O III], neutral-density, and very broad "white light" filters. The observatory in Chile (SARA-CT) comprises $UBV\,RI$, SDSS $ugriz$, white light, and zero-redshift Hα filters. The telescope in Spain (SARA-RM) includes $UBV\,RI$, $ugriz$, and "white-light" filters. In Arizona and Chile, identical single-fiber echelle spectrographs are also installed on the telescopes. The SARA-KP and SARA-RM have an f-ratio of 7.5 and 8, respectively. The CCD pixel scale of the SARA telescopes varies from 0.14″ to 0.61″.

The scientific program of the observatories includes studies of the Solar System (asteroids and comets), research on stellar astrophysics (Mira variables, binary stars, exoplanet transits, pulsating white dwarfs, or cataclysmic variables), studies of AGNs, blazar variations and the variability of Seyfert galaxies, and rapid follow-up of transient sources, e.g., GRBs, novae, and SNe (for references, see [183]).

4.1.18. SkyNet

Aimed at observations of GRB afterglows, the Skynet Robotic Telescope Network consists of ∼20 small (0.4–1 m aperture) optical telescopes in the Americas, Australia, and Europe and a 20 m radio telescope in West Virginia, USA, operating under the control of the software TERMINATOR based on the ASCOM standards [184]. The Panchromatic Robotic Optical Monitoring and Polarimetry Telescopes (PROMPTs), which form the main branch of SkyNet, are located in Chile ($3 \times 16''$ telescopes + $3 \times 24''$ + $32''$ + $40''$, proposed $60''$, polarimeter and spectrograph in development), Australia ($4 \times 17''$, proposed $17''$ or $40''$), and Canada ($16''$). Besides, Skynet comprises a number of partnering university telescopes. The scientific goals of the network include observations of GRBs, GW sources, FRBs, blazars, SNe, SN remnants in radio, novae, white dwarfs and subdwarfs, variable stars, eclipsing binaries, exoplanets, and Solar System objects, especially NEOs.

4.1.19. Swift/UVOT

Developed for rapid follow-up and long-term observations of GRB afterglows in the UV and optical 170–600 nm range, UVOT (the UV/Optical Telescope mounted on Swift spacecraft—see Section 2.2.3) has an optical configuration with a 30 cm primary mirror (which in terms of imaging sensitivity is equivalent to a 4 m ground-based telescope) with an f-number of 12.7 [69]. The instrument is characterized by a $17' \times 17'$ FoV, a PSF of $0.9'$ FWHM at 350 nm, and a 256×256 pixel^2 CCD with a $0.5''$-pixel scale. The photon detectors are able to image the incoming photons and operate in a photon counting mode, i.e., measure both individual photon positions and timing information. The instrument is aimed at GRB studies: rapid follow-up and sub-arcsecond localization, identification of the GRB environment, redshift estimation, timing of GRB afterglows, and shedding light on dark bursts.

4.1.20. TAROT

The 25 cm Télescope à Action Rapide pour les Objets Transitoires-South (TAROT—Rapid Action Telescope for Transient Objects) is a very-fast-moving optical robotic telescope in La Silla (Chile), active since 9 September 2006 [185]. An original twin TAROT telescope is located at the Calern observatory, France. TAROT is able to react very quickly, with pointing speed $\lesssim 80°$ s^{-1} and acceleration $\lesssim 120°$ s^{-2} and a pointing time of 1–1.5 s, to a signal from a satellite indicating that a GRB is in progress and can provide fast (the standard processing time is one minute) and accurate (better than $1''$) positions of transient events in $2° \times 2°$ FoV. The speed ratio of the telescope is $f/3.5$.

One of the primary scientific goals of the telescope is the GRB follow-up observations. The data acquired by TAROT are also useful for studies of GRB evolution and the physics of the fireball and of the surrounding material. Moreover, TAROT contributed to the discovery of the seven planets orbiting the nearby ultra-cool dwarf star TRAPPIST-1, which are all made mostly of rock, and some could potentially hold more water than Earth.

4.1.21. TORTORA and Mini-MegaTORTORA

The Telescopio Ottimizzato per la Ricerca dei Transienti Ottici RApidi (TORTORA) wide-field camera is mounted on top of the REM robotic telescope at La-Silla Observatory in Chile and has been operating since May 2006 [186] and till 2015. The instrument was optimized for photometry of fast transients with a best time resolution of about 0.1 s and is capable of autonomously detecting and classifying optical transients up to 10^m–11^m on a sub-second time scale in a $24° \times 32° = 768$ deg^2 FoV. It has a diameter of 120 mm, focal length of 150 mm, and focal ratio of 1/1.2.

TORTORA is the second version of a prototype FAVOR camera that was placed at North Caucasus near the 6 m BTA telescope [187–189]. One of the important results of the TORTORA routine observation was the estimation of the detection rate of the short-lived orphan transients. The prompt optical transient detection rate determined from the observations with TORTORA is $<8 \times 10^{-9}$ deg^{-2} s^{-1} for the GRB counterparts brighter

than 10.5^m on a 0.13 s timescale [190]. The TORTORA camera was running the observations in three automated operation modes: the survey mode (scheduled programs of the REM telescope), the alert mode (notifications from GCN network), and the follow-up mode (tracking Swift/BAT).

The Mini-MegaTORTORA (MMT-9) multichannel wide-field monitoring system is a successor to TORTORA and started routinely observing the sky in June 2014. MMT-9 is aimed at detecting meteors, comets, and asteroids, tracking satellites, finding flashes of flaring stars and novae, studying variable stars of various classes, observing transits of exoplanets, and searching for bright SNe and optical counterparts of GRBs. The importance of such instruments became evident after the discovery and detailed study of the brightest optical afterglow of GRB 080319B [149,191] with the TORTORA camera. Installed on five independent equatorial mounts, nine individual channels, which constitute the basis of MMT-9, allow mosaicking of a larger FoV, or pointing all the channels in one direction. In the primary "monitoring" (white light, wide field of view) regime, the system acquires images with 0.1 s exposures and analyzes them in real time using a dedicated fast differential imaging algorithm, able to detect and classify various classes of transients with sub-second time scales (rapid flashes, meteors, satellites, etc.) [192]. Upon detection of the flashing transients, the system switches to the narrow-field "follow-up" regime, with different channels observing its position in different photometric and polarimetric filters simultaneously for several minutes. Every sky field is observed this way for 1000 s. Before and after the high-resolution observations, the system switches to the "survey" mode, in which it takes deeper images with a 60 s exposure in white light, which allow studying the variability of 14–15 mag objects.

Mini-MegaTORTORA routinely follows the fields of view of the Swift and Fermi satellites in order to maximize the probability of simultaneously observing the optical counterparts of GRBs. Furthermore, upon receiving the GRB triggers from these telescopes, it initiates the follow-up of the events even if they occurred outside of its monitoring field of view, thus acting as a more traditional robotic telescope.

4.1.22. WATCHER

Installed at Boyden Observatory, South Africa, in April 2006, the Watcher, which is a 40 cm classical Cassegrain reflecting telescope equipped with standard B, V, R, I filters, was aimed towards follow-up observations of GRBs detected by Fermi, INTEGRAL, Swift, XMM-Newton, and NuSTAR [193]. A highlight result for GRB research is a detailed early-time observation of GRB 120711A [194]. AGNs and variable stars are among the observation targets of the telescope in the absence of GRBs [195].

4.2. Surveys

In the classic model of astronomical observation, astronomers study a selected class of objects in a small region of sky. However, some of the most exciting cosmological and astrophysical results in recent years have been made possible by the study of millions of objects over thousands of square degrees of sky by means of large-scale optical surveys. Thanks to these surveys, we often have the information on the GRB host galaxies without any additional observations. Furthermore, the ones with finer temporal resolution may actually detect the afterglows of GRBs independently of gamma-ray triggers [196–198].

The volumetric survey speed, i.e., the spatial volume within which an object of a given absolute magnitude could be detected, per the total time per exposure, can represent the ability of a survey camera to detect transients [199]. This quantity combines limiting magnitude, FoV, and exposure and overhead times into a single metric capturing how quickly a survey can probe physical space for new events. Figure 4 shows relative volumetric survey speeds for different projects.

Again, we do not pursue the goal of reviewing all the surveys in the optical range. The selection of referenced projects is subjective. To the best of our knowledge, apart from the surveys briefly reviewed below as examples, there are several projects able to detect

GRB optical counterparts, which is, however, not their primary goal, e.g., the Asteroid Terrestrial-impact Last Alert System (ATLAS [200]), SDSS ([201–203]), Gaia [204], the Visible and Infrared Survey Telescope for Astronomy (VISTA [205,206]), and Two MicronAll Sky Survey (2MASS [207]).

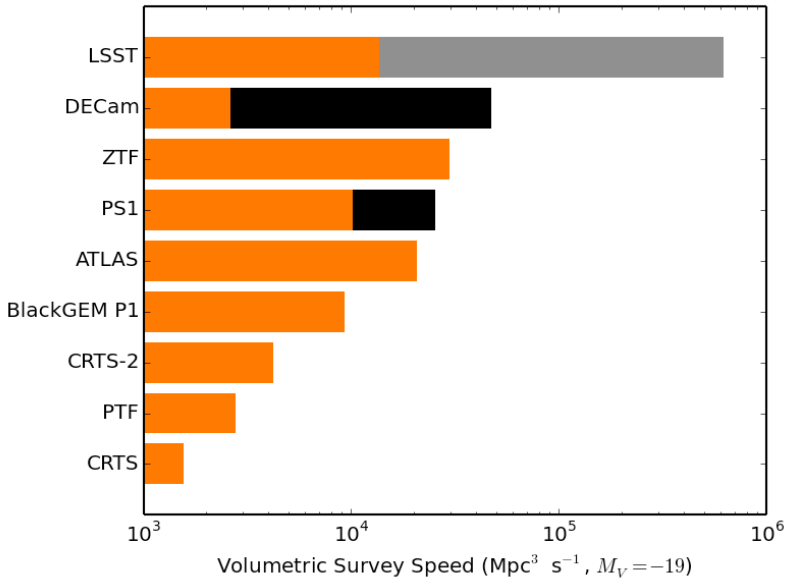

Figure 4. Comparison of volumetric survey speeds adopted from https://www.oir.caltech.edu/twiki_oir/pub/Palomar/ZTF/140724NSFSite/Bellm_ZTF_overview_NSF_site_visit.pdf (accessed on 23 May 2022).

4.2.1. Pan-STARRS

The Panoramic Survey Telescope and Rapid Response System (Pan-STARRS) located at Haleakala Observatory, Hawaii, USA, is a wide-field astronomical imaging and data processing facility [208,209]. The first telescope of the Pan-STARRS Observatory was the Pan-STARRS Telescope #1, (Pan-STARRS1 or informally PS1). PS2 is due north of PS1; the center of the two telescope piers is separated by 20.05 m. PS1 has a focal length of 8000 mm, a nominal FoV of a 3°-diameter circle, a 1800 mm-diameter primary mirror, a $f/4.44$ focal ratio, and a 4800 × 4800 pixel CCD matrix.

The 3π Steradian Survey, the Medium Deep Survey, and other synoptic imaging surveys were carried out in $grizy_{P1}$ filters. For the 3π Steradian Survey, the 5σ point source limiting magnitudes were 23.3, 23.2, 23.1, 22.3, and 21.4, respectively. Pan-STARRS spends ∼90% of its time observing near-Earth objects. Apart from this, Pan-STARRS is supposed to study the Milky Way and the Local Group structure, galaxy formation, SNe, and cosmology; survey the Solar System; provide new constraints on dark energy and dark matter; explore the astrophysical time domain, including, but not limited to, explosive transients and microlensing events in M31; and a transit search for exoplanets [210].

Apart for the observations of GRB candidates, the major contribution of Pan-STARRS telescopes to the field of transient science is the creation of the Pan-STARRS (PS1) catalog and imaging atlas, covering about 70% of the sky and providing uniform and accurate photometric data, which are widely used for selecting secondary standards for calibrating the GRB observations by other groups, as well as often providing pre-discovery images of the GRB host galaxies.

4.2.2. PTF/iPTF/ZTF

The PTF project has three stages: the Palomar Transient Factory (PTF, 2008–2012), a general synoptic transient survey; the Intermediate Palomar Transient Factory (iPTF, 2013–2017), focused mini-surveys; and the Zwicky Transient Facility (ZTF, 2017–present), a high-

cadence survey. All of them are based on the same 1.2-m (48-inch, P48) Samuel Oschin Telescope at the Palomar Observatory in California, USA, which has been historically used for the photographic Palomar All-Sky Survey. The surveys are supplemented by a nearby Palomar 60-inch telescope (P60) used for photometric follow-up observations, which allows the flexibility of a closed-loop follow-up program and high survey performance [211].

PTF could observe 4×10^4 events/night, while ZTF detects 3×10^5 events/night (for comparison, the upcoming Legacy Survey of Space and Time (LSST) described in Section 4.2.3 is expected to record 2×10^6 events/night[13]).

The PTF camera had 101 megapixels, a 1″ sampling, and a 8.1 deg^2 FoV. Operating in one of two broad-band filters (Mould-R, SDSS-g′) under median seeing conditions, the camera achieved 2.0″ FWHM images and reached $m_{g'} \approx 21.3$ and $m_R \approx 20.6$ 5σ limiting AB magnitudes in 60 s exposures. PTF scientific goals included novae, luminous red novae, SNe, cataclysmic variables, TDE, RR Lyrae variable stars, compact binaries (AM CVn star), AGNs, transiting Extrasolar planets, microlensing events, and small bodies of the Solar System [212].

iPTF, built upon the legacy of PTF, was a fully automated, wide-field survey, which used a large field (7.8 deg^2) camera having 11 active 2048×4096 CCDs [211]. The survey was conducted with different cadences, varying from 5 days to 90 s in the R-band nominally, along with additional observations made in the g-band. With a standard 60 s per frame exposure, the 5σ limiting magnitudes were $m_R = 20.6$ and $m_{g'} = 21.3$ [211]. With respect to the original PTF, iPTF has the major improvements of the data reduction pipelines (see [213] for further details).

Using an extremely wide $7.50° \times 7.32°$ FoV camera with a 47.7 deg^2 light-sensitive area, ZTF currently scans the entire northern sky every two days [214]. The new camera is made up of 16 CCDs of 6144×6160 pixels each, with a 15 µm pixel size. ZTF has a complement of three custom filters, ZTF-g, ZTF-r, and ZTF-i. The median ZTF sensitivity is $m_g = 21.1$, $m_r = 20.9$, and $m_i = 20.2$ (new moon). The resulting large area survey enables the astronomical community to pursue a broad range of time domain science, including explosive extragalactic transients, optical counterparts of multiwavelength and multi-messenger phenomena (e.g., GRBs), variable stars, TDEs, AGN, and Solar System objects.

4.2.3. Vera C. Rubin Observatory (LSST)

The Vera C. Rubin Observatory, also referred to as LSST (Legacy Survey of Space and Time or, previously, the Large Synoptic Survey Telescope), will be aimed at exploring the transient optical sky, mapping the Milky Way, probing dark energy and dark matter, and monitoring the Solar System [215]. Having an 8.4 m (6.5 m effective) primary mirror, a 9.6 deg^2 FoV, an $f/1.234$ focal ratio, a 3.2-gigapixel camera, and six *ugrizy* filters covering the 320–1050 nm band, the telescope will acquire images of the sky visible from Cerro Pachón, Chile. The facility is expected to be commissioned by 2024.

Most of its observation time, LSST will operate in the deep–wide–fast survey mode, uniformly observing a 18,000 deg^2 region of the sky during the planned 10 years of operation, which will produce a co-added map with $r \sim 27.5$. The remaining 10% of the observing time will be dedicated to very deep and very fast time domain surveys and other projects. An important contribution of LSST to time domain science will be a 50–100-time extension of the current time–volume–color space 50–100 surveys. The LSST goals in time domain science include studies of transients and variables, e.g., variability in blazars, transients associated with TDE flares, and counterparts to SNe, GRBs, and FRBs.

4.3. Telescopes for Spectroscopic and Photometric Studies

One of the primary goals of the spectroscopic observations of GRB afterglows and host galaxies is to probe the early Universe. GRB afterglows are keys to the properties of the intergalactic medium, including its reionization, interstellar medium, and the metal enrichment history [15]. Photometric observations of GRB optical counterparts allow

roughly estimating GRB redshifts and mapping the SED evolution to measure circumburst parameters.

We, again, do not pursue the goal of reviewing all the telescopes observing GRB counterparts in the optical range. The selection of referenced projects is subjective. To our knowledge, apart from the instruments briefly reviewed below as examples, there are several projects able to detect GRB optical counterparts, e.g., Subaru [216]; spectrographs IRCS [217,218], Suprime-Cam [219], HSC [220–223], FOCAS [224,225], MOIRCS [226–229], AO188 [230,231]; SALT (the 10 m Southern African Large Telescope [232])/Robert Stobie Spectrograph (RSS) [233,234], Telescopio Nazionale Galileo (TNG)/Device Optimized for the LOw RESolution (DOLORES)[14], MMT and Magellan Infrared Spectrograph (MMIRS) [235] for spectroscopic observations and SALT/SALTICAM [236]; and MITSuME [237] for photometry. The recently launched James Webb Space Telescope (JWST [238]) is supposed to be able to observe afterglows from the earliest GRBs.

4.3.1. BTA/SCORPIO

The Spectral Camera with Optical Reducer for Photometric and Interferometric Observations (SCORPIO-1) has been operated at the primary focus of the 6 m BTA (the Big Telescope Alt-azimuthal, located in Northern Caucasus, Russia) since September 2000 [239,240]. The SCORPIO-1 focal reducer had a focal ratio of $f/2.6$, spectral range 3600–10,000 Å, limiting magnitudes for images $R = 26.8$ (S/N = 5 for $T_{exp} = 1800$ s, seeing $1.5''$), and limiting magnitude for low-resolution spectra $r = 24.0$ (S/N = 10 in continuum, $T_{exp} = 7200$ s). SCORPIO has a $6.1' \times 6.1'$ total FoV and $2.9' \times 5.9'$ in the multislit mode, CCD image scale of $0.18''$/pixel, and spectral resolution of 1.5–20 Å with grisms (for $1''$ slit width) and 0.8–2.5 Å with FPI. Its successor, SCORPIO-2, has expanded opportunities for polarimetric observations. SCORPIO-2 has -5 filter wheels for 10 positions in each for the changeable elements in the beam (filters, grisms, Wallaston prisms), a focal plane slide, a slide with analyzers of polarization, and a FPI holder.

SCORPIO is aimed to study Solar System objects; stars and the interstellar medium; nearby galaxies; nearby AGNs; distant objects (extragalactic radio sources, wide separation gravitational lens systems); and optical transients.

4.3.2. CAHA/CAFOS

The Calar Alto Faint Object Spectrograph (CAFOS), a focal reducer mounted on the 2.2 m Centro Astronómico Hispano Alemán (CAHA) telescope at Calar Alto, Spain, can change the focal ratio of the telescope from $f/8$ to $f/4.4$. The instrument with a $16'$-diameter FoV and $0.53''$/pix scale is designed to work in visible light and has imaging, spectroscopy, polarimetry, and Fabry–Pérot–Etalon capabilities [241]. CAFOS is equipped with standard filters (Johnson, Cousins, Gunn, SDSS) and a large set of interference filters[15], along with a Wollaston prism and a rotatable $\lambda/2$ plate that provides polarimetry. Imaging polarimetry is carried out with or without a stripe mask, two polarized images separated by $18''$. Spectropolarimetry is conducted in combination with the grisms 400 Å/mm, 200 Å/mm, and 100 Å/mm. Apart from GRB follow-ups, CAFOS is contributing to SNe [242], binary star [243], and galaxy studies.

4.3.3. Gemini/GMOS

The Gemini Observatory comprises two 8.1 m $f/16$ telescopes: Gemini-North (called the"Frederick C. Gillett Gemini Telescope") and Gemini-South, which observe the Northern and Southern Hemispheres and are located in Hawaii, USA, and the Chilean Andes, respectively. Both telescopes began scientific operations in 2000 and cover almost all the sky except for two areas near the celestial poles (with a $\pm 89°$ declination). The Gemini Multi-Object Spectrographs (GMOSs), installed on both telescopes, operate in 360–1030 nm wavelength range covering a $5.5' \times 5.5'$ FoV with $\sim 0.08''$/pixel spatial sampling [244–246]. GMOS-N was delivered in July 2001, with GMOS-S following in December 2002. The GMOS detector comprises an array of three CCDs 4608 × 2048 pixels each with a $0.07''$/pixel scale.

The GMOSs are equipped with the broad-band $u'g'r'i'z'$ imaging filters similar to the Sloan Digital Sky Survey (SDSS) ones, narrow-band imaging filters, and spectroscopy-blocking filters. The instruments operate in four modes: direct imaging, long-slit spectroscopy, multi-slit spectroscopy using custom-made masks, and integral field spectroscopy. The scientific highlights of the GMOSs include research on SNe, massive stars, compact stars, BHs, GW events, galaxies, Solar System bodies, and detection of GRB and FRB optical counterparts.

4.3.4. GROND

Installed at the $\varnothing$2.2 m $f/8$ Ritchey–Chretien telescope on an equatorial fork mount in La Silla (Chile), the Gamma-Ray Burst Optical Near-IR Detector (GROND) performs imaging in the Sloan $g'r'i'z'$ filters and NIR JHK bands with a $0.4''$ intrinsic image quality in a $5.4' \times 5.4'$ FoV in each visual band and a $10' \times 10'$ FoV in the NIR (2048×2048 CCD with the $0.158''$/pixel plate scale) using a focal reducer (1024×1024 array with a plate scale of $0.60''$/pixel) with a $0.6''$ FWHM, allowing the linear increase of sensitivity with additional exposure up to 3–4 h [151,247].

The primary goal of GROND is a rapid follow-up of GRB afterglows and estimation of their redshifts. The main scientific highlights include the start of systematic GRB afterglow follow-up in the near-infrared (JHKs) band, enabling the discovery of high-redshift GRBs, studying the abundance of dust along the GRB line-of-sight, i.e., assessment of the "dark burst" incidence, measurements of GRB afterglow SEDs, studies of the GRB–SNe connection, observations of the black widow binaries, and blazar redshift estimates [151].

4.3.5. GTC/OSIRIS

The Optical System for Imaging and low-Intermediate-Resolution Integrated Spectroscopy (OSIRIS) is a broad-band optical imager and spectrograph, placed in the Nasmyth-B (supposed to be displaced to the Main Cassegrain Station) focus of Gran Telescopio de Canarias (GTC) with a $\varnothing$10.4 m mirror comprising 36 individual hexagonal segments acting as a single surface, which is currently the largest optical–IR telescope in the world. The telescope is hosted at Observatorio del Roque de Los Muchachos in La Palma (Spain), benefiting from the excellent observing conditions. OSIRIS covers a $7.8' \times 7.8'$ FoV in a spectral range from λ3650Å to λ10,000 Å covered by the Sloan system broad-band filters: u' (λ3500 Å), g' (λ4750 Å), r' (λ6300 Å), i' (λ7800 Å), z' (λ9250 Å) over [248,249]. The instrument is primarily aimed at galaxy surveys. Hubble has five scientific instruments, which include cameras and spectrographs: (1) The Wide Field Camera 3 (WFC3) is Hubble's main camera, which studies all kinds of phenomena from the formation of distant galaxies to the planets in the Solar System. The camera can see three different kinds of light: near-UF, visible, and near-IR, only one at a time; (2) the Advanced Camera for Surveys (ACS) captures images of large areas of space to study some of the earliest activity in the Universe; (3) the Cosmic Origins Spectrograph (COS) reads ultraviolet light. This spectrograph studies how galaxies, stars, and planets formed and changed.

The Space Telescope Imaging Spectrograph helps scientists determine the temperature, chemical composition, density, and motion of objects in space. It also has been used to detect black holes.

The Near Infrared Camera and Multi-Object Spectrometer (NICMOS) sees objects in deep space by sensing the heat they emit to capture images, and it is also a spectrograph.

4.3.6. HST

Launched to LEO on 24 April 1990, the Hubble Space Telescope (HST) is one of NASA's Great Observatories (built in collaboration with the ESA). HST has a 2.4 m primary mirror and a collection of five science instruments that work across the entire optical spectrum.

(1) The Advanced Camera for Surveys (ACS), which replaced Hubble's Faint Object Camera, can map large areas of the sky in great detail and perform spectroscopy using grisms. ACS comprises three instruments: Wide Field Channel (WFC), High Resolution

Channel (HRC), and Solar Blind Channel (SBC). They cover the FoVs of $202'' \times 202''$ (WFC), $29.1'' \times 26.1''$ (HRC), and $34.6'' \times 30.8''$ (SBC) in the ranges of 350–1050 nm (WFC), 200–1050 nm (HRC), and 115–180 nm (SBC) with 4096×4096 (WFC), 1024×1024 (HRC), and 1024×1024 (SBC) detectors.

(2) The Wide Field Camera 3 (WFC3) offers comparable performance to the ACS instrument, but over a wider range of wavelengths. WFC3 has two channels: one for ultraviolet and visible light (UVIS) and the other for near-infrared (NIR). The instrument operates in the 200–1000 nm (UVIS) and 850–1700 nm (NIR) spectral range covering a $160'' \times 160''$ (UVIS) and $123'' \times 137''$ (NIR) FoV with 4096×4096 (UVIS) and 1024×1024 (NIR) detectors having a $0.04''$/pixel (UVIS) and $0.13''$/pixel (NIR) pixel scale.

(3) The Cosmic Origins Spectrograph (COS) has two channels: the far-ultraviolet (FUV) channel and the near-ultraviolet (NUV) channel and maximizes efficiency or throughput. COS covers the 115–205 nm (FUV) and 170–320 nm (NUV) spectral range using 32768×1024 (FUV) and 1024×1024 (NUV) detectors. The spectral resolution is 16,000–24,000 (med.), 2000–3000 (low) for FUV and 16,000–24,000 (med.), 2000–3000 (low) for NUV.

(4) The Space Telescope Imaging Spectrograph (STIS) combines a camera with a spectrograph and covers a wide range of wavelengths from the NIR to UV (115–1000 nm). Its spectrograph can operate in two different modes: "long slit spectroscopy", where spectra of many different points across an object are obtained simultaneously, and "echelle spectroscopy", where the spectrum of one object is spread over the detector, giving better wavelength resolution in a single exposure. STIS covers a $25'' \times 25''$ (MAMA) and a $50'' \times 50''$ (CCD) FoV. STIS also has a chronograph, which can block light from bright objects, enabling investigations of nearby fainter objects.

(5) The Near Infrared Camera and Multi-Object Spectrometer (NICMOS) is an instrument providing the capability of infrared imaging and spectroscopy. However, NICMOS's infrared capabilities have been largely superseded by WFC3 since that instrument's installation in 2009. NICMOS operates in the 800–2500 nm wavelength range covering $51.5'' \times 51.5''$ (low resolution), $17.5'' \times 17.5''$ (medium resolution), and $11.0'' \times 11.0''$ (high resolution).

The HST science highlights include estimation of the age and expansion of the Universe and studies of exoplanets, distant galaxies, black holes, SNe, asteroids, and other Solar System bodies, including the discovery of two moons of Pluto and the water vapor erupting off the surface of Jupiter's moon Europa. HST discovered that nearly every major galaxy is anchored by a black hole at the center, helped make a 3D map of dark matter, and estimated the mass and size of the Milky Way.

4.3.7. Keck-II/DEIMOS

Located in Hawaii, USA, the W. M. Keck Observatory comprises twin telescopes both having 10 m primary mirrors, a real focal ratio of $f/13.7$, and covering a $20'$-diameter FoV at the Cassegrain. Both funded by the William Myron Keck Foundation, Keck-I and Keck-II started scientific observations in May 1993 and October 1996, respectively. The equipment most relevant for GRB studies comprises the DEIMOS [250], HIRES [251]), and LRIS [252,253] spectrographs and spectrometers

The DEep Imaging Multi-Object Spectrograph (DEIMOS) is a wide-field, visible-wavelength, faint-object, multi-slit imaging spectrograph in operation at the Nasmyth focus of the Keck-II telescope since June 2002 [250]. It was designed for long-exposure extra-Galactic work, particularly the observation of distant, early, galaxies. DEIMOS operates in three modes: direct imaging, single-object spectroscopy, and multi-object, long-slit spectroscopy. The instrument was designed to achieve high performance across the blue and visible regions for >4200 Å. Its polychromatic and monochromatic focal ratios are $f/1.3$ and $\sim f/2.5$, respectively. The camera consists of a 2×4 mosaic of 2048×4096 CCDs with a total detector array of 8192×8192 pixel. The DEIMOS science FoV is $16.7' \times 5'$ with a pixel scale of $0.1185''$/pixel for both the spectrograph and imager. In "Mega Mask" mode, the instrument can acquire spectra of more than 1200 objects simultaneously, using a special

narrow-band filter. The scientific highlights of DEIMOS include studies of distant galaxy populations, their formation and evolution (e.g., the DEEP2 Galaxy Redshift Survey [254]), and observations of the intergalactic medium (IGM), AGNs, and QSOs (e.g., [255]).

4.3.8. Keck-I/HIRES

The High Resolution Echelle Spectrometer (HIRES) is a grating cross-dispersed, echelle spectrograph operating in the 0.3–1.1 μm wavelength range [251]. It is installed on the right Nasmyth platform of the Keck-I telescope. There are two equally efficient (at ∼4200 Å) configurations of instruments: HIRESb and HIRESr optimized for short- and long-wavelength observations, respectively. The figure of merit of the power of a hi-res spectrometer is the throughput, the product of slit width times resolving power: higher spectral resolution requires a narrower slit, which loses more light. HIRES achieves a relatively large throughput (∼39,000″), despite the large diameter of the telescope primary, by a combination of a large 12″ collimated beam, a large (48″ long) echelle grating (mosaic), and a very fast ($f/1.0$) exquisitely achromatic camera. The instrument has a spectral resolution up to 84,000, a spatial resolution 0.191″/pixel, and a slit length up to 28″. The detector is equipped with a 2048 × 2048 CCD. The main science highlights of the instrument include research on the cosmic origin and evolution of deuterium/hydrogen and beryllium, studies of QSOs, stars, star clusters, and galaxies, the measurement of the temperature of the Universe at distant redshifts, and the search for exoplanets [256].

4.3.9. Keck-I/LRIS

Commissioned in 1993, the Low Resolution Imaging Spectrometer (LRIS) is a visible-wavelength imaging and spectroscopy instrument operating at the Cassegrain focus of Keck-I [252,253]. LRIS has two separate cameras, a blue (LRISb) side and a red (LRISr) side. The upgraded LRISr achieved first light on 27 April 2021. These cameras can be operated simultaneously, though both must be operated using the same basic mode: optical imaging or low-dispersion spectroscopy. An optional polarimeter module enables spectropolarimetry. In the optical imaging mode, the instrument covers a 6′ × 8′ FoV for imaging and a 25″ × 25″ FoV for polarimetry. LRISr uses a mosaic of two 2 K × 4 K CCDs, and LRISb has a mosaic of two 2 K × 4 K CCDs, with a pixel scale of 0.135″/pixel for both sides. The standard imaging filters include the $UBVGRI$ passbands along with some narrow-band imaging filters. Thanks to the wide wavelength range and high sensitivity, the instrument can study different phenomena: from the blue light from star formation, to the red light of very distant objects. A remarkable science highlight achieved with LRIS is the observations of distant supernovae, which led to the discovery of the accelerating expansion of the Universe and awarded the Nobel Prize in Physics in 2011. The science goals of the instrument also include exploration of AGN, QSOs, distant clusters of galaxies, and comets.

4.3.10. LDT/LMI

Being one of the most sophisticated ground-based telescopes of its size, the 4.3 m Lowell Discovery Telescope (LDT), formerly called the Discovery Channel Telescope (DCT), allows for the simultaneous attachment of five instruments [257]. The telescope with the effective focal length of 26.04 m and $f/$ratio of 6.2 is hosted by the Lowell Observatory in Arizona, USA. The Large Monolithic Imager (LMI) covers a 12.3′ × 12.3′ FoV with the 6144 × 6150 pixel CCD having a base pixel scale of 0.120″/pixel (unbinned) and 0.24″/pixel (binned 2 × 2), and it saw first light on September 12, 2012 [258]. The instrument is equipped with 17 filters, which are Johnson–Cousins $UBVRI$, SDSS $u'g'r'i'z'$, VR, HalphaOn, HalphaOff, OIII, Y-ish (a UKIDSS/WFCAM Y, extended in the red) filters, and three Wolf–Rayet emission line filters (WC, WN, and CT) along with the set of 11 narrow-band comet filters. Apart from the GRB follow-ups, LDT/LMI carries out studies of stars [259–261] and comets [262].

4.3.11. NOT

Inaugurated in 1989, the Nordic Optical Telescope (NOT) is a 2.56 m optical/IR telescope located in La Palma, Spain. It has a 2.56 m $f/2.0$ primary mirror of the Ritchey–Chretien type with focal and aspect ratios of $f/2.0$ and 13.5, respectively, and a secondary 51 cn mirror. The effective aperture ratio of system is $f/11$ [263–265]. The Andalucía (Or Alhambra) Faint Object Spectrograph and Camera (ALFOSC) [266] is a CCD camera and spectrograph, which includes includes a polarimetry module that allows it to be used not only for low-/medium-resolution spectroscopy, but also for polarimetry and spectropolarimetry. ALFOSC has a 2048×2064 pixel CCD detector with a $6.4' \times 6.4'$ FoV in imaging mode and a plate scale of $0.2138''$/pixel. The optical filter set comprises $UBVRi$, IR, and other filters[16]. ALFOSC is used to study GRBs, SNe, TDEs, AGNs, and other transient phenomena, as well as planetary nebulae.

4.3.12. VLT/X-Shooter

Installed at the Cassegrain focus of UT2 of the ESO Very Large Telescope (VLT), Chile, in 2009, the X-shooter spectrograph operates in the 300–2500 nm spectral range at intermediate spectral resolution ($R \sim$ 4000–17,000, depending on slit width and wavelength) with an echelle spectral format maximizing its sensitivity via dichroic splitting in three arms with optimized optics, coatings, dispersive elements, and detectors and comprises a $1.8'' \times 4''$ integral field unit. See [267] for further details on the instrument. The main scientific goals of the instrument include studies of young stellar objects, brown dwarfs, T Tauri stars, the progenitors of SNe Type Ia, GRBs, QSO absorption lines, and lensed high-redshift galaxies. The research performed using the X-shooter benefits from its wide spectral band, allowing observations of objects in a wide range of redshifts.

4.3.13. VLT/FORS

FORS, the visual and near-UV FOcal Reducer and low dispersion Spectrograph for VLT, was developed as an all-dioptric instrument for the 330–1100 nm wavelength range [268]. Two instruments, FORS1 and FORS2, were installed on the Cassegrain foci of distinct telescopes. However, in April 2009, FORS1 was dismounted in favor of X-shooter, leaving only FORS2 in operation. The instrument has a $0''.25$/pixel image scale with the standard-resolution collimator or $0''.125$/pixel with the high-resolution one and corresponding FoV sizes of $6.8' \times 6.8'$ and $4.25' \times 4.25'$. FORS2 is installed on UT1 (Antu) and is by default equipped with a detector system that is optimized for the red with a very low level of fringes thanks to a mosaic of two 2 k $\times$ 4 k MIT CCDs (with 15 µm pixels). However, the blue-optimized detector system that was previously available on FORS1 has been commissioned on FORS2 and can be requested for Visitor Mode observation. Operating in different modes, FORS can perform long-slit and multi-object spectroscopy with exchangeable masks, imaging and spectroscopy with high-time resolution, and spectro-polarimetry.

The main results obtained by the instrument include a description of the morphological properties of the first interstellar asteroid, observations of first light from a GW source, studies of the chemical composition of exoplanets, galaxy formation, and observations of NSs, galaxy clusters, supermassive BHs, and planetary nebulae.

5. Observations in the Radio Band

Radio afterglows of GRBs can help unveil the physics of the forward and reverse shocks (e.g., [269]), test the Cocoon model [270], constrain the scale of magnetic fields in ejecta [271], and study the environments around the massive stars exploding as GRBs in the early Universe [272]. Unfortunately, the GRB model cannot explain all features of GRB radio afterglows, e.g., (1) a population of radio-quiet GRBs [273–275]; (2) ν_a would be increased by a factor of $\sim$30, and an additional emission is supposed to be detected on top of the expected synchrotron spectrum caused by a population of quasi-thermal electrons [276–279]; (3) no post-jet-break decline seen in the radio light curve even a factor of 10 or 20 later than the observed optical/X-ray break [280], and radio light curves of

GRBs are flatter than expected [281]. Possible explanations of (3) included the model of a two-component jet, where a wider, less-energetic Cocoon surrounds the core of the jet and would be responsible for the radio emission [282–284], and the model of semirelativistic reverse shock in a continuous inflow of ejecta [285].

The key radio telescopes detecting GRB afterglows are the Arcminute Microkelvin Imager—Large Array (AMI-LA [286]), Karl G. Jansky Very Large Array (VLA [287]), Australian Square Kilometre Array Pathfinder (ASKAP [288]), Low Frequency Array (LOFAR [289]), Karoo Array Telescope (MeerKAT [290]), Australia Telescope Compact Array (ATCA[17]), upgraded Giant Metrewave Radio Telescope (uGMRT), European VLBI Network (EVN[18]), enhanced-Multi-Element Remotely Linked Interferometer Network (e-MERLIN [291]), and Murchison Wide Field Array (MWA [292]).

ATCA

Commissioned on 2 September 1988, the Australia Telescope Compact Array (ATCA) located in New South Wales, Australia, is a part of the Australia Telescope National Facility (ATNF). ATCA is a radio interferometer comprising six 22 m Cassegrain antennas [293] arranged primarily along a 6 km east–west track; towards the middle of this, there is also a short north–south track or "spur". While one antenna is fixed, the rest are movable along a 3 km-long east–west track and a 214 m-long north–south "spur", allowing changes of the beam size or resolution available at each observing frequency. ATCA operates in the millimeter and centimeter wavebands (3 mm–30 cm), specifically those centered on 20-, 13-, 6-, 3-, 1.2-, 0.7-, and 0.3 cm (see [294] and the references therein). The ATCA science highlights include the detection of the first image of a forming radio SN remnant (SNR 1987A), studies of Jupiter's magnetic field, protoplanetary discs, water masers, QSOs, jets from microquasars, star formation regions, radio galaxies and galaxy clusters, mapping of hydrogen in the Magellanic Clouds, giving evidence of SN-GRB connection, and the observation of GRBs and neutron stars including pulsars (see, e.g., [294]).

6. Very High Energy Observations

In GRBs, γ-rays above $\sim$100 MeV are believed to be produced from the electron synchrotron in the afterglow shocks [295–298]. Moreover, joint observations of many GRBs by XRT and LAT are consistent with a single spectral component [299]. However, it is complicated to produce photons above a few GeV in the context of the synchrotron mechanism unless an unrealistically large bulk Lorentz factor is employed [300]. The fireball model also predicts the origin of GeV–TeV photons, and the emission can last from minutes to several hours [131,301]. The synchrotron self-Compton (SSC) process is the favored one and a widely used mechanism to interpret the very-high-energy ($>$100 GeV) photons in the afterglow era, where the relativistic electrons upscatter their own synchrotron radiation [295,301–303]. In this scenario, the SSC emission takes place from a constant density circumburst medium or from the Comptonization of X-ray photons in the afterglow shock [304,305]. This highlights the importance of VHE and joint observations of GRBs.

The VHE γ-ray observatories have been searching for the GRB emission for years, which led to many multiwavelength follow-up campaigns, e.g., for GRB 180720B, which was detected in its deep afterglow phase, up to 3 days after the observations by Fermi and Swift [306] or GRB 180720B[19]. The fact that the VHE emission is observed in the GRB afterglows at such late times is game changing for the modeling of the afterglow emission and scheduling GRB follow-up campaigns. MAGIC and HESS detected several LGRBs with >5σ significance. Among the SGRBs, the famous BNS-SGRB event GW 170817 (GRB 170817A) was also observed in VHE by MAGIC [307] and HESS [308].

Another example of an SGRB observed in a wide band of wavelengths is GRB 160821B [309]. This is one of the nearest SGRBs known ($z = 0.162$), and it has an optical–infrared kilonova component found in its afterglow emission, which is characteristic of heavy-element nucleosynthesis in a BNS merger. The emission of this burst was observed by several facilities covering the spectral range from radio to $\gtrsim$0.5 TeV (at 3σ significance). Figure 5 shows the

multiwavelength light curves of this burst along with the afterglow modeling (left panel) and the SEDs of the radiation at approximately 3 h (right panel).

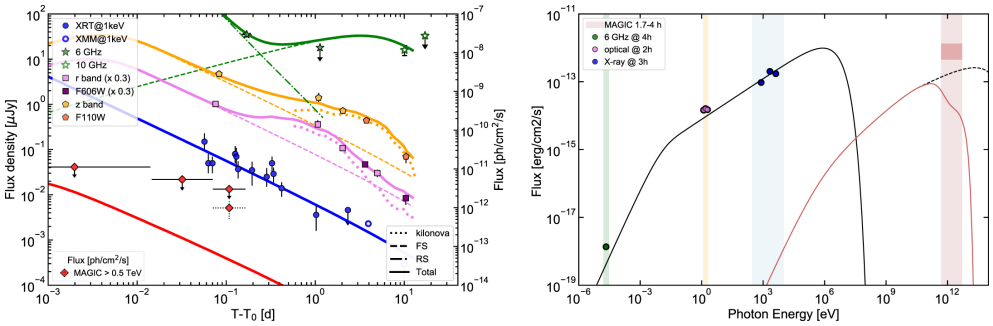

Figure 5. Multiwavelength light curve (left) and SED (right) of GRB 160821B compared with afterglow modeling (Figure 4 adopted from [309]). ©AAS. Reproduced with permission.

In the VHE range, the main contributors to the GRB observations are Imaging Atmospheric Cherenkov Telescopes (IACTs), such as the Major Atmospheric Gamma Imaging Cherenkov Telescope (MAGIC [310]), Very Energetic Radiation Imaging Telescope Array System (VERITAS [311]), and High Energy Stereoscopic System (HESS [312]), which, however, have duty cycles of ∼15% constrained by darkness conditions to perform observations, and Water Cherenkov Detectors (WCDs), such as the High Altitude Water Cherenkov Experiment (HAWC [313]), which is the most prolific in detecting GRBs, as well as the future Southern Wide-field Gamma-ray Observatory (SWGO [314]), having much larger duty cycles as they can observe during daytime, although with a higher low-energy threshold.

6.1. HAWC

The High Altitude Water Cherenkov Experiment or Observatory (HAWC [313]) is a facility designed to observe gamma- and cosmic-rays in the 100 GeV–100 TeV range. Located at an altitude of 4100 m in La Puebla, Mexico, HAWC is the successor to the Milagro γ-ray observatory in New Mexico, USA. HAWC uses the water Cherenkov method: an array of 300 WCDs detects the Cherenkov light produced in the water by the individual charged particles of air showers. Each WCD is a cylindrical (7.3 m diameter and 5 m height) stainless steel tank that contains a plastic bladder holding up to 200,000 L of water. The collection area of HAWC is of the order of the physical area of the detector, ∼104 m^2 above 500 GeV for a source at the Crab declination.

Being a survey instrument, HAWC continuously monitors the sky covering an instantaneous FoV of ∼2 sr and two-thirds of the sky from approximately $-20°$ to $+60°$ in declination daily. The achieved sensitivity is ∼2% of the Crab flux for sources with declination 0°–40°, assuming a spectral index of -2.5, and degrades to 8% of the Crab flux for sources at the edge of the HAWC observable sky ($\delta = -20°$ and $+60°$). HAWC has been taking data with its full configuration since its inauguration on 20 March 2015. The HAWC science highlights include obtain an all-TeV γ-ray sky map, studies of the cosmic-ray anisotropy and antiproton-to-proton ratio [315], and GRB detections [316].

6.2. HESS

Situated at an altitude of 1800 m in Namibia, the High Energy Stereoscopic System (HESS) comprises five telescopes: four IACTs with mirrors just under 12 m in diameter, arranged as a square with 120 m sides and operating since 2004, and one larger IACT with a 28 m mirror, commissioned in 2012 and located at the center of the array. Thanks to its low-energy threshold and fast slewing (200°/min), the latter IACT is well suited for the observation of soft-spectrum transient sources. HESS is sensitive to γ-rays in the energy range from tens of GeV to tens of TeV. Each 12 m telescope has a focal length of 15 m, a d/f ratio of 0.8, and a total mirror area of 108 m^2 [312]. The biggest mirror has a focal length of 36 m and a total mirror area of 614 m^2. The cameras of the small mirrors consist

of 960 pixels of a 0.16° angular size, providing a total field of view of 5°. The camera of the biggest mirror covers a 3.2° FoV with an image recording rate of 3600 images/s. The HESS science highlights include the first spatial resolution of a source of cosmic–γ-rays, studies of the sources of PeV protons, conducting the Galactic plane survey and extragalactic observations, and searching for the sources of cosmic accelerators.

6.3. Fermi/LAT

The Large Area Telescope (LAT), the primary instrument for the Fermi Gamma-ray Space Telescope (Fermi) mission, is an imaging, wide field of view, high-energy γ-ray telescope, covering the energy range from 30 MeV to more than 300 GeV [79]. Commissioning of LAT began on 24 June 2008. LAT is a pair-conversion telescope with a precision tracker and calorimeter, each comprising 16 modules (4×4 array), a segmented anticoincidence detector that covers the tracker array, and a programmable trigger. Every calorimeter module comprises 96 CsI(Tl) crystals, arranged in an eight-layer hodoscopic configuration with a total depth of 8.6 radiation lengths, providing information about the energy deposition pattern. Having an aspect ratio (height/width) of 0.4, the tracker has a large FoV (2.4 sr) and measures energy of most pair-conversion showers initiated in the tracker. The main characteristics of LAT are the timing accuracy of <10 μs, $<10'$ GRB location accuracy on board, GRB notification time to spacecraft of <5 s, point source location determination of $<0.5'$, and point source sensitivity (>100 MeV) of 3×10^{-9} ph cm^{-2} s^{-1}.

GBM and LAT have a significant impact on multimessenger astrophysics [317], e.g., LAT followed the GBM detection of GRB 170817A/GW 170817, the first neutron star–neutron star merger observed by its gravitational radiation with the LIGO and Virgo detectors [22] and on the studies of GRBs. Another LAT science highlights are the detection of the flaring of γ-ray emission from an active galaxy associated with the detection of a high-energy neutrino from the same direction by the IceCube neutrino detector, being the first association between photon and neutrino emission from an active galaxy [318].

6.4. MAGIC

Major Atmospheric Gamma Imaging Cherenkov Telescope (MAGIC), located in the Canary Islands (Spain), is an array of two IACTs detecting γ-ray emission in the range from a few tens of GeV to a few tens of TeV. The first IACT was commissioned in 2004 and worked in the stand-alone mode until the commissioning of the second IACT, built 85 m away from the first, in 2009. The IACTs have a 17 m diameter reflective surface and fine pixelated cameras covering a 3.5° FoV. Currently, the energy threshold of the telescope is ∼70 GeV for low-zenith-angle observations and an integral sensitivity above 300 GeV of 0.6% of the Crab Nebula flux in 50 h of observation [310]. The energy resolution is 15–17% at ∼1 TeV.

The MAGIC scientific highlights include the discovery of the highest-energy photons from GRB 190114C [319,320], tracing the origin of a rare cosmic neutrino, observations of a gravitational lens at very high energies and the Crab Pulsar at TeV, and the first detection of the distant galaxy PKS1441+25.

7. Summary and Future Prospect

The investigation of GRBs started a half century ago with their discovery in the soft gamma-rays [16]. More than twenty years later, in 1997, the discovery of the first GRB radio, optical, and X-ray afterglows [19,33,281] opened the era of the multiwavelength GRB studies. The discovery of the first gravitational wave event GW-170817A from NS–NS coalescence accompanied by the observation of short GRB-170817A, the optical/infrared kilonova AT2017gfo, and further X-ray, optical, infrared, and radio emission ([22] and the references therein) opened a new era for the multimessenger observations of GRBs. The multiwavelength and multimessenger observations of GRBs, including sGRBs and "kilonovae" features such as GW-170817, are vital to establish the progenitors' nature and emission mechanisms, probe the properties of high-redshift galaxies, and test fundamental

physics. The equipment for the observation of GRBs has advanced from simple scintillation gamma detectors to specialized multiwavelength observatories supported by dozens of ground-based instruments across the entire range of the electromagnetic spectrum, from radio to TeV (see Figure 6). In contrast, the ultra-violet (UV; 100–300 nm) variable sky is relatively poorly explored as the detection of the afterglow in the near-UV (NUV) is limited to the closest GRBs, since above $z \sim 1.2$, host galaxy Lyman limit absorption will suppress the signal. In [321], the fraction of GRB afterglows detectable in the UV at a fiducial sensitivity is estimated to be four events per 1000 (or per year).

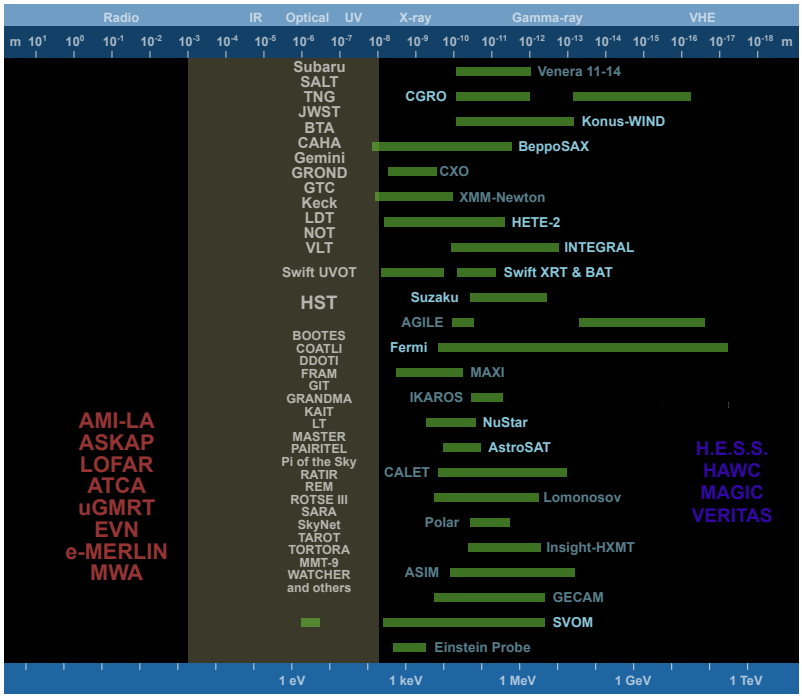

instruments can routinely measure precise redshifts onboard (except Swift-UVOT, which measured a few redshifts). From this perspective, THESEUS [325,326] could provide a significant advancement of multi-messenger and time domain astrophysics, enabling the identification, accurate localization, and study of GRBs and electromagnetic counterparts to sources of gravitational waves and neutrinos, which are expected to be routinely detected in a decade. THESEUS could also show a great synergy with future large observing facilities in both the electromagnetic (such as, e.g., Advanced Telescope for High ENergy Astrophysics (ATHENA [327]), an X-ray observatory planned for launch in 2034, LSST (see Section 4.2.3), the Extremely Large Telescope (ELT [328]), the Thirty Meter Telescope (TMT [328]) in optical, the Square Kilometre Array Telescope (SKA [329]) in radio, the Cherenkov Telescope Array (CTA [330,331]) in VHE, which have GRB-related science in their core-science programs), and multi-messenger (e.g., advanced LIGO/VIRGO KAGRA [332] and, in perspective, 3G detectors: the Einstein Telescope (ET [333]), the Cosmic Explorer (CE [334]) and, possibly, the Laser Interferometer Space Antenna (LISA [335]) for GW and Km3NET [336] and IceCube-Gen2 [337] for neutrinos). The All-sky Medium Energy Gamma-ray Observatory (AMEGO [338]), the Energetic X-ray Imaging Survey Telescope (EXIST [339]), the High-z Gamma-ray bursts for Unraveling the Dark Ages Mission (HiZ-GUNDAM [340]), the Transient Astrophysics Probe (TAP [341]), and Gamow Explorer [342] are also expected to advance the research on the physics of prompt emission and internal engines and progenitors of GRBs and provide tests on cosmology and fundamental physics.

Despite several decades of observations, the physical properties of highly relativistic jets that produce the GRB prompt emission (i.e., their structure and magnetic topology) remain unknown. The polarization degree and angle of γ-emission can shed light on the nature of the highly relativistic jets and prompt emission mechanisms. In particular, the linear polarization properties of the γ-rays are highly dependent on the prompt emission processes and the magnetic fields along with their structure within the emitting jets (see, e.g., [343,344] for a overview). New advanced missions with spectropolarimetry capability, such as the enhanced X-ray Timing and Polarimetry mission (eXTP [345]) or POLAR-2 [346], could constrain theoretical emission models.

In this paper, we briefly described the key facilities for GRB studies, briefly reviewed the game-changing decommissioned missions, and concisely presented a handful of new experiments supposed to contribute significantly to GRB science. We hope this review may serve as a guide for the newcomers to GRB science.

Author Contributions: Conceptualization, A.T., D.S. and D.F.; writing—original draft preparation, A.T., D.S., D.F. and S.K.; writing—review and editing, A.T., D.F., D.S. and S.K.; funding acquisition, D.F. and S.K. All authors have read and agreed to the published version of the manuscript.

Funding: A.T. acknowledges support from the PRIN 2017 Agreement No. 20179ZF5KS. D.F. acknowledges support from RSF Grant 21-12-00250. S.K. acknowledges support from the European Structural and Investment Fund and the Czech Ministry of Education, Youth and Sports (Project CoGraDS – CZ.02.1.01/0.0/0.0/15_003/0000437). This work was partially supported within the framework of the government contract of the Special Astrophysical Observatory of the Russian Academy of Sciences in its part entitled "Conducting Fundamental Research". The work was also partially performed according to the Russian Government Program of Competitive Growth of Kazan Federal University.

Institutional Review Board Statement: Not applicable.

Informed Consent Statement: Not applicable.

Data Availability Statement: Not applicable.

Acknowledgments: We thank Mikhail Ulanov for help in preparing the figures. We also thank the anonymous referees for their comments and suggestions, which significantly improved the manuscript.

Conflicts of Interest: The authors declare no conflict of interest. The funders had no role in the design of the study; in the collection, analyses, or interpretation of the data; in the writing of the manuscript; nor in the decision to publish the results.

Abbreviations

The following abbreviations are used in this manuscript:

AGN	Active galactic nuclei
BH	Black hole
CCD	Charge coupled devices
FoV	Field of view
FRB	Fast Radio Burst
GRB	Gamma-ray burst
GW	Gravitational wave
HEN	High-energy neutrino
HEO	High-Earth orbit
IACT	Imaging Atmospheric Cherenkov Telescope
IGM	Intergalactic medium
LGRB	Long gamma-ray burst
LEO	Low-Earth orbit
NEO	Near-Earth object
NIR	Near-infrared
NS	Neutron star
OT	Optical transient
PMT	Photomultiplier tube
PSF	Point spread function
QSO	Quasar (quasi-stellar object)
SED	Spectral energy distribution
SGR	Soft gamma-repeater
SGRB	Short gamma-ray burst
SF	Solar flare
SNe	Supernovae
SNR	Signal-to-noise ratio
TDE	Tidal disruption event
TGF	Terrestrial gamma-ray flash
ToO	Target of opportunity
VHE	Very high energy
WCD	Water Cherenkov Detector
YSO	Young stellar object

Notes

1 http://www.ioffe.ru/LEA/ (accessed on 23 May 2022).
2 BAT is able to perform imaging, which allows obtaining the GRB position, in the 14–150 keV energy range and record the data with no information on the GRB localization up to 350 keV.
3 https://swift.gsfc.nasa.gov/archive/grb_table/ (accessed on 23 May 2022).
4 https://swift.gsfc.nasa.gov/results/ (accessed on 23 May 2022).
5 https://heasarc.gsfc.nasa.gov/W3Browse/fermi/fermigbrst.html (accessed on 23 May 2022).
6 http://astrosat.iucaa.in/czti/?q=grb (accessed on 23 May 2022).
7 https://gcn.gsfc.nasa.gov/gcn3_archive.html (accessed on 23 May 2022).
8 https://gcn.gsfc.nasa.gov (accessed on 23 May 2022).
9 https://www.swift.ac.uk/about/swifteranongrb.php (accessed on 23 May 2022).
10 http://maxi.riken.jp/grbs/ (accessed on 23 May 2022).
11 https://www.jpl.nasa.gov/missions/nuclear-spectroscopic-telescope-array-nustar (accessed on 23 May 2022).
12 https://sites.google.com/view/growthindia (accessed on 23 May 2022).
13 https://www.oir.caltech.edu/twiki_oir/pub/Palomar/ZTF/140724NSFSite/Bellm_ZTF_overview_NSF_site_visit.pdf (accessed on 23 May 2022).
14 https://www.tng.iac.es/instruments/lrs/ (accessed on 23 May 2022).
15 https://www.caha.es/CAHA/Instruments/filterlist.html (accessed on 23 May 2022).
16 http://www.not.iac.es/instruments/filters/ (accessed on 23 May 2022).

[17] https://www.narrabri.atnf.csiro.au (accessed on 23 May 2022).
[18] https://www.evlbi.org (accessed on 23 May 2022).
[19] http://tevcat.uchicago.edu/?mode=1;id=329 (accessed on 23 May 2022).

References

1. Frederiks, D.D.; Hurley, K.; Svinkin, D.S.; Pal'shin, V.D.; Mangano, V.; Oates, S.; Aptekar, R.L.; Golenetskii, S.V.; Mazets, E.P.; Oleynik, P.P.; et al. The Ultraluminous GRB 110918A. *Astrophys. J.* **2013**, *779*, 151. [CrossRef]
2. Cucchiara, A.; Levan, A.J.; Fox, D.B.; Tanvir, N.R.; Ukwatta, T.N.; Berger, E.; Krühler, T.; Küpcü Yoldaş, A.; Wu, X.F.; Toma, K.; et al. A Photometric Redshift of z ˜ 9.4 for GRB 090429B. *Astrophys. J.* **2011**, *736*, 7. [CrossRef]
3. Zhang, B.; Zhang, B.B.; Virgili, F.J.; Liang, E.W.; Kann, D.A.; Wu, X.F.; Proga, D.; Lv, H.J.; Toma, K.; Mészáros, P.; et al. Discerning the Physical Origins of Cosmological Gamma-ray Bursts Based on Multiple Observational Criteria: The Cases of z = 6.7 GRB 080913, z = 8.2 GRB 090423, and Some Short/Hard GRBs. *Astrophys. J.* **2009**, *703*, 1696–1724. [CrossRef]
4. Blinnikov, S.I.; Novikov, I.D.; Perevodchikova, T.V.; Polnarev, A.G. Exploding Neutron Stars in Close Binaries. *Sov. Astron. Lett.* **1984**, *10*, 177–179.
5. Paczynski, B. Gamma-ray bursters at cosmological distances. *Astrophys. J. Lett.* **1986**, *308*, L43–L46. [CrossRef]
6. Eichler, D.; Livio, M.; Piran, T.; Schramm, D.N. Nucleosynthesis, neutrino bursts and gamma-rays from coalescing neutron stars. *Nature* **1989**, *340*, 126–128. [CrossRef]
7. Paczynski, B. Cosmological gamma-ray bursts. *Acta Astron.* **1991**, *41*, 257–267.
8. Narayan, R.; Paczynski, B.; Piran, T. Gamma-ray bursts as the death throes of massive binary stars. *Astrophys. J. Lett.* **1992**, *395*, L83–L86. [CrossRef]
9. Mazets, E.P.; Golenetskii, S.V.; Ilinskii, V.N.; Panov, V.N.; Aptekar, R.L.; Gurian, I.A.; Proskura, M.P.; Sokolov, I.A.; Sokolova, Z.I.; Kharitonova, T.V. Catalog of cosmic gamma-ray bursts from the KONUS experiment data. I. *Astrophys. Space Sci.* **1981**, *80*, 3–83. [CrossRef]
10. Kouveliotou, C.; Meegan, C.A.; Fishman, G.J.; Bhat, N.P.; Briggs, M.S.; Koshut, T.M.; Paciesas, W.S.; Pendleton, G.N. Identification of Two Classes of Gamma-Ray Bursts. *Astrophys. J. Lett.* **1993**, *413*, L101. [CrossRef]
11. Woosley, S.E. Gamma-ray bursts from stellar mass accretion disks around black holes. *Astrophys. J.* **1993**, *405*, 273–277. [CrossRef]
12. Paczyński, B. Are Gamma-Ray Bursts in Star-Forming Regions? *Astrophys. J. Lett.* **1998**, *494*, L45–L48. [CrossRef]
13. MacFadyen, A.I.; Woosley, S.E. Collapsars: Gamma-Ray Bursts and Explosions in "Failed Supernovae". *Astrophys. J.* **1999**, *524*, 262–289. [CrossRef]
14. Woosley, S.E.; Bloom, J.S. The Supernova Gamma-Ray Burst Connection. *Annu. Rev. Astron Astrophys.* **2006**, *44*, 507–556. [CrossRef]
15. Petitjean, P.; Wang, F.Y.; Wu, X.F.; Wei, J.J. GRBs and Fundamental Physics. *Space Sci. Rev.* **2016**, *202*, 195–234. [CrossRef]
16. Klebesadel, R.W.; Strong, I.B.; Olson, R.A. Observations of Gamma-Ray Bursts of Cosmic Origin. *Astrophys. J. Lett.* **1973**, *182*, L85. [CrossRef]
17. Golenetskii, S.V.; Mazets, E.P.; Aptekar, R.L.; Ilinskii, V.N. Correlation between luminosity and temperature in γ-ray burst sources. *Nature* **1983**, *306*, 451–453. [CrossRef]
18. Meegan, C.A.; Fishman, G.J.; Wilson, R.B.; Paciesas, W.S.; Pendleton, G.N.; Horack, J.M.; Brock, M.N.; Kouveliotou, C. Spatial distribution of γ-ray bursts observed by BATSE. *Nature* **1992**, *355*, 143–145. [CrossRef]
19. Costa, E.; Frontera, F.; Heise, J.; Feroci, M.; in't Zand, J.; Fiore, F.; Cinti, M.N.; Dal Fiume, D.; Nicastro, L.; Orlandini, M.; et al. Discovery of an X-ray afterglow associated with the γ-ray burst of 28 February 1997. *Nature* **1997**, *387*, 783–785. [CrossRef]
20. Lamb, D.Q.; Reichart, D.E. Gamma-Ray Bursts as a Probe of the Very High Redshift Universe. *Astrophys. J.* **2000**, *536*, 1–18. [CrossRef]
21. Vanderspek, R.; Crew, G.; Doty, J.; Villasenor, J.; Monnelly, G.; Butler, N.; Cline, T.; Jernigan, J.G.; Levine, A.; Martel, F.; et al. GRB030329 (=H2652): A long, extremely bright GRB localized by the HETE WXM and SXC. *GRB Coord. Netw.* **2003**, *1997*, 1.
22. Abbott, B.P.; Abbott, R.; Abbott, T.D.; Aceari, R.X.; Adyrnese, F.; Ackley, K.; Adams, C.; Adams, T.; Addesso, P.; Adhika, V.B.; et al. Multi-messenger Observations of a Binary Neutron Star Merger. *Astrophys. J. Lett.* **2017**, *848*, L12. [CrossRef]
23. Sacahui, J.R.; Penacchioni, A.V.; Braga, J.; Castro, M.A.; D'Amico, F. MIRAX sensitivity for Gamma Ray Bursts. *J. High Energy Astrophys.* **2016**, *9*, 16–24. [CrossRef]
24. Yamaoka, K.; Ohno, M.; Tashiro, M.S.; Hurley, K.; Krimm, H.A.; Lien, A.Y.; Ohmori, N.; Sugita, S.; Urata, Y.; Yasuda, T.; et al. Suzaku Wide-band All-sky Monitor (WAM) observations of GRBs and SGRs. *Publ. Astron. Soc. Jpn.* **2017**, *69*, R2. [CrossRef]
25. Lipunov, V.M.; Gorosabel, J.; Pruzhinskaya, M.V.; Postigo, A.d.U.; Pelassa, V.; Tsvetkova, A.E.; Sokolov, I.V.; Kann, D.A.; Xu, D.; Gorbovskoy, E.S.; et al. The optical identification of events with poorly defined locations: The case of the Fermi GBM GRB 140801A. *Mon. Not. R. Astron. Soc.* **2016**, *455*, 712–724. [CrossRef]
26. Mazets, E.P.; Golenetskii, S.V.; Il'Inskii, V.N. Flare of cosmic gamma radiation as observed with "Cosmos-461" satellite. *Sov. J. Exp. Theor. Phys. Lett.* **1974**, *19*, 77.
27. Horack, J.M. *Development of the Burst And Transient Source Experiment (BATSE)*; NASA: Washington, DC, USA, 1991.
28. Goldstein, A.; Preece, R.D.; Mallozzi, R.S.; Briggs, M.S.; Fishman, G.J.; Kouveliotou, C.; Paciesas, W.S.; Burgess, J.M. The BATSE 5B Gamma-Ray Burst Spectral Catalog. *Astrophys. J. Suppl.* **2013**, *208*, 21. [CrossRef]

29. Band, D.; Matteson, J.; Ford, L.; Schaefer, B.; Palmer, D.; Teegarden, B.; Cline, T.; Briggs, M.; Paciesas, W.; Pendleton, G.; et al. BATSE Observations of Gamma-Ray Burst Spectra. I. Spectral Diversity. *Astrophys. J.* **1993**, *413*, 281. [CrossRef]
30. Ford, L.A.; Band, D.L.; Matteson, J.L.; Briggs, M.S.; Pendleton, G.N.; Preece, R.D.; Paciesas, W.S.; Teegarden, B.J.; Palmer, D.M.; Schaefer, B.E.; et al. BATSE Observations of Gamma-Ray Burst Spectra. II. Peak Energy Evolution in Bright, Long Bursts. *Astrophys. J.* **1995**, *439*, 307. [CrossRef]
31. Boella, G.; Butler, R.C.; Perola, G.C.; Piro, L.; Scarsi, L.; Bleeker, J.A.M. BeppoSAX, the wide band mission for X-ray astronomy. *Astron. Astrophys. Suppl.* **1997**, *122*, 299–307. [CrossRef]
32. Jager, R.; Mels, W.A.; Brinkman, A.C.; Galama, M.Y.; Goulooze, H.; Heise, J.; Lowes, P.; Muller, J.M.; Naber, A.; Rook, A.; et al. The Wide Field Cameras onboard the BeppoSAX X-ray Astronomy Satellite. *Astron. Astrophys. Suppl.* **1997**, *125*, 557–572. [CrossRef]
33. van Paradijs, J.; Groot, P.J.; Galama, T.; Kouveliotou, C.; Strom, R.G.; Telting, J.; Rutten, R.G.M.; Fishman, G.J.; Meegan, C.A.; Pettini, M.; et al. Transient optical emission from the error box of the γ-ray burst of 28 February 1997. *Nature* **1997**, *386*, 686–689. [CrossRef]
34. Metzger, M.R.; Djorgovski, S.G.; Kulkarni, S.R.; Steidel, C.C.; Adelberger, K.L.; Frail, D.A.; Costa, E.; Frontera, F. Spectral constraints on the redshift of the optical counterpart to the γ-ray burst of 8 May 1997. *Nature* **1997**, *387*, 878–880. [CrossRef]
35. Reichart, D.E. The Redshift of GRB 970508. *Astrophys. J. Lett.* **1998**, *495*, L99–L101. [CrossRef]
36. Frontera, F. The key role of BeppoSAX in the GRB history. *Rend. Lincei. Sci. Fis. Nat.* **2019**, *30*, 171–184. [CrossRef]
37. Galama, T.J.; Vreeswijk, P.M.; van Paradijs, J.; Kouveliotou, C.; Augusteijn, T.; Böhnhardt, H.; Brewer, J.P.; Doublier, V.; Gonzalez, J.F.; Leibundgut, B.; et al. An unusual supernova in the error box of the γ-ray burst of 25 April 1998. *Nature* **1998**, *395*, 670–672. [CrossRef]
38. Amati, L.; Frontera, F.; Tavani, M.; in't Zand, J.J.M.; Antonelli, A.; Costa, E.; Feroci, M.; Guidorzi, C.; Heise, J.; Masetti, N.; et al. Intrinsic spectra and energetics of BeppoSAX Gamma-Ray Bursts with known redshifts. *Astron. Astrophys.* **2002**, *390*, 81–89. [CrossRef]
39. Ricker, G.R.; Atteia, J.L.; Crew, G.B.; Doty, J.P.; Fenimore, E.E.; Galassi, M.; Graziani, C.; Hurley, K.; Jernigan, J.G.; Kawai, N.; et al. The High Energy Transient Explorer (HETE): Mission and Science Overview. In *Gamma-Ray Burst and Afterglow Astronomy 2001: A Workshop Celebrating the First Year of the HETE Mission*; Ricker, G.R., Vanderspek, R.K., Eds.; American Institute of Physics Conference Series; American Institute of Physics: College Park, MD, USA, 2003; Volume 662, pp. 3–16. [CrossRef]
40. Lamb, D.Q.; Ricker, G.R.; Atteia, J.L.; Barraud, C.; Boer, M.; Braga, J.; Butler, N.; Cline, T.; Crew, G.B.; Dezalay, J.P.; et al. Scientific highlights of the HETE-2 mission. *New Astron. Rev.* **2004**, *48*, 423–430. [CrossRef]
41. Yamaoka, K.; Endo, A.; Enoto, T.; Fukazawa, Y.; Hara, R.; Hanabata, Y.; Hong, S.; Kamae, T.; Kira, C.; Kodaka, N.; et al. Design and In-Orbit Performance of the Suzaku Wide-Band All-Sky Monitor. *Publ. Astron. Soc. Jpn.* **2009**, *61*, S35–S53. [CrossRef]
42. Mitsuda, K.; Bautz, M.; Inoue, H.; Kelley, R.L.; Koyama, K.; Kunieda, H.; Makishima, K.; Ogawara, Y.; Petre, R.; Takahashi, T.; et al. The X-Ray Observatory Suzaku. *Publ. Astron. Soc. Jpn.* **2007**, *59*, S1–S7. [CrossRef]
43. Yonetoku, D.; Murakami, T.; Gunji, S.; Mihara, T.; Sakashita, T.; Morihara, Y.; Kikuchi, Y.; Takahashi, T.; Fujimoto, H.; Toukairin, N.; et al. Gamma-Ray Burst Polarimeter (GAP) aboard the Small Solar Power Sail Demonstrator IKAROS. *Publ. Astron. Soc. Jpn.* **2011**, *63*, 625. [CrossRef]
44. Yonetoku, D.; Murakami, T.; Gunji, S.; Mihara, T.; Toma, K.; Sakashita, T.; Morihara, Y.; Takahashi, T.; Toukairin, N.; Fujimoto, H.; et al. Detection of Gamma-Ray Polarization in Prompt Emission of GRB 100826A. *Astrophys. J. Lett.* **2011**, *743*, L30. [CrossRef]
45. Amelushkin, A.; Bogomolov, V.; Benghin, V.; Garipov, G.; Gorbovskoy, E.; Grossan, B.; Klimov, P.; Khrenov, B.; Lee, J.; Lipunov, V.; et al. Space experiments on-board of lomonosov mission to study gamma-ray bursts and UHECRS. *Eur. Astron. Soc. Publ. Ser.* **2013**, *61*, 545–552. [CrossRef]
46. Park, I.H.; Grossan, B.; Lim, H.; Nam, J.W.; Chen, P.; Khrenov, B.A.; Kim, Y.K.; Lee, C.H.; Lee, J.; Linder, E.V.; et al. The UFFO (Ultra-Fast Flash Observatory) Pathfinder. *arXiv* **2009**, arXiv:0912.0773.
47. Park, I.H.; Brandt, S.; Budtz-Jørgensen, C.; Castro-Tirado, A.J.; Chen, P.; Connell, P.; Eyles, C.; Grossan, B.; Huang, M.H.A.; Jeong, S.; et al. Ultra-Fast Flash Observatory for the observation of early photons from gamma-ray bursts. *New J. Phys.* **2013**, *15*, 023031. [CrossRef]
48. Amelyushkin, A.M.; Galkin, V.I.; Goncharov, B.V.; Gorbovskoy, E.S.; Kornilov, V.G.; Lipunov, V.M.; Panasyuk, M.I.; Petrov, V.L.; Smoot, G.F.; Svertilov, S.I.; et al. The BDRG and SHOK instruments for studying gamma-ray burst prompt emission onboard the Lomonosov spacecraft. *Cosm. Res.* **2013**, *51*, 434–438. [CrossRef]
49. Sadovnichy, V.A.; Panasyuk, M.I.; Svertilov, S.I.; Lipunov, V.M.; Bogomolov, V.V.; Bogomolov, A.V.; Gorbovskoy, E.S.; Iyudin, A.F.; Kalegaev, V.V.; Kornilov, V.G.; et al. Lomonosov GRB Catalogue: The First Experience of Prompt Emission Multi-Wavelength Observations. *Universe* **2021**, *7*, 375. [CrossRef]
50. Produit, N.; Barao, F.; Deluit, S.; Hajdas, W.; Leluc, C.; Pohl, M.; Rapin, D.; Vialle, J.P.; Walter, R.; Wigger, C. POLAR, a compact detector for gamma-ray bursts photon polarization measurements. *Nucl. Instrum. Methods Phys. Res. A* **2005**, *550*, 616–625. [CrossRef]
51. Zhang, S.N.; Kole, M.; Bao, T.W.; Batsch, T.; Bernasconi, T.; Cadoux, F.; Chai, J.Y.; Dai, Z.G.; Dong, Y.W.; Gauvin, N.; et al. Detailed polarization measurements of the prompt emission of five gamma-ray bursts. *Nat. Astron.* **2019**, *3*, 258–264. [CrossRef]
52. Aptekar, R.L.; Frederiks, D.D.; Golenetskii, S.V.; Ilynskii, V.N.; Mazets, E.P.; Panov, V.N.; Sokolova, Z.J.; Terekhov, M.M.; Sheshin, L.O.; Cline, T.L.; et al. Konus-W Gamma-Ray Burst Experiment for the GGS Wind Spacecraft. *Space Sci. Rev.* **1995**, *71*, 265–272. [CrossRef]

53. Svinkin, D.S.; Frederiks, D.D.; Aptekar, R.L.; Golenetskii, S.V.; Pal'shin, V.D.; Oleynik, P.P.; Tsvetkova, A.E.; Ulanov, M.V.; Cline, T.L.; Hurley, K. The Second Konus-Wind Catalog of Short Gamma-Ray Bursts. *Astrophys. J. Suppl.* **2016**, *224*, 10. [CrossRef]
54. Tsvetkova, A.; Frederiks, D.; Golenetskii, S.; Lysenko, A.; Oleynik, P.; Pal'shin, V.; Svinkin, D.; Ulanov, M.; Cline, T.; Hurley, K.; et al. The Konus-Wind Catalog of Gamma-Ray Bursts with Known Redshifts. I. Bursts Detected in the Triggered Mode. *Astrophys. J.* **2017**, *850*, 161. [CrossRef]
55. Tsvetkova, A.; Frederiks, D.; Svinkin, D.; Aptekar, R.; Cline, T.L.; Golenetskii, S.; Hurley, K.; Lysenko, A.; Ridnaia, A.; Ulanov, M. The Konus-Wind Catalog of Gamma-Ray Bursts with Known Redshifts. II. Waiting-Mode Bursts Simultaneously Detected by Swift/BAT. *Astrophys. J.* **2021**, *908*, 83. [CrossRef]
56. Kozlova, A.V.; Svinkin, D.S.; Lysenko, A.L.; Ulanov, M.V.; Tsvetkova, A.E.; Frederiks, D.D. A search for transient events in Konus-Wind data. *J. Phys. Conf. Ser.* **2019**, *1400*, 022014. [CrossRef]
57. Aptekar, R.L.; Butterworth, P.S.; Cline, T.L.; Frederiks, D.D.; Golenetskii, S.V.; Il'inskii, V.N.; Mazets, E.P.; Stilwell, D.E.; Terekhov, M.M. Hard X-Ray Bursts from GRO J1744-28. I. Observations by the Konus-Wind and Konus-A Experiments. *Astrophys. J.* **1998**, *493*, 404–407. [CrossRef]
58. Ubertini, P.; Lebrun, F.; Di Cocco, G.; Bazzano, A.; Bird, A.J.; Broenstad, K.; Goldwurm, A.; La Rosa, G.; Labanti, C.; Laurent, P.; et al. IBIS: The Imager on-board INTEGRAL. *Astron. Astrophys.* **2003**, *411*, L131–L139. [CrossRef]
59. Vedrenne, G.; Roques, J.P.; Schönfelder, V.; Mandrou, P.; Lichti, G.G.; von Kienlin, A.; Cordier, B.; Schanne, S.; Knödlseder, J.; Skinner, G.; et al. SPI: The spectrometer aboard INTEGRAL. *Astron. Astrophys.* **2003**, *411*, L63–L70. [CrossRef]
60. von Kienlin, A.; Beckmann, V.; Rau, A.; Arend, N.; Bennett, K.; McBreen, B.; Connell, P.; Deluit, S.; Hanlon, L.; Hurley, K.; et al. INTEGRAL Spectrometer SPI's GRB detection capabilities. GRBs detected inside SPI's FoV and with the anticoincidence system ACS. *Astron. Astrophys.* **2003**, *411*, L299–L305. [CrossRef]
61. Forot, M.; Laurent, P.; Grenier, I.A.; Gouiffès, C.; Lebrun, F. Polarization of the Crab Pulsar and Nebula as Observed by the INTEGRAL/IBIS Telescope. *Astrophys. J. Lett.* **2008**, *688*, L29. [CrossRef]
62. Marcinkowski, R.; Denis, M.; Bulik, T.; Goldoni, P.; Laurent, P.; Rau, A. GRB 030406 —An extremely hard burst outside of the INTEGRAL field of view. *Astron. Astrophys.* **2006**, *452*, 113–117. [CrossRef]
63. Götz, D.; Gouiffès, C.; Rodriguez, J.; Laurent, P.; Jourdain, E.; Roques, J.P.; Mereghetti, S.; Lutovinov, A.; Savchenko, V.; Hanlon, L.; et al. INTEGRAL results on gamma-ray bursts and polarization of hard X-ray sources. *New Astron. Rev.* **2019**, *87*, 101537. [CrossRef]
64. Kuulkers, E.; Ferrigno, C.; Kretschmar, P.; Alfonso-Garzón, J.; Baab, M.; Bazzano, A.; Bélanger, G.; Benson, I.; Bird, A.J.; Bozzo, E.; et al. INTEGRAL reloaded: Spacecraft, instruments and ground system. *New Astron. Rev.* **2021**, *93*, 101629. [CrossRef]
65. Gehrels, N.; Chincarini, G.; Giommi, P.; Mason, K.O.; Nousek, J.A.; Wells, A.A.; White, N.E.; Barthelmy, S.D.; Burrows, D.N.; Cominsky, L.R.; et al. The Swift Gamma-Ray Burst Mission. *Astrophys. J.* **2004**, *611*, 1005–1020. [CrossRef]
66. Barthelmy, S.D.; Barbier, L.M.; Cummings, J.R.; Fenimore, E.E.; Gehrels, N.; Hullinger, D.; Krimm, H.A.; Markwardt, C.B.; Palmer, D.M.; Parsons, A.; et al. The Burst Alert Telescope (BAT) on the SWIFT Midex Mission. *Space Sci. Rev.* **2005**, *120*, 143–164. [CrossRef]
67. Hill, J.E.; Zugger, M.E.; Shoemaker, J.; Witherite, M.E.; Koch, T.S.; Chou, L.L.; Case, T.; Burrows, D.N. Laboratory x-ray CCD camera electronics: A test bed for the Swift X-Ray Telescope. In *X-ray and Gamma-Ray Instrumentation for Astronomy XI*; Flanagan, K.A., Siegmund, O.H., Eds.; Society of Photo-Optical Instrumentation Engineers (SPIE) Conference Series; SPIE Press: Bellingham, DC, USA, 2000; Volume 4140, pp. 87–98. [CrossRef]
68. Burrows, D.N.; Hill, J.E.; Nousek, J.A.; Kennea, J.A.; Wells, A.; Osborne, J.P.; Abbey, A.F.; Beardmore, A.; Mukerjee, K.; Short, A.D.T.; et al. The Swift X-Ray Telescope. *Space Sci. Rev.* **2005**, *120*, 165–195. [CrossRef]
69. Roming, P.W.A.; Kennedy, T.E.; Mason, K.O.; Nousek, J.A.; Ahr, L.; Bingham, R.E.; Broos, P.S.; Carter, M.J.; Hancock, B.K.; Huckle, H.E.; et al. The Swift Ultra-Violet/Optical Telescope. *Space Sci. Rev.* **2005**, *120*, 95–142. [CrossRef]
70. Sakamoto, T.; Barthelmy, S.D.; Barbier, L.; Cummings, J.R.; Fenimore, E.E.; Gehrels, N.; Hullinger, D.; Krimm, H.A.; Markwardt, C.B.; Palmer, D.M.; et al. The First Swift BAT Gamma-Ray Burst Catalog. *Astrophys. J. Suppl.* **2008**, *175*, 179–190. [CrossRef]
71. Sakamoto, T.; Barthelmy, S.D.; Baumgartner, W.H.; Cummings, J.R.; Fenimore, E.E.; Gehrels, N.; Krimm, H.A.; Markwardt, C.B.; Palmer, D.M.; Parsons, A.M.; et al. The Second Swift Burst Alert 76 Telescope Gamma-Ray Burst Catalog. *Astrophys. J. Suppl.* **2011**, *195*, 2. [CrossRef]
72. Lien, A.; Sakamoto, T.; Barthelmy, S.D.; Baumgartner, W.H.; Cannizzo, J.K.; Chen, K.; Collins, N.R.; Cummings, J.R.; Gehrels, N.; Krimm, H.A.; et al. The Third Swift Burst Alert Telescope Gamma-Ray Burst Catalog. *Astrophys. J.* **2016**, *829*, 7. [CrossRef]
73. Tavani, M.; Barbiellini, G.; Argan, A.; Boffelli, F.; Bulgarelli, A.; Caraveo, P.; Cattaneo, P.W.; Chen, A.W.; Cocco, V.; Costa, E.; et al. The AGILE Mission. *Astron. Astrophys.* **2009**, *502*, 995–1013. [CrossRef]
74. Ursi, A.; Romani, M.; Verrecchia, F.; Pittori, C.; Tavani, M.; Marisaldi, M.; Galli, M.; Labanti, C.; Parmiggiani, N.; Bulgarelli, A.; et al. The Second AGILE MCAL Gamma-Ray Burst Catalog: 13 yr of Observations. *Astrophys. J.* **2022**, *925*, 152. [CrossRef]
75. Labanti, C.; Marisaldi, M.; Fuschino, F.; Galli, M.; Argan, A.; Bulgarelli, A.; Di Cocco, G.; Gianotti, F.; Tavani, M.; Trifoglio, M. Design and construction of the Mini-Calorimeter of the AGILE satellite. *Nucl. Instrum. Methods Phys. Res. A* **2009**, *598*, 470–479. [CrossRef]
76. Marisaldi, M.; Fuschino, F.; Labanti, C.; Galli, M.; Longo, F.; Del Monte, E.; Barbiellini, G.; Tavani, M.; Giuliani, A.; Moretti, E.; et al. Detection of terrestrial gamma ray flashes up to 40 MeV by the AGILE satellite. *J. Geophys. Res. Space Phys.* **2010**, *115*, A00E13. [CrossRef]

77. Marisaldi, M.; Fuschino, F.; Tavani, M.; Dietrich, S.; Price, C.; Galli, M.; Pittori, C.; Verrecchia, F.; Mereghetti, S.; Cattaneo, P.W.; et al. Properties of terrestrial gamma ray flashes detected by AGILE MCAL below 30 MeV. *J. Geophys. Res. Space Phys.* **2014**, *119*, 1337–1355. [CrossRef]
78. Meegan, C.; Lichti, G.; Bhat, P.N.; Bissaldi, E.; Briggs, M.S.; Connaughton, V.; Diehl, R.; Fishman, G.; Greiner, J.; Hoover, A.S.; et al. The Fermi Gamma-ray Burst Monitor. *Astrophys. J.* **2009**, *702*, 791–804. [CrossRef]
79. Atwood, W.B.; Abdo, A.A.; Ackermann, M.; Althouse, W.; Anderson, B.; Axelsson, M.; Baldini, L.; Ballet, J.; Band, D.L.; Barbiellini, G.; et al. The Large Area Telescope on the Fermi Gamma-Ray Space Telescope Mission. *Astrophys. J.* **2009**, *697*, 1071–1102. [CrossRef]
80. Goldstein, A.; Fletcher, C.; Veres, P.; Briggs, M.S.; Cleveland, W.H.; Gibby, M.H.; Hui, C.M.; Bissaldi, E.; Burns, E.; Hamburg, R.; et al. Evaluation of Automated Fermi GBM Localizations of Gamma-Ray Bursts. *Astrophys. J.* **2020**, *895*, 40. [CrossRef]
81. Hoover, A.S.; Kippen, R.M.; Wallace, M.S.; Pendleton, G.N.; Fishman, G.J.; Meegan, C.A.; Kouveliotou, C.; Wilson-Hodge, C.A.; Bissaldi, E.; Diehl, R.; et al. GLAST Burst Monitor Instrument Simulation and Modeling. In *Gamma-ray Bursts 2007*; Galassi, M., Palmer, D., Fenimore, E., Eds.; American Institute of Physics Conference Series; American Institute of Physics: College Park, MA, USA, 2008; Volume 1000, pp. 565–568. [CrossRef]
82. Bissaldi, E.; von Kienlin, A.; Lichti, G.; Steinle, H.; Bhat, P.N.; Briggs, M.S.; Fishman, G.J.; Hoover, A.S.; Kippen, R.M.; Krumrey, M.; et al. Ground-based calibration and characterization of the Fermi gamma-ray burst monitor detectors. *Exp. Astron.* **2009**, *24*, 47–88. [CrossRef]
83. Wilson-Hodge, C.A.; Cherry, M.L.; Case, G.L.; Baumgartner, W.H.; Beklen, E.; Narayana Bhat, P.; Briggs, M.S.; Camero-Arranz, A.; Chaplin, V.; Connaughton, V.; et al. When a Standard Candle Flickers. *Astrophys. J. Lett.* **2011**, *727*, L40. [CrossRef]
84. Paciesas, W.S.; Meegan, C.A.; von Kienlin, A.; Bhat, P.N.; Bissaldi, E.; Briggs, M.S.; Burgess, J.M.; Chaplin, V.; Connaughton, V.; Diehl, R.; et al. The Fermi GBM Gamma-Ray Burst Catalog: The First Two Years. *Astrophys. J. Suppl.* **2012**, *199*, 18. [CrossRef]
85. von Kienlin, A.; Meegan, C.A.; Paciesas, W.S.; Bhat, P.N.; Bissaldi, E.; Briggs, M.S.; Burns, E.; Cleveland, W.H.; Gibby, M.H.; Giles, M.M.; et al. The Fourth Fermi-GBM Gamma-Ray Burst Catalog: A Decade of Data. *Astrophys. J.* **2020**, *893*, 46. [CrossRef]
86. Chattopadhyay, T.; Vadawale, S.V.; Rao, A.R.; Sreekumar, S.; Bhattacharya, D. Prospects of hard X-ray polarimetry with Astrosat-CZTI. *Exp. Astron.* **2014**, *37*, 555–577. [CrossRef]
87. Vadawale, S.V.; Chattopadhyay, T.; Rao, A.R.; Bhattacharya, D.; Bhalerao, V.B.; Vagshette, N.; Pawar, P.; Sreekumar, S. Hard X-ray polarimetry with Astrosat-CZTI. *Astron. Astrophys.* **2015**, *578*, A73. [CrossRef]
88. Chattopadhyay, T.; Vadawale, S.V.; Aarthy, E.; Mithun, N.P.S.; Chand, V.; Ratheesh, A.; Basak, R.; Rao, A.R.; Bhalerao, V.; Mate, S.; et al. Prompt Emission Polarimetry of Gamma-Ray Bursts with the AstroSat CZT Imager. *Astrophys. J.* **2019**, *884*, 123. [CrossRef]
89. Chand, V.; Chattopadhyay, T.; Oganesyan, G.; Rao, A.R.; Vadawale, S.V.; Bhattacharya, D.; Bhalerao, V.B.; Misra, K. AstroSat-CZTI Detection of Variable Prompt Emission Polarization in GRB 171010A. *Astrophys. J.* **2019**, *874*, 70. [CrossRef]
90. Torii, S.; Marrocchesi, P.S.; Calet Collaboration. The CALorimetric Electron Telescope (CALET) on the International Space Station. *Adv. Space Res.* **2019**, *64*, 2531–2537. [CrossRef]
91. Yamaoka, K.; Yoshida, A.; Sakamoto, T.; Takahashi, I.; Hara, T.; Yamamoto, T.; Kawakubo, Y.; Inoue, R.; Terazawa, S.; Fujioka, R.; et al. CALET Gamma-ray Burst Monitor (CGBM). *Int. Cosm. Ray Conf.* **2013**, *33*, 2948,
92. Kawakubo, Y. Gamma-ray burst observations with the CALET Gamma-ray Burst Monitor. In Proceedings of the 36th International Cosmic Ray Conference (ICRC2019), Madison, WI, USA, 24 July–1 August 2019; p. 571. [CrossRef]
93. Liu, C.; Zhang, Y.; Li, X.; Lu, X.; Chang, Z.; Li, Z.; Zhang, A.; Jin, Y.; Yu, H.; Zhang, Z.; et al. The High Energy X-ray telescope (HE) onboard the Insight-HXMT astronomy satellite. *Sci. China Phys. Mech. Astron.* **2020**, *63*, 249503. [CrossRef]
94. Cao, X.; Jiang, W.; Meng, B.; Zhang, W.; Luo, T.; Yang, S.; Zhang, C.; Gu, Y.; Sun, L.; Liu, X.; et al. The Medium Energy X-ray telescope (ME) onboard the Insight-HXMT astronomy satellite. *Sci. China Phys. Mech. Astron.* **2020**, *63*, 249504. [CrossRef]
95. Chen, Y.; Cui, W.; Li, W.; Wang, J.; Xu, Y.; Lu, F.; Wang, Y.; Chen, T.; Han, D.; Hu, W.; et al. The Low Energy X-ray telescope (LE) onboard the Insight-HXMT astronomy satellite. *Sci. China Phys. Mech. Astron.* **2020**, *63*, 249505. [CrossRef]
96. Neubert, T.; Østgaard, N.; Reglero, V.; Blanc, E.; Chanrion, O.; Oxborrow, C.A.; Orr, A.; Tacconi, M.; Hartnack, O.; Bhanderi, D.D. The ASIM Mission on the International Space Station. *Space Sci. Rev.* **2019**, *215*, 26. [CrossRef]
97. Østgaard, N.; Balling, J.E.; Bjørnsen, T.; Brauer, P.; Budtz-Jørgensen, C.; Bujwan, W.; Carlson, B.; Christiansen, F.; Connell, P.; Eyles, C.; et al. The Modular X- and Gamma-Ray Sensor (MXGS) of the ASIM Payload on the International Space Station. *Space Sci. Rev.* **2019**, *215*, 23. [CrossRef]
98. Castro-Tirado, A.J.; Østgaard, N.; Göğüş, E.; Sánchez-Gil, C.; Pascual-Granado, J.; Reglero, V.; Mezentsev, A.; Gabler, M.; Marisaldi, M.; Neubert, T.; et al. Very-high-frequency oscillations in the main peak of a magnetar giant flare. *Nature* **2021**, *600*, 621–624. [CrossRef]
99. Hurley, K.; Mitrofanov, I.G.; Golovin, D.; Litvak, M.L.; Sanin, A.B.; Boynton, W.; Fellows, C.; Harshman, K.; Starr, R.; Golenetskii, S.; et al. *The Interplanetary Network*; Castro-Tirado, A.J., Gorosabel, J., Park, I.H., Eds.; EAS Publications Series; EAS: Les Ulis, France, 2013; Volume 61, pp. 459–464. [CrossRef]
100. Saunders, R.S.; Arvidson, R.E.; Badhwar, G.D.; Boynton, W.V.; Christensen, P.R.; Cucinotta, F.A.; Feldman, W.C.; Gibbs, R.G.; Kloss, C.J.; Landano, M.R.; et al. 2001 Mars Odyssey Mission Summary. *Space Sci. Rev.* **2004**, *110*, 1–36. [CrossRef]
101. Boynton, W.V.; Feldman, W.C.; Mitrofanov, I.G.; Evans, L.G.; Reedy, R.C.; Squyres, S.W.; Starr, R.; Trombka, J.I.; D'Uston, C.; Arnold, J.R.; et al. The Mars Odyssey Gamma-Ray Spectrometer Instrument Suite. *Space Sci. Rev.* **2004**, *110*, 37–83. [CrossRef]

102. Hurley, K.; Mitrofanov, I.; Kozyrev, A.; Litvak, M.; Grinkov, V.; Sanin, A.; Charyshnikov, S.; Boynton, W.; Fellows, C.; Harshman, K.; et al. Mars Odyssey Joins the Third Interplanetary Network. *Astrophys. J. Suppl.* **2006**, *164*, 124–129. [CrossRef]
103. Benkhoff, J.; Murakami, G.; Baumjohann, W.; Besse, S.; Bunce, E.; Casale, M.; Cremosese, G.; Glassmeier, K.H.; Hayakawa, H.; Heyner, D.; et al. BepiColombo—Mission Overview and Science Goals. *Space Sci. Rev.* **2021**, *217*, 90. [CrossRef]
104. Mitrofanov, I.G.; Kozyrev, A.S.; Konovalov, A.; Litvak, M.L.; Malakhov, A.A.; Mokrousov, M.I.; Sanin, A.B.; Tret'ykov, V.I.; Vostrukhin, A.V.; Bobrovnitskij, Y.I.; et al. The Mercury Gamma and Neutron Spectrometer (MGNS) on board the Planetary Orbiter of the BepiColombo mission. *Planet. Space Sci.* **2010**, *58*, 116–124. [CrossRef]
105. Mitrofanov, I.G.; Kozyrev, A.S.; Lisov, D.I.; Litvak, M.L.; Malakhov, A.A.; Mokrousov, M.I.; Benkhoff, J.; Owens, A.; Schulz, R.; Quarati, F. The Mercury Gamma-Ray and Neutron Spectrometer (MGNS) Onboard the Mercury Planetary Orbiter of the BepiColombo Mission: Design Updates and First Measurements in Space. *Space Sci. Rev.* **2021**, *217*, 67. [CrossRef]
106. Goldsten, J.O.; Rhodes, E.A.; Boynton, W.V.; Feldman, W.C.; Lawrence, D.J.; Trombka, J.I.; Smith, D.M.; Evans, L.G.; White, J.; Madden, N.W.; et al. The MESSENGER Gamma-Ray and Neutron Spectrometer. *Space Sci. Rev.* **2007**, *131*, 339–391. [CrossRef]
107. Gold, R.E.; Solomon, S.C.; McNutt, R.L.; Santo, A.G.; Abshire, J.B.; Acuña, M.H.; Afzal, R.S.; Anderson, B.J.; Andrews, G.B.; Bedini, P.D.; et al. The MESSENGER mission to Mercury: Scientific payload. *Planet. Space Sci.* **2001**, *49*, 1467–1479. [CrossRef]
108. Solomon, S.C.; McNutt, R.L.; Gold, R.E.; Domingue, D.L. MESSENGER Mission Overview. *Space Sci. Rev.* **2007**, *131*, 3–39. [CrossRef]
109. Lin, R.P.; Dennis, B.R.; Hurford, G.J.; Smith, D.M.; Zehnder, A.; Harvey, P.R.; Curtis, D.W.; Pankow, D.; Turin, P.; Bester, M.; et al. The Reuven Ramaty High-Energy Solar Spectroscopic Imager (RHESSI). *Sol. Phys.* **2002**, *210*, 3–32. [CrossRef]
110. Smith, D.M.; Lin, R.P.; Turin, P.; Curtis, D.W.; Primbsch, J.H.; Campbell, R.D.; Abiad, R.; Schroeder, P.; Cork, C.P.; Hull, E.L.; et al. The RHESSI Spectrometer. *Sol. Phys.* **2002**, *210*, 33–60. [CrossRef]
111. Svinkin, D.; Frederiks, D.; Hurley, K.; Aptekar, R.; Golenetskii, S.; Lysenko, A.; Ridnaia, A.V.; Tsvetkova, A.; Ulanov, M.; Cline, T.L.; et al. A bright γ-ray flare interpreted as a giant magnetar flare in NGC 253. *Nature* **2021**, *589*, 211–213. [CrossRef]
112. Ahumada, T.; Singer, L.P.; Anand, S.; Coughlin, M.W.; Kasliwal, M.M.; Ryan, G.; Andreoni, I.; Cenko, S.B.; Fremling, C.; Kumar, H.; et al. Discovery and confirmation of the shortest gamma-ray burst from a collapsar. *Nat. Astron.* **2021**, *5*, 917–927. [CrossRef]
113. Ho, A.Y.Q.; Perley, D.A.; Yao, Y.; Svinkin, D.; de Ugarte Postigo, A.; Perley, R.A.; Kann, D.A.; Burns, E.; Andreoni, I.; Bellm, E.C.; et al. Cosmological Fast Optical Transients with the Zwicky Transient Facility: A Search for Dirty Fireballs. *arXiv* **2022**, arXiv:2201.12366.
114. Hurley, K.C. Gamma-Ray Burst Triangulation with a Near-Earth Network. *Astrophys. J.* **2020**, *905*, 82. [CrossRef]
115. Racusin, J.; Perkins, J.S.; Briggs, M.S.; de Nolfo, G.; Krizmanic, J.; Caputo, R.; McEnery, J.E.; Shawhan, P.; Morris, D.; Connaughton, V.; et al. BurstCube: A CubeSat for Gravitational Wave Counterparts. *arXiv* **2017**, arXiv:1708.09292.
116. Smith, J. BurstCube: Mission Concept, Performance, and Status. In Proceedings of the 36th International Cosmic Ray Conference (ICRC2019), Madison, WI, USA, 24 July–1 August 2019; Volume 36, p. 604.
117. Wen, J.X.; Zheng, X.T.; Yu, J.D.; Che, Y.P.; Yang, D.X.; Gao, H.Z.; Jin, Y.F.; Long, X.Y.; Liu, Y.H.; Xu, D.C.; et al. Compact CubeSat Gamma-Ray Detector for GRID Mission. *arXiv* **2021**, arXiv:2104.14228.
118. Werner, N.; Řípa, J.; Pál, A.; Ohno, M.; Tarcai, N.; Torigoe, K.; Tanaka, K.; Uchida, N.; Mészáros, L.; Galgóczi, G.; et al. CAMELOT: Cubesats Applied for MEasuring and LOcalising Transients mission overview. In *Space Telescopes and Instrumentation 2018: Ultraviolet to Gamma Ray*; den Herder, J.W.A., Nikzad, S., Nakazawa, K., Eds.; Society of Photo-Optical Instrumentation Engineers (SPIE) Conference Series; SPIE Press: Bellingham, DC, USA, 2018; Volume 10699, pp. 672–686. [CrossRef]
119. Fuschino, F.; Campana, R.; Labanti, C.; Evangelista, Y.; Feroci, M.; Burderi, L.; Fiore, F.; Ambrosino, F.; Baldazzi, G.; Bellutti, P.; et al. HERMES: An ultra-wide band X and gamma-ray transient monitor on board a nano-satellite constellation. *Nucl. Instruments Methods Phys. Res. A* **2019**, *936*, 199–203. [CrossRef]
120. Fiore, F.; Burderi, L.; Lavagna, M.; Bertacin, R.; Evangelista, Y.; Campana, R.; Fuschino, F.; Lunghi, P.; Monge, A.; Negri, B.; et al. *The HERMES-Technologic and Scientific Pathfinder*; Society of Photo-Optical Instrumentation Engineers (SPIE) Conference Series; SPIE Press: Bellingham, DC, USA, 2020; Volume 11444, pp. 214–228. [CrossRef]
121. Inceoglu, F.; Hernández Marcano, N.J.; Jacobsen, R.H.; Karoff, C. A General Overview for Localising Short Gamma-ray Bursts with a CubeSat Mega-Constellation. *Front. Astron. Space Sci.* **2020**, *7*, 75. [CrossRef]
122. Pál, A.; Ohno, M.; Mészáros, L.; Werner, N.; Ripa, J.; Frajt, M.; Hirade, N.; Hudec, J.; Kapuš, J.; Koleda, M.; et al. *GRBAlpha: A 1U CubeSat Mission for Validating Timing-Based Gamma-Ray Burst Localization*; Society of Photo-Optical Instrumentation Engineers (SPIE) Conference Series; SPIE Press: Bellingham, DC, USA, 2020; Volume 11444, pp. 825–833. [CrossRef]
123. Granja, C.; Hudec, R.; Maršíková, V.; Inneman, A.; Pína, L.; Doubravova, D.; Matej, Z.; Daniel, V.; Oberta, P. Directional-Sensitive X-ray/Gamma-ray Imager on Board the VZLUSAT-2 CubeSat for Wide Field-of-View Observation of GRBs in Low Earth Orbit. *Universe* **2022**, *8*, 241. [CrossRef]
124. Murphy, D.; Joe, F.; Thompson, J.W.; Doyle, M.; Erkal, J.; Gloster, A.; O'Toole, C.; Salmon, L.; Sherwin, D.; Walsh, S.; et al. EIRSAT-1 - The Educational Irish Research Satellite. In Proceedings of the 2nd Symposium on Space Educational Activities, Budapest, Hungary, 11–13 April 2018.
125. Sanna, A.; Burderi, L.; Di Salvo, T.; Fiore, F.; Riggio, A.; Gambino, A.; Lavagna, M.; Bertacin, R.; Evangelista, Y.; Campana, R.; et al. *Timing Techniques Applied to Distributed Modular High-Energy Astronomy: The H.E.R.M.E.S. Project*; Society of Photo-Optical Instrumentation Engineers (SPIE) Conference Series; SPIE Press: Bellingham, DC, USA, 2020; Volume 11444, pp. 844–862. [CrossRef]

126. Burderi, L.; Di Salvo, T.; Riggio, A.; Gambino, A.F.; Sanna, A.; Fiore, F.; Amarilli, F.; Amati, L.; Ambrosino, F.; Amelino-Camelia, G.; et al. *GrailQuest and HERMES: Hunting for Gravitational Wave Electromagnetic Counterparts and Probing Space-Time Quantum Foam*; Society of Photo-Optical Instrumentation Engineers (SPIE) Conference Series; SPIE Press: Bellingham, DC, USA, 2020; Volume 11444, pp. 863–881. [CrossRef]
127. Evangelista, Y.; Fiore, F.; Fuschino, F.; Campana, R.; Ceraudo, F.; Demenev, E.; Guzman, A.; Labanti, C.; La Rosa, G.; Fiorini, M.; et al. *The Scientific Payload On-Board the HERMES-TP and HERMES-SP CubeSat Missions*; Society of Photo-Optical Instrumentation Engineers (SPIE) Conference Series; SPIE Press: Bellingham, DC, USA, 2020; Volume 11444, pp. 241–256. [CrossRef]
128. Burderi, L.; Sanna, A.; Di Salvo, T.; Amati, L.; Amelino-Camelia, G.; Branchesi, M.; Capozziello, S.; Coccia, E.; Colpi, M.; Costa, E.; et al. GrailQuest: Hunting for atoms of space and time hidden in the wrinkle of Space-Time. *Exp. Astron.* **2021**, *51*, 1255–1297. [CrossRef]
129. Paczynski, B.; Rhoads, J.E. Radio Transients from Gamma-Ray Bursters. *Astrophys. J. Lett.* **1993**, *418*, L5. [CrossRef]
130. Sari, R.; Piran, T.; Narayan, R. Spectra and Light Curves of Gamma-Ray Burst Afterglows. *Astrophys. J. Lett.* **1998**, *497*, L17–L20. [CrossRef]
131. Piran, T. The physics of gamma-ray bursts. *Rev. Mod. Phys.* **2004**, *76*, 1143–1210. [CrossRef]
132. Granot, J.; Sari, R. The Shape of Spectral Breaks in Gamma-Ray Burst Afterglows. *Astrophys. J.* **2002**, *568*, 820–829. [CrossRef]
133. Mészáros, P.; Rees, M.J. GRB 990123: Reverse and internal shock flashes and late afterglow behaviour. *Mon. Not. R. Astron. Soc.* **1999**, *306*, L39–L43. [CrossRef]
134. Rhoads, J.E. The Dynamics and Light Curves of Beamed Gamma-Ray Burst Afterglows. *Astrophys. J.* **1999**, *525*, 737–749. [CrossRef]
135. Sari, R.; Piran, T.; Halpern, J.P. Jets in Gamma-Ray Bursts. *Astrophys. J. Lett.* **1999**, *519*, L17–L20. [CrossRef]
136. Weisskopf, M.C.; Tananbaum, H.D.; Van Speybroeck, L.P.; O'Dell, S.L. Chandra X-ray Observatory (CXO): Overview. In *X-Ray Optics, Instruments, and Missions III*; Truemper, J.E., Aschenbach, B., Eds.; Society of Photo-Optical Instrumentation Engineers (SPIE) Conference Series; SPIE Press: Bellingham, DC, USA, 2000; Volume 4012, pp. 2–16. [CrossRef]
137. Weisskopf, M.C.; Brinkman, B.; Canizares, C.; Garmire, G.; Murray, S.; Van Speybroeck, L.P. An Overview of the Performance and Scientific Results from the Chandra X-Ray Observatory. *Publ. Astron. Soc. Pac.* **2002**, *114*, 1–24. [CrossRef]
138. Schwartz, D.A. The Development and Scientific Impact of the Chandra X-Ray Observatory. *Int. J. Mod. Phys. D* **2004**, *13*, 1239–1247. [CrossRef]
139. Jansen, F.; Lumb, D.; Altieri, B.; Clavel, J.; Ehle, M.; Erd, C.; Gabriel, C.; Guainazzi, M.; Gondoin, P.; Much, R.; et al. XMM-Newton observatory. I. The spacecraft and operations. *Astron. Astrophys.* **2001**, *365*, L1–L6. [CrossRef]
140. Burrows, D.N.; Kennea, J.A.; Abbey, A.F.; Beardmore, A.P.; Campana, S.; Capalbi, M.; Chincarini, G.L.; Cusumano, G.; Evans, P.A.; Hill, J.E.; et al. The swift x-ray telescope: Status and performance. In *SPIE Optical Engineering + Applications*; SPIE Press: Bellingham, DC, USA, 2007.
141. Racusin, J.L.; Liang, E.W.; Burrows, D.N.; Falcone, A.; Sakamoto, T.; Zhang, B.B.; Zhang, B.; Evans, P.; Osborne, J. Jet Breaks and Energetics of Swift Gamma-Ray Burst X-Ray Afterglows. *Astrophys. J.* **2009**, *698*, 43–74. [CrossRef]
142. Dainotti, M.G.; Lenart, A.Ł.; Fraija, N.; Nagataki, S.; Warren, D.C.; De Simone, B.; Srinivasaragavan, G.; Mata, A. Closure relations during the plateau emission of Swift GRBs and the fundamental plane. *Publ. Astron. Soc. Jpn.* **2021**, *73*, 970–1000. [CrossRef]
143. Klingler, N.J.; Kennea, J.A.; Evans, P.A.; Tohuvavohu, A.; Cenko, S.B.; Barthelmy, S.D.; Beardmore, A.P.; Breeveld, A.A.; Brown, P.J.; Burrows, D.N.; et al. Swift-XRT Follow-up of Gravitational-wave Triggers in the Second Advanced LIGO/Virgo Observing Run. *Astrophys. J. Suppl.* **2019**, *245*, 15. [CrossRef]
144. Page, K.L.; Evans, P.A.; Tohuvavohu, A.; Kennea, J.A.; Klingler, N.J.; Cenko, S.B.; Oates, S.R.; Ambrosi, E.; Barthelmy, S.D.; Beardmore, A.P.; et al. Swift-XRT follow-up of gravitational wave triggers during the third aLIGO/Virgo observing run. *Mon. Not. R. Astron. Soc.* **2020**, *499*, 3459–3480. [CrossRef]
145. Serino, M.; Sakamoto, T.; Kawai, N.; Yoshida, A.; Ohno, M.; Ogawa, Y.; Nishimura, Y.; Fukushima, K.; Higa, M.; Ishikawa, K.; et al. MAXI observations of gamma-ray bursts. *Publ. Astron. Soc. Jpn.* **2014**, *66*, 87. [CrossRef]
146. Sugizaki, M.; Mihara, T.; Serino, M.; Yamamoto, T.; Matsuoka, M.; Kohama, M.; Tomida, H.; Ueno, S.; Kawai, N.; Morii, M.; et al. In-Orbit Performance of MAXI Gas Slit Camera (GSC) on ISS. *Publ. Astron. Soc. Jpn.* **2011**, *63*, S635–S644. [CrossRef]
147. Harrison, F.A.; Craig, W.W.; Christensen, F.E.; Hailey, C.J.; Zhang, W.W.; Boggs, S.E.; Stern, D.; Cook, W.R.; Forster, K.; Giommi, P.; et al. The Nuclear Spectroscopic Telescope Array (NuSTAR) High-energy X-Ray Mission. *Astrophys. J.* **2013**, *770*, 103. [CrossRef]
148. Racusin, J.L.; Karpov, S.V.; Sokolowski, M.; Granot, J.; Wu, X.F.; Pal'Shin, V.; Covino, S.; van der Horst, A.J.; Oates, S.R.; Schady, P.; et al. Broadband observations of the naked-eye γ-ray burst GRB080319B. *Nature* **2008**, *455*, 183–188. [CrossRef] [PubMed]
149. Beskin, G.; Karpov, S.; Bondar, S.; Greco, G.; Guarnieri, A.; Bartolini, C.; Piccioni, A. Fast Optical Variability of a Naked-eye Burst—Manifestation of the Periodic Activity of an Internal Engine. *Astrophys. J. Lett.* **2010**, *719*, L10–L14. [CrossRef]
150. Zhang, B.B.; Zhang, B.; Castro-Tirado, A.J.; Dai, Z.G.; Tam, P.H.T.; Wang, X.Y.; Hu, Y.D.; Karpov, S.; Pozanenko, A.; Zhang, F.W.; et al. Transition from fireball to Poynting-flux-dominated outflow in the three-episode GRB 160625B. *Nat. Astron.* **2018**, *2*, 69–75. [CrossRef]
151. Greiner, J. The Benefit of Simultaneous Seven-filter Imaging: 10 Years of GROND Observations. *Publ. Astron. Soc. Pac.* **2019**, *131*, 015002. [CrossRef]

152. Castro-Tirado, A.J.; Soldán, J.; Bernas, M.; Páta, P.; Rezek, T.; Hudec, R.; Mateo Sanguino, T.J.; de La Morena, B.; Berná, J.A.; Rodríguez, J.; et al. The Burst Observer and Optical Transient Exploring System (BOOTES). *Astron. Astrophys. Suppl.* **1999**, *138*, 583–585. [CrossRef]
153. Castro-Tirado, A.J.; Jelínek, M.; Gorosabel, J.; Kubánek, P.; Cunniffe, R.; Guziy, S.; Lara-Gil, O.; Rabaza-Castillo, O.; de Ugarte Postigo, A.; Sánchez-Ramírez, R.; et al. *Building the BOOTES World-Wide Network of Robotic Telescopes*; Astronomical Society of India Conference Series; Astronomical Society of India: Hyderabad, India, 2012; Volume 7, pp. 313–320.
154. Hu, Y.D.; Li, X.Y.; Castro-Tirado, A.J.; Fernandez-García, E.J.; Castellón, A.; Carrasco-García, I.; Perez del Pulgar, C.; Caballero-García, M.D.; Querel, R.; Bai, J.; et al. *The BOOTES Network in the Gravitational Wave Era*; Revista Mexicana de Astronomia y Astrofisica Conference Series; The Astronomical Institute (Instituto de Astronomia) of the National Autonomous University of Mexico: Mexico City, Mexico, 2021; Volume 53, pp. 75–82. [CrossRef]
155. Watson, A.M.; Cuevas Cardona, S.; Alvarez Nuñez, L.C.; Ángeles, F.; Becerra-Godínez, R.L.; Chapa, O.; Farah, A.S.; Fuentes-Fernández, J.; Figueroa, L.; Langarica Lebre, R.; et al. COATLI: An all-sky robotic optical imager with 0.3 arcsec image quality. In *Ground-Based and Airborne Instrumentation for Astronomy VI*; Evans, C.J., Simard, L., Takami, H., Eds.; SPIE Press: Bellingham, DC, USA, 2016; Volume 9908, p. 99100G. [CrossRef]
156. Watson, A.M.; Lee, W.H.; Troja, E.; Román-Zúñiga, C.G.; Butler, N.R.; Kutyrev, A.S.; Gehrels, N.A.; Ángeles, F.; Basa, S.; Blanc, P.E.; et al. DDOTI: The deca-degree optical transient imager. In *Observatory Operations: Strategies, Processes, and Systems VI*; Peck, A.B., Seaman, R.L., Benn, C.R., Eds.; Society of Photo-Optical Instrumentation Engineers (SPIE) Conference Series; SPIE Press: Bellingham, DC, USA, 2016; Volume 9910. [CrossRef]
157. Ebr, J.; Janeček, P.; Prouza, M.; Kubánek, P.; Jelínek, M.; Mašek, M.; Ebrová, I.; Černý, J. *FRAM: Showers, Comets, GRBs and Popular Science*; Revista Mexicana de Astronomia y Astrofisica Conference Series; The Astronomical Institute (Instituto de Astronomia) of the National Autonomous University of Mexico: Mexico City, Mexico, 2014; Volume 45, p. 114.
158. Janeček, P.; Ebr, J.; Juryšek, J.; Prouza, M.; Blažek, J.; Trávníček, P.; Mandát, D.; Pech, M.; Karpov, S.; Cunniffe, R.; et al. FRAM telescopes and their measurements of aerosol content at the Pierre Auger Observatory and at future sites of the Cherenkov Telescope Array. *Eur. Phys. J. Web Conf.* **2019,** *197*, 02008. [CrossRef]
159. Antier, S.; Agayeva, S.; Aivazyan, V.; Alishov, S.; Arbouch, E.; Baransky, A.; Barynova, K.; Bai, J.M.; Basa, S.; Beradze, S.; et al. The first six months of the Advanced LIGO's and Advanced Virgo's third observing run with GRANDMA. *Mon. Not. R. Astron. Soc.* **2020**, *492*, 3904–3927. [CrossRef]
160. Agayeva, S.; Alishov, S.; Antier, S.; Ayvazian, V.R.; Bai, J.M.; Baransky, A.; Barynova, K.; Basa, S.; Beradze, S.; Bertin, E.; et al. *Grandma: A Network to Coordinate Them All*; Revista Mexicana de Astronomia y Astrofisica Conference Series; The Astronomical Institute (Instituto de Astronomia) of the National Autonomous University of Mexico: Mexico City, Mexico, 2021; Volume 53, pp. 198–205. [CrossRef]
161. Volnova, A.; Pozanenko, A.; Mazaeva, E.; Belkin, S.; Molotov, I.; Elenin, L.; Tungalag, N.; Buckley, D. IKI GRB-FuN: Observations of GRBs with small-aperture telescopes. *An. Acad. Bras. Ciências* **2021**, *93*, 1. [CrossRef]
162. Pozanenko, A.; Elenin, L.; Litvinenko, E.; Volnova, A.; Erofeeva, A.; Matkin, A.; Ivanov, A.; Ivanov, V.; Varda, D.; Sinyakov, E.; et al. *Gamma-Ray Burst Observations with Ison Network*; Castro-Tirado, A.J., Gorosabel, J., Park, I.H., Eds.; EAS Publications Series; EDP Sciences: Les Ulis, France, 2013; Volume 61, pp. 259–261. [CrossRef]
163. Pozanenko, A.; Mazaeva, E.; Volnova, A.; Elenin, L.; Inasaridze, R.; Aivazyan, V.; Reva, I.; Kusakin, A.; Tungalag, N.; Schmalz, S.; et al. GRB Afterglow Observations by International Scientific Optical Network (ISON). In *Eighth Huntsville Gamma-Ray Burst Symposium*; LPI Contributions; Lunar and Planetary Institute: Houston, TX, USA, 2016; Volume 1962, p. 4074.
164. Richmond, M.; Treffers, R.R.; Filippenko, A.V. The Berkeley Automatic Imaging Telescope. *Publ. Astron. Soc. Pac.* **1993**, *105*, 1164. [CrossRef]
165. Filippenko, A.V.; Li, W.D.; Treffers, R.R.; Modjaz, M. The Lick Observatory Supernova Search with the Katzman Automatic Imaging Telescope. In *IAU Colloq. 183: Small Telescope Astronomy on Global Scales*; Paczynski, B., Chen, W.P., Lemme, C., Eds.; Astronomical Society of the Pacific Conference Series; Astronomical Society of the Pacific: San Francisco, CA, USA, 2001; Volume 246, p. 121.
166. Butler, N.; Bloom, J.; Filippenko, A.; Li, W.; Foley, R.; Alatalo, K.; Kocevski, D.; Perley, D.; Pooley, D. Rapidly Detecting Extincted Bursts with KAIT and PAIRITEL. In *Gamma-Ray Bursts in the Swift Era*; Holt, S.S., Gehrels, N., Nousek, J.A., Eds.; American Institute of Physics Conference Series; American Institute of Physics: College Park, MA, USA, 2006; Volume 836, pp. 277–280. [CrossRef]
167. Guidorzi, C.; Monfardini, A.; Gomboc, A.; Mottram, C.J.; Mundell, C.G.; Steele, I.A.; Carter, D.; Bode, M.F.; Smith, R.J.; Fraser, S.N.; et al. The Automatic Real-Time Gamma-Ray Burst Pipeline of the 2 m Liverpool Telescope. *Publ. Astron. Soc. Pac.* **2006**, *118*, 288–296. [CrossRef]
168. Lipunov, V.; Kornilov, V.; Gorbovskoy, E.; Shatskij, N.; Kuvshinov, D.; Tyurina, N.; Belinski, A.; Krylov, A.; Balanutsa, P.; Chazov, V.; et al. Master Robotic Net. *Adv. Astron.* **2010**, *2010*, 349171. [CrossRef]
169. Troja, E.; Lipunov, V.M.; Mundell, C.G.; Butler, N.R.; Watson, A.M.; Kobayashi, S.; Cenko, S.B.; Marshall, F.E.; Ricci, R.; Fruchter, A.; et al. Significant and variable linear polarization during the prompt optical flash of GRB 160625B. *Nature* **2017**, *547*, 425–427. [CrossRef]

170. Gorbovskoy, E.S.; Lipunova, G.V.; Lipunov, V.M.; Kornilov, V.G.; Belinski, A.A.; Shatskiy, N.I.; Tyurina, N.V.; Kuvshinov, D.A.; Balanutsa, P.V.; Chazov, V.V.; et al. Prompt, early and afterglow optical observations of five γ-ray bursts: GRB 100901A, GRB 100902A, GRB 100905A, GRB 100906A and GRB 101020A. *Mon. Not. R. Astron. Soc.* **2012**, *421*, 1874–1890. [CrossRef]
171. Pruzhinskaya, M.V.; Krushinsky, V.V.; Lipunova, G.V.; Gorbovskoy, E.S.; Balanutsa, P.V.; Kuznetsov, A.S.; Denisenko, D.V.; Kornilov, V.G.; Tyurina, N.V.; Lipunov, V.M.; et al. Optical polarization observations with the MASTER robotic net. *New Astron.* **2014**, *29*, 65–74. [CrossRef]
172. Tyurina, N.; Lipunov, V.; Kornilov, V.; Gorbovskoy, E.; Shatskij, N.; Kuvshinov, D.; Balanutsa, P.; Belinski, A.; Krushinsky, V.; Zalozhnyh, I.; et al. MASTER Prompt and Follow-Up GRB Observations. *Adv. Astron.* **2010**, *2010*, 763629. [CrossRef]
173. Bloom, J.S.; Starr, D.L.; Blake, C.H.; Skrutskie, M.F.; Falco, E.E. Autonomous Observing and Control Systems for PAIRITEL, a 1.3m Infrared Imaging Telescope. In *Astronomical Data Analysis Software and Systems XV*; Gabriel, C., Arviset, C., Ponz, D., Enrique, S., Eds.; Astronomical Society of the Pacific Conference Series; Astronomical Society of the Pacific: San Francisco, CA, USA, 2006; Volume 351, p. 751.
174. Burd, A.; Cwiok, M.; Czyrkowski, H.; Dabrowski, R.; Dominik, W.; Grajda, M.; Husejko, M.; Jegier, M.; Kalicki, A.; Kasprowicz, G.; et al. Pi of the Sky - all-sky, real-time search for fast optical transients. *New Astron.* **2005**, *10*, 409–416. [CrossRef]
175. Mankiewicz, L.; Batsch, T.; Castro-Tirado, A.; Czyrkowski, H.; Cwiek, A.; Cwiok, M.; Dabrowski, R.; Jelínek, M.; Kasprowicz, G.; Majcher, A.; et al. *Pi of the Sky Full System and the New Telescope*; Revista Mexicana de Astronomia y Astrofisica Conference Series; The Astronomical Institute (Instituto de Astronomia) of the National Autonomous University of Mexico: Mexico City, Mexico, 2014; Volume 45, p. 7.
176. Vestrand, W.T.; Borozdin, K.N.; Brumby, S.P.; Casperson, D.E.; Fenimore, E.E.; Galassi, M.C.; McGowan, K.; Perkins, S.J.; Priedhorsky, W.C.; Starr, D.; et al. The RAPTOR experiment: A system for monitoring the optical sky in real time. In *Advanced Global Communications Technologies for Astronomy II*; Kibrick, R.I., Ed.; Society of Photo-Optical Instrumentation Engineers (SPIE) Conference Series; SPIE Press: Bellingham, DC, USA,2002; Volume 4845, pp. 126–136. [CrossRef]
177. Borozdin, K.N.; Brumby, S.P.; Galassi, M.C.; McGowan, K.; Starr, D.; Vestrand, T.; White, R.; Wozniak, P.; Wren, J.A. Real-Time Detection of Optical Transients with RAPTOR. In *Astronomical Data Analysis II*; Starck, J.L., Murtagh, F.D., Eds.; Society of Photo-Optical Instrumentation Engineers (SPIE) Conference Series; SPIE Press: Bellingham, DC, USA, 2002; Volume 4847, pp. 344–353. [CrossRef]
178. Butler, N.; Klein, C.; Fox, O.; Lotkin, G.; Bloom, J.; Prochaska, J.X.; Ramirez-Ruiz, E.; de Diego, J.A.; Georgiev, L.; González, J.; et al. First Light with RATIR: An Automated 6-band Optical/NIR Imaging Camera. In *Ground-based and Airborne Instrumentation for Astronomy IV*; McLean, I.S., Ramsay, S.K., Takami, H., Eds.; Society of Photo-Optical Instrumentation Engineers (SPIE) Conference Series; SPIE Press: Bellingham, DC, USA, 2012; Volume 8446, p. 844610. [CrossRef]
179. Watson, A.M.; Richer, M.G.; Bloom, J.S.; Butler, N.R.; Ceseña, U.; Clark, D.; Colorado, E.; Córdova, A.; Farah, A.; Fox-Machado, L.; et al. Automation of the OAN/SPM 1.5-meter Johnson telescope for operations with RATIR. In *Ground-based and Airborne Telescopes IV*; Stepp, L.M., Gilmozzi, R., Hall, H.J., Eds.; Society of Photo-Optical Instrumentation Engineers (SPIE) Conference Series; SPIE Press: Bellingham, DC, USA, 2012; Volume 8444, p. 84445L. [CrossRef]
180. Fox, O.D.; Kutyrev, A.S.; Rapchun, D.A.; Klein, C.R.; Butler, N.R.; Bloom, J.; de Diego, J.A.; Farah, A.; Gehrels, N.A.; Georgiev, L.; et al. Performance and calibration of H2RG detectors and SIDECAR ASICs for the RATIR camera. In *High Energy, Optical, and Infrared Detectors for Astronomy V*; Holland, A.D., Beletic, J.W., Eds.; Society of Photo-Optical Instrumentation Engineers (SPIE) Conference Series; SPIE Press: Bellingham, DC, USA, 2012; Volume 8453, pp. 508–517. [CrossRef]
181. Antonelli, L.A.; Zerbi, F.M.; Chincarini, G.; Rodonò, M.; Palazzi, E.; Tosti, G.; Conconi, P.; Covino, S.; Cutispoto, G.; Molinari, E.; et al. The REM telescope: A robotic facility for wide band prompt observations of Gamma Ray Bursts. In *Frontier Objects in Astrophysics and Particle Physics*; Italian Physical Society: Bologna, Italy, 2005; p. 657.
182. Akerlof, C.W.; Kehoe, R.L.; McKay, T.A.; Rykoff, E.S.; Smith, D.A.; Casperson, D.E.; McGowan, K.E.; Vestrand, W.T.; Wozniak, P.R.; Wren, J.A.; et al. The ROTSE-III Robotic Telescope System. *Publ. Astron. Soc. Pac.* **2003**, *115*, 132–140. [CrossRef]
183. Keel, W.C.; Oswalt, T.; Mack, P.; Henson, G.; Hillwig, T.; Batcheldor, D.; Berrington, R.; De Pree, C.; Hartmann, D.; Leake, M.; et al. The Remote Observatories of the Southeastern Association for Research in Astronomy (SARA). *Publ. Astron. Soc. Pac.* **2021**, *129*, 015002; Corrigendum in *Publ. Astron. Soc. Pac.* **2021**, *133*, 069201. [CrossRef]
184. Zola, S.; Kouprianov, V.; Reichart, D.E.; Bhatta, G.; Caton, D.B. *Long-Term Photometry with Skynet Robotic Telescope Network*; Revista Mexicana de Astronomia y Astrofisica Conference Series; The Astronomical Institute (Instituto de Astronomia) of the National Autonomous University of Mexico: Mexico City, Mexico, 2021; Volume 53, pp. 206–214. [CrossRef]
185. Boer, M.; Klotz, A.; Atteia, J.L.; Buchholtz, G.; Daigne, F.; Eysseric, J.; Goldoni, P.; Jean, P.; Lecavelier Des Etangs, A.; Lopez, M.; et al. The Gamma-Ray Burst Hunt at La Silla the TAROT-S Very Fast Moving Telescope. *Messenger* **2003**, *113*, 45–48.
186. Molinari, E.; Bondar, S.; Karpov, S.; Beskin, G.; Biryukov, A.; Ivanov, E.; Bartolini, C.; Greco, G.; Guarnieri, A.; Piccioni, A.; et al. TORTOREM: Two-telescope complex for detection and investigation of optical transients. *Nuovo Cimento B Ser.* **2006**, *121*, 1525–1526. [CrossRef]
187. Zolotukhin, I.; Beskin, G.; Biryukov, A.; Bondar, S.; Hurley, K.; Ivanov, E.; Karpov, S.; Katkova, E.; Pozanenko, A. Optical camera with high temporal resolution to search for transients in the wide field. *Astron. Nachrichten* **2004**, *325*, 675. [CrossRef]
188. Karpov, S.; Beskin, G.; Biryukov, A.; Bondar, S.; Hurley, K.; Ivanov, E.; Katkova, E.; Pozanenko, A.; Zolotukhin, I. Optical camera with high temporal resolution to search for transients in the wide field. *Nuovo Cimento C Geophys. Space Phys. C* **2005**, *28*, 747. [CrossRef]

189. Karpov, S.; Beskin, G.; Bondar, S.; Guarnieri, A.; Bartolini, C.; Greco, G.; Piccioni, A. Wide and Fast: Monitoring the Sky in Subsecond Domain with the FAVOR and TORTORA Cameras. *Adv. Astron.* **2010**, *2010*, 784141. [CrossRef]
190. Greco, G.; Beskin, G.; Karpov, S.; Guarnieri, A.; Bartolini, C.; Bondar, S.; Piccioni, A.; Molinari, E. The High-Speed and Wide-Field TORTORA Camera: Description & results. *Mem. Della Soc. Astron. Ital. Suppl.* **2010**, *14*, 267.
191. Beskin, G.M.; Karpov, S.V.; Bondar, S.F.; Plokhotnichenko, V.L.; Guarnieri, A.; Bartolini, C.; Greco, G.; Piccioni, A. CONFERENCES AND SYMPOSIA: Discovery of the fast optical variability of GRB 080319B and the prospects for wide-field optical monitoring with high time resolution. *Phys. Uspekhi* **2010**, *53*, 406–414. [CrossRef]
192. Karpov, S.; Beskin, G.; Biryukov, A.; Bondar, S.; Ivanov, E.; Katkova, E.; Perkov, A.; Sasyuk, V. *Mini-Mega-TORTORA Wide-Field Monitoring System with Sub-Second Temporal Resolution: First Year of Operation*; Revista Mexicana de Astronomia y Astrofisica Conference Series; The Astronomical Institute (Instituto de Astronomia) of the National Autonomous University of Mexico: Mexico City, Mexico, 2016; Volume 48, pp. 91–96.
193. French, J.; Hanlon, L.; McBreen, B.; McBreen, S.; Moran, L.; Smith, N.; Giltinan, A.; Meintjes, P.; Hoffman, M. Watcher: A Telescope for Rapid Gamma-Ray Burst Follow-Up Observations. In *Gamma-Ray Bursts: 30 Years of Discovery*; Fenimore, E., Galassi, M., Eds.; American Institute of Physics Conference Series; American Institute of Physics: College Park, MA, USA, 2004; Volume 727, pp. 741–744. [CrossRef]
194. Martin-Carrillo, A.; Hanlon, L.; Topinka, M.; LaCluyzé, A.P.; Savchenko, V.; Kann, D.A.; Trotter, A.S.; Covino, S.; Krühler, T.; Greiner, J.; et al. GRB 120711A: An intense INTEGRAL burst with long-lasting soft γ-ray emission and a powerful optical flash. *Astron. Astrophys.* **2014**, *567*, A84. [CrossRef]
195. Tisdall, P.; Hanlon, L.; Murphy, D.; Topinka, M.; Meehan, S.; Martin-Carillo, A.; Jelínek, M.; Meintjes, P.; van Soelen, B.; Hoffman, M. *Blazar Monitoring with the Watcher Robotic Telescope*; Revista Mexicana de Astronomia y Astrofisica Conference Series; The Astronomical Institute (Instituto de Astronomia) of the National Autonomous University of Mexico: Mexico City, Mexico, 2014; Volume 45, p. 71.
196. Cenko, S.B.; Urban, A.L.; Perley, D.A.; Horesh, A.; Corsi, A.; Fox, D.B.; Cao, Y.; Kasliwal, M.M.; Lien, A.; Arcavi, I.; et al. iPTF14yb: The First Discovery of a Gamma-Ray Burst Afterglow Independent of a High-energy Trigger. *Astrophys. J. Lett.* **2015**, *803*, L24. [CrossRef]
197. Stalder, B.; Tonry, J.; Smartt, S.J.; Coughlin, M.; Chambers, K.C.; Stubbs, C.W.; Chen, T.W.; Kankare, E.; Smith, K.W.; Denneau, L.; et al. Observations of the GRB Afterglow ATLAS17aeu and Its Possible Association with GW 170104. *Astrophys. J.* **2017**, *850*, 149. [CrossRef]
198. Andreoni, I.; Coughlin, M.W.; Kool, E.C.; Kasliwal, M.M.; Kumar, H.; Bhalerao, V.; Carracedo, A.S.; Ho, A.Y.Q.; Pang, P.T.H.; Saraogi, D.; et al. Fast-transient Searches in Real Time with ZTFReST: Identification of Three Optically Discovered Gamma-Ray Burst Afterglows and New Constraints on the Kilonova Rate. *Astrophys. J.* **2021**, *918*, 63. [CrossRef]
199. Bellm, E.C. Volumetric Survey Speed: A Figure of Merit for Transient Surveys. *Publ. Astron. Soc. Pac.* **2016**, *128*, 084501. [CrossRef]
200. Tonry, J.L.; Denneau, L.; Heinze, A.N.; Stalder, B.; Smith, K.W.; Smartt, S.J.; Stubbs, C.W.; Weiland, H.J.; Rest, A. ATLAS: A High-cadence All-sky Survey System. *Publ. Astron. Soc. Pac.* **2018**, *130*, 064505. [CrossRef]
201. York, D.G.; Adelman, J.; Anderson, J.E., Jr.; Anderson, S.F.; Annis, J.; Bahcall, N.A.; Bakken, J.A.; Barkhouser, R.; Bastian, S.; Berman, E.; et al. The Sloan Digital Sky Survey: Technical Summary. *Astron. J.* **2000**, *120*, 1579–1587. [CrossRef]
202. Eisenstein, D.J.; Weinberg, D.H.; Agol, E.; Aihara, H.; Allende Prieto, C.; Anderson, S.F.; Arns, J.A.; Aubourg, É.; Bailey, S.; Balbinot, E.; et al. SDSS-III: Massive Spectroscopic Surveys of the Distant Universe, the Milky Way, and Extra-Solar Planetary Systems. *Astron. J.* **2011**, *142*, 72. [CrossRef]
203. Blanton, M.R.; Bershady, M.A.; Abolfathi, B.; Albareti, F.D.; Allende Prieto, C.; Almeida, A.; Alonso-García, J.; Anders, F.; Anderson, S.F.; Andrews, B.; et al. Sloan Digital Sky Survey IV: Mapping the Milky Way, Nearby Galaxies, and the Distant Universe. *Astron. J.* **2017**, *154*, 28. [CrossRef]
204. Gaia Collaboration; Prusti, T.; de Bruijne, J.H.J.; Brown, A.G.A.; Vallenari, A.; Babusiaux, C.; Bailer-Jones, C.A.L.; Bastian, U.; Biermann, M.; Evans, D.W.; et al. The Gaia mission. *Astron. Astrophys.* **2016**, *595*, A1. [CrossRef]
205. Emerson, J.P.; Sutherland, W. Visible and Infrared Survey Telescope for Astronomy: Overview. In *Survey and Other Telescope Technologies and Discoveries*; Tyson, J.A., Wolff, S., Eds.; Society of Photo-Optical Instrumentation Engineers (SPIE) Conference Series; SPIE Press: Bellingham, DC, USA, 2002; Volume 4836, pp. 35–42. [CrossRef]
206. Sutherland, W.; Emerson, J.; Dalton, G.; Atad-Ettedgui, E.; Beard, S.; Bennett, R.; Bezawada, N.; Born, A.; Caldwell, M.; Clark, P.; et al. The Visible and Infrared Survey Telescope for Astronomy (VISTA): Design, technical overview, and performance. *Astron. Astrophys.* **2015**, *575*, A25. [CrossRef]
207. Skrutskie, M.F.; Cutri, R.M.; Stiening, R.; Weinberg, M.D.; Schneider, S.; Carpenter, J.M.; Beichman, C.; Capps, R.; Chester, T.; Elias, J.; et al. The Two Micron All Sky Survey (2MASS). *Astron. J.* **2006**, *131*, 1163–1183. [CrossRef]
208. Kaiser, N.; Aussel, H.; Burke, B.E.; Boesgaard, H.; Chambers, K.; Chun, M.R.; Heasley, J.N.; Hodapp, K.W.; Hunt, B.; Jedicke, R.; et al. Pan-STARRS: A Large Synoptic Survey Telescope Array. In *Survey and Other Telescope Technologies and Discoveries*; Tyson, J.A., Wolff, S., Eds.; Society of Photo-Optical Instrumentation Engineers (SPIE) Conference Series; SPIE Press: Bellingham, DC, USA, 2002; Volume 4836, pp. 154–164. [CrossRef]

209. Kaiser, N.; Burgett, W.; Chambers, K.; Denneau, L.; Heasley, J.; Jedicke, R.; Magnier, E.; Morgan, J.; Onaka, P.; Tonry, J. The Pan-STARRS wide-field optical/NIR imaging survey. In *Ground-Based and Airborne Telescopes III*; Stepp, L.M., Gilmozzi, R., Hall, H.J., Eds.; Society of Photo-Optical Instrumentation Engineers (SPIE) Conference Series; SPIE Press: Bellingham, DC, USA, 2010; Volume 7733, pp. 59–172. [CrossRef]
210. Chambers, K.; Pan-STARRS Team. The Pan-STARRS1 Surveys. In *American Astronomical Society Meeting Abstracts #231*; American Astronomical Society: Washington, DC, USA, 2018; Volume 231, p. 102.01.
211. Law, N.M.; Kulkarni, S.R.; Dekany, R.G.; Ofek, E.O.; Quimby, R.M.; Nugent, P.E.; Surace, J.; Grillmair, C.C.; Bloom, J.S.; Kasliwal, M.M.; et al. The Palomar Transient Factory: System Overview, Performance, and First Results. *Publ. Astron. Soc. Pac.* **2009**, *121*, 1395. [CrossRef]
212. Rau, A.; Kulkarni, S.R.; Law, N.M.; Bloom, J.S.; Ciardi, D.; Djorgovski, G.S.; Fox, D.B.; Gal-Yam, A.; Grillmair, C.C.; Kasliwal, M.M.; et al. Exploring the Optical Transient Sky with the Palomar Transient Factory. *Publ. Astron. Soc. Pac.* **2009**, *121*, 1334. [CrossRef]
213. Kulkarni, S.R. The intermediate Palomar Transient Factory (iPTF) begins. *Astron. Telegr.* **2013**, *4807*, 1.
214. Bellm, E.C.; Kulkarni, S.R.; Graham, M.J.; Dekany, R.; Smith, R.M.; Riddle, R.; Masci, F.J.; Helou, G.; Prince, T.A.; Adams, S.M.; et al. The Zwicky Transient Facility: System Overview, Performance, and First Results. *Publ. Astron. Soc. Pac.* **2019**, *131*, 018002. [CrossRef]
215. Ivezić, Ž.; Kahn, S.M.; Tyson, J.A.; Abel, B.; Acosta, E.; Allsman, R.; Alonso, D.; AlSayyad, Y.; Anderson, S.F.; Andrew, J.; et al. LSST: From Science Drivers to Reference Design and Anticipated Data Products. *Astrophys. J.* **2019**, *873*, 111. [CrossRef]
216. Iye, M.; Karoji, H.; Ando, H.; Kaifu, N.; Kodaira, K.; Aoki, K.; Aoki, W.; Chikada, Y.; Doi, Y.; Ebizuka, N.; et al. Current Performance and On-Going Improvements of the 8.2 m Subaru Telescope. *Publ. Astron. Soc. Jpn.* **2004**, *56*, 381–397. [CrossRef]
217. Tokunaga, A.T.; Kobayashi, N.; Bell, J.; Ching, G.K.; Hodapp, K.W.; Hora, J.L.; Neill, D.; Onaka, P.M.; Rayner, J.T.; Robertson, L.; et al. Infrared camera and spectrograph for the SUBARU Telescope. In *Infrared Astronomical Instrumentation*; Fowler, A.M., Ed.; Society of Photo-Optical Instrumentation Engineers (SPIE) Conference Series; SPIE Press: Bellingham, DC, USA, 1998; Volume 3354, pp. 512–524. [CrossRef]
218. Kobayashi, N.; Tokunaga, A.T.; Terada, H.; Goto, M.; Weber, M.; Potter, R.; Onaka, P.M.; Ching, G.K.; Young, T.T.; Fletcher, K.; et al. IRCS: Infrared camera and spectrograph for the Subaru Telescope. In *Optical and IR Telescope Instrumentation and Detectors*; Iye, M., Moorwood, A.F., Eds.; Society of Photo-Optical Instrumentation Engineers (SPIE) Conference Series; SPIE Press: Bellingham, DC, USA, 2000; Volume 4008, pp. 1056–1066. [CrossRef]
219. Miyazaki, S.; Komiyama, Y.; Sekiguchi, M.; Okamura, S.; Doi, M.; Furusawa, H.; Hamabe, M.; Imi, K.; Kimura, M.; Nakata, F.; et al. Subaru Prime Focus Camera—Suprime-Cam. *Publ. Astron. Soc. Jpn.* **2002**, *54*, 833–853. [CrossRef]
220. Miyazaki, S.; Komiyama, Y.; Kawanomoto, S.; Doi, Y.; Furusawa, H.; Hamana, T.; Hayashi, Y.; Ikeda, H.; Kamata, Y.; Karoji, H.; et al. Hyper Suprime-Cam: System design and verification of image quality. *Publ. Astron. Soc. Jpn.* **2018**, *70*, S1. [CrossRef]
221. Komiyama, Y.; Obuchi, Y.; Nakaya, H.; Kamata, Y.; Kawanomoto, S.; Utsumi, Y.; Miyazaki, S.; Uraguchi, F.; Furusawa, H.; Morokuma, T.; et al. Hyper Suprime-Cam: Camera dewar design. *Publ. Astron. Soc. Jpn.* **2018**, *70*, S2. [CrossRef]
222. Kawanomoto, S.; Uraguchi, F.; Komiyama, Y.; Miyazaki, S.; Furusawa, H.; Finet, F.; Hattori, T.; Wang, S.Y.; Yasuda, N.; Suzuki, N. Hyper Suprime-Cam: Filters. *Publ. Astron. Soc. Jpn.* **2018**, *70*, 66. [CrossRef]
223. Furusawa, H.; Koike, M.; Takata, T.; Okura, Y.; Miyatake, H.; Lupton, R.H.; Bickerton, S.; Price, P.A.; Bosch, J.; Yasuda, N.; et al. The on-site quality-assurance system for Hyper Suprime-Cam: OSQAH. *Publ. Astron. Soc. Jpn.* **2018**, *70*, S3. [CrossRef]
224. Yoshida, M.; Shimizu, Y.; Sasaki, T.; Kosugi, G.; Takata, T.; Sekiguchi, K.; Kashikawa, N.; Aoki, K.; Asai, R.; Ohyama, Y.; et al. Software structure and its performance on FOCAS instrument control, a MOS design, and an analyzing package. In *Advanced Telescope and Instrumentation Control Software*; Lewis, H., Ed.; Society of Photo-Optical Instrumentation Engineers (SPIE) Conference Series; SPIE Press: Bellingham, DC, USA, 2000; Volume 4009, pp. 240–249. [CrossRef]
225. Kashikawa, N.; Aoki, K.; Asai, R.; Ebizuka, N.; Inata, M.; Iye, M.; Kawabata, K.S.; Kosugi, G.; Ohyama, Y.; Okita, K.; et al. FOCAS: The Faint Object Camera and Spectrograph for the Subaru Telescope. *Publ. Astron. Soc. Jpn.* **2002**, *54*, 819–832. [CrossRef]
226. Suzuki, R.; Tokoku, C.; Ichikawa, T.; Uchimoto, Y.K.; Konishi, M.; Yoshikawa, T.; Tanaka, I.; Yamada, T.; Omata, K.; Nishimura, T. Multi-Object Infrared Camera and Spectrograph (MOIRCS) for the Subaru Telescope I. Imaging. *Publ. Astron. Soc. Jpn.* **2008**, *60*, 1347. [CrossRef]
227. Ichikawa, T.; Suzuki, R.; Tokoku, C.; Uchimoto, Y.K.; Konishi, M.; Yoshikawa, T.; Yamada, T.; Tanaka, I.; Omata, K.; Nishimura, T. *MOIRCS: Multi-Object Infrared Camera and Spectrograph for SUBARU*; McLean, I.S., Iye, M., Eds.; Society of Photo-Optical Instrumentation Engineers (SPIE) Conference Series; SPIE Press: Bellingham, DC, USA, 2006; Volume 6269, p. 626916. [CrossRef]
228. Walawender, J.; Wung, M.; Fabricius, M.; Tanaka, I.; Arimoto, N.; Cook, D.; Elms, B.; Hashiba, Y.; Hu, Y.S.; Iwata, I.; et al. The nuMOIRCS project: Detector upgrade overview and early commissioning results. In *Ground-Based and Airborne Instrumentation for Astronomy VI*; Evans, C.J.; Simard, L.; Takami, H., Eds.; Society of Photo-Optical Instrumentation Engineers (SPIE) Conference Series; SPIE Press: Bellingham, DC, USA, 2016; Volume 9908, pp. 772–780. [CrossRef]
229. Fabricius, M.; Walawender, J.; Arimoto, N.; Cook, D.; Elms, B.; Hashiba, Y.; Hattori, T.; Hu, Y.S.; Iwata, I.; Nishimura, T.; et al. Detector upgrade of Subaru's Multi-object Infrared Camera and Spectrograph (MOIRCS). In *Ground-Based and Airborne Instrumentation for Astronomy VI*; Evans, C.J., Simard, L., Takami, H., Eds.; Society of Photo-Optical Instrumentation Engineers (SPIE) Conference Series; SPIE Press: Bellingham, DC, USA, 2016; Volume 9908, p. 990828. [CrossRef]

230. Hayano, Y.; Takami, H.; Guyon, O.; Oya, S.; Hattori, M.; Saito, Y.; Watanabe, M.; Murakami, N.; Minowa, Y.; Ito, M.; et al. Current status of the laser guide star adaptive optics system for Subaru Telescope. In *Adaptive Optics Systems*; Hubin, N., Max, C.E., Wizinowich, P.L., Eds.; Society of Photo-Optical Instrumentation Engineers (SPIE) Conference Series; SPIE Press: Bellingham, DC, USA, 2008; Volume 7015, p. 701510. [CrossRef]
231. Hayano, Y.; Takami, H.; Oya, S.; Hattori, M.; Saito, Y.; Watanabe, M.; Guyon, O.; Minowa, Y.; Egner, S.E.; Ito, M.; et al. Commissioning status of Subaru laser guide star adaptive optics system. In *Adaptive Optics Systems II*; Ellerbroek, B.L., Hart, M., Hubin, N., Wizinowich, P.L., Eds.; Society of Photo-Optical Instrumentation Engineers (SPIE) Conference Series; SPIE Press: Bellingham, DC, USA, 2010; Volume 7736, pp. 260–267. [CrossRef]
232. Buckley, D.A.H.; Swart, G.P.; Meiring, J.G. *Completion and Commissioning of the Southern African Large Telescope*; Stepp, L.M., Ed.; Society of Photo-Optical Instrumentation Engineers (SPIE) Conference Series; SPIE Press: Bellingham, DC, USA, 2006; Volume 6267, pp. 333–347. [CrossRef]
233. Burgh, E.B.; Nordsieck, K.H.; Kobulnicky, H.A.; Williams, T.B.; O'Donoghue, D.; Smith, M.P.; Percival, J.W. Prime Focus Imaging Spectrograph for the Southern African Large Telescope: Optical design. In *Instrument Design and Performance for Optical/Infrared Ground-Based Telescopes*; Iye, M., Moorwood, A.F.M., Eds.; Society of Photo-Optical Instrumentation Engineers (SPIE) Conference Series; SPIE Press: Bellingham, DC, USA, 2003; Volume 4841, pp. 1463–1471. [CrossRef]
234. Kobulnicky, H.A.; Nordsieck, K.H.; Burgh, E.B.; Smith, M.P.; Percival, J.W.; Williams, T.B.; O'Donoghue, D. Prime focus imaging spectrograph for the Southern African large telescope: Operational modes. In *Instrument Design and Performance for Optical/Infrared Ground-Based Telescopes*; Iye, M., Moorwood, A.F.M., Eds.; Society of Photo-Optical Instrumentation Engineers (SPIE) Conference Series; SPIE Press: Bellingham, DC, USA, 2003; Volume 4841, pp. 1634–1644. [CrossRef]
235. McLeod, B.; Fabricant, D.; Nystrom, G.; McCracken, K.; Amato, S.; Bergner, H.; Brown, W.; Burke, M.; Chilingarian, I.; Conroy, M.; et al. MMT and Magellan Infrared Spectrograph. *Publ. Astron. Soc. Pac.* **2012**, *124*, 1318. [CrossRef]
236. O'Donoghue, D.; Buckley, D.A.H.; Balona, L.A.; Bester, D.; Botha, L.; Brink, J.; Carter, D.B.; Charles, P.A.; Christians, A.; Ebrahim, F.; et al. First science with the Southern African Large Telescope: Peering at the accreting polar caps of the eclipsing polar SDSS J015543.40+002807.2. *Mon. Not. R. Astron. Soc.* **2006**, *372*, 151–162. [CrossRef]
237. Kotani, T.; Kawai, N.; Yanagisawa, K.; Watanabe, J.; Arimoto, M.; Fukushima, H.; Hattori, T.; Inata, M.; Izumiura, H.; Kataoka, J.; et al. MITSuME—Multicolor Imaging Telescopes for Survey and Monstrous Explosions. *Nuovo Cimento C Geophys. Space Phys. C* **2005**, *28*, 755. [CrossRef]
238. Gardner, J.P.; Mather, J.C.; Clampin, M.; Doyon, R.; Greenhouse, M.A.; Hammel, H.B.; Hutchings, J.B.; Jakobsen, P.; Lilly, S.J.; Long, K.S.; et al. The James Webb Space Telescope. *Space Sci. Rev.* **2006**, *123*, 485–606. [CrossRef]
239. Afanasiev, V.L.; Moiseev, A.V. The SCORPIO Universal Focal Reducer of the 6-m Telescope. *Astron. Lett.* **2005**, *31*, 194–204. [CrossRef]
240. Afanasiev, V.L.; Moiseev, A.V. Scorpio on the 6 m Telescope: Current State and Perspectives for Spectroscopy of Galactic and Extragalactic Objects. *Balt. Astron.* **2011**, *20*, 363–370. [CrossRef]
241. Patat, F.; Taubenberger, S. Characterisation of the CAFOS linear spectropolarimeter. *Astron. Astrophys.* **2011**, *529*, A57. [CrossRef]
242. Inserra, C.; Pastorello, A.; Turatto, M.; Pumo, M.L.; Benetti, S.; Cappellaro, E.; Botticella, M.T.; Bufano, F.; Elias-Rosa, N.; Harutyunyan, A.; et al. Moderately luminous Type II supernovae. *Astron. Astrophys.* **2013**, *555*, A142. [CrossRef]
243. Caballero, J.A.; Montes, D.; Klutsch, A.; Genebriera, J.; Miret, F.X.; Tobal, T.; Cairol, J.; Pedraz, S. The magnetically-active, low-mass, triple system WDS 19312+3607. *Astron. Astrophys.* **2010**, *520*, A91. [CrossRef]
244. Hook, I.M.; Jørgensen, I.; Allington-Smith, J.R.; Davies, R.L.; Metcalfe, N.; Murowinski, R.G.; Crampton, D. The Gemini-North Multi-Object Spectrograph: Performance in Imaging, Long-Slit, and Multi-Object Spectroscopic Modes. *Publ. Astron. Soc. Pac.* **2004**, *116*, 425–440. [CrossRef]
245. Allington-Smith, J.; Murray, G.; Content, R.; Dodsworth, G.; Davies, R.; Miller, B.W.; Jorgensen, I.; Hook, I.; Crampton, D.; Murowinski, R. Integral Field Spectroscopy with the Gemini Multiobject Spectrograph. I. Design, Construction, and Testing. *Publ. Astron. Soc. Pac.* **2002**, *114*, 892–912. [CrossRef]
246. Gimeno, G.; Roth, K.; Chiboucas, K.; Hibon, P.; Boucher, L.; White, J.; Rippa, M.; Labrie, K.; Turner, J.; Hanna, K.; et al. On-sky commissioning of Hamamatsu CCDs in GMOS-S. In *Ground-Based and Airborne Instrumentation for Astronomy VI*; Evans, C.J., Simard, L., Takami, H., Eds.; Society of Photo-Optical Instrumentation Engineers (SPIE) Conference Series; SPIE Press: Bellingham, DC, USA, 2016; Volume 9908, pp. 872–885. [CrossRef]
247. Greiner, J.; Bornemann, W.; Clemens, C.; Deuter, M.; Hasinger, G.; Honsberg, M.; Huber, H.; Huber, S.; Krauss, M.; Krühler, T.; et al. GROND—A 7-Channel Imager. *Publ. Astron. Soc. Pac.* **2008**, *120*, 405. [CrossRef]
248. Cepa, J.; Aguiar, M.; Escalera, V.G.; Gonzalez-Serrano, I.; Joven-Alvarez, E.; Peraza, L.; Rasilla, J.L.; Rodriguez-Ramos, L.F.; Gonzalez, J.J.; Cobos Duenas, F.J.; et al. OSIRIS tunable imager and spectrograph. In *Optical and IR Telescope Instrumentation and Detectors*; Iye, M., Moorwood, A.F., Eds.; Society of Photo-Optical Instrumentation Engineers (SPIE) Conference Series; SPIE Press: Bellingham, DC, USA, 2000; Volume 4008, pp. 623–631. [CrossRef]
249. Cortés-Contreras, M.; Bouy, H.; Solano, E.; Mahlke, M.; Jiménez-Esteban, F.; Alacid, J.M.; Rodrigo, C. The Gran Telescopio Canarias OSIRIS broad-band first data release. *Mon. Not. R. Astron. Soc.* **2020**, *491*, 129–152. [CrossRef]

250. Faber, S.M.; Phillips, A.C.; Kibrick, R.I.; Alcott, B.; Allen, S.L.; Burrous, J.; Cantrall, T.; Clarke, D.; Coil, A.L.; Cowley, D.J.; et al. The DEIMOS spectrograph for the Keck II Telescope: Integration and testing. In *Instrument Design and Performance for Optical/Infrared Ground-Based Telescopes*; Iye, M., Moorwood, A.F.M., Eds.; Society of Photo-Optical Instrumentation Engineers (SPIE) Conference Series; SPIE Press: Bellingham, DC, USA, 2003; Volume 4841, pp. 1657–1669. [CrossRef]
251. Vogt, S.S.; Allen, S.L.; Bigelow, B.C.; Bresee, L.; Brown, B.; Cantrall, T.; Conrad, A.; Couture, M.; Delaney, C.; Epps, H.W.; et al. HIRES: The high-resolution echelle spectrometer on the Keck 10-m Telescope. In *Instrumentation in Astronomy VIII*; Crawford, D.L., Craine, E.R., Eds.; Society of Photo-Optical Instrumentation Engineers (SPIE) Conference Series; SPIE Press: Bellingham, DC, USA, 1994; Volume 2198, p. 362. [CrossRef]
252. Oke, J.B.; Cohen, J.G.; Carr, M.; Cromer, J.; Dingizian, A.; Harris, F.H.; Labrecque, S.; Lucinio, R.; Schaal, W.; Epps, H.; et al. The Keck Low-Resolution Imaging Spectrometer. *Publ. Astron. Soc. Pac.* **1995**, *107*, 375. [CrossRef]
253. Rockosi, C.; Stover, R.; Kibrick, R.; Lockwood, C.; Peck, M.; Cowley, D.; Bolte, M.; Adkins, S.; Alcott, B.; Allen, S.L.; et al. The low-resolution imaging spectrograph red channel CCD upgrade: Fully depleted, high-resistivity CCDs for Keck. In *Ground-Based and Airborne Instrumentation for Astronomy III*; McLean, I.S., Ramsay, S.K., Takami, H., Eds.; Society of Photo-Optical Instrumentation Engineers (SPIE) Conference Series; SPIE Press: Bellingham, DC, USA, 2010; Volume 7735, pp. 355–365. [CrossRef]
254. Newman, J.A.; Cooper, M.C.; Davis, M.; Faber, S.M.; Coil, A.L.; Guhathakurta, P.; Koo, D.C.; Phillips, A.C.; Conroy, C.; Dutton, A.A.; et al. The DEEP2 Galaxy Redshift Survey: Design, Observations, Data Reduction, and Redshifts. *Astrophys. J. Suppl.* **2013**, *208*, 5. [CrossRef]
255. Meyer, R.A.; Kakiichi, K.; Bosman, S.E.I.; Ellis, R.S.; Laporte, N.; Robertson, B.E.; Ryan-Weber, E.V.; Mawatari, K.; Zitrin, A. The role of galaxies and AGN in reionizing the IGM - III. IGM-galaxy cross-correlations at z $\sim$ 6 from eight quasar fields with DEIMOS and MUSE. *Mon. Not. R. Astron. Soc.* **2020**, *494*, 1560–1578. [CrossRef]
256. Vogt, S.S. An Overview of Science Results from HIRES: The First 6 Years. In *Astronomical Instrumentation and Astrophysics*; Bash, F.N., Sneden, C., Eds.; Astronomical Society of the Pacific Conference Series; Astronomical Society of the Pacific: San Francisco, CA, USA, 2002; Volume 270, p. 5.
257. Levine, S.E.; DeGroff, W.T. Status and imaging performance of Lowell Observatory's Discovery Channel Telescope in its first year of full science operations. In *Ground-Based and Airborne Telescopes VI*; Hall, H.J., Gilmozzi, R., Marshall, H.K., Eds.; Society of Photo-Optical Instrumentation Engineers (SPIE) Conference Series; SPIE Press: Bellingham, DC, USA, 2016; Volume 9906, p. 990621. [CrossRef]
258. Massey, P.; Dunham, E.W.; Bida, T.A.; Collins, P.; Hall, J.C.; Hunter, D.A.; Lauman, S.; Levine, S.; Neugent, K.; Nye, R.; et al. As Big and As Good As It Gets: The Large Monolithic Imager for Lowell Observatory's 4.3-m Discovery Channel Telescope. In *American Astronomical Society Meeting Abstracts #221*; NASA: Washington, DC, USA, 2013; Volume 221, p. 345.02.
259. Scholz, A.; Llama, J.; Muzic, K.; Faller, S.; Froebrich, D.; Stelzer, B. Discovery of a Magnetic White Dwarf with Unusual Short-period Variability. *Res. Notes Am. Astron. Soc.* **2018**, *2*, 27. [CrossRef]
260. Hussaini, M.; Mace, G.N.; López-Valdivia, R.; Honaker, E.J.; Han, E. The Impact of Rotation Velocity on Measuring Magnetic Fields of K and M Stars. *Res. Notes Am. Astron. Soc.* **2020**, *4*, 241. [CrossRef]
261. Clark, C.A.; van Belle, G.T.; Horch, E.P. A New Stellar Companion to TYC 5493-889-1. *Res. Notes Am. Astron. Soc.* **2021**, *5*, 280. [CrossRef]
262. Ye, Q.; Farnham, T.L.; Knight, M.M.; Holt, C.E.; Feaga, L.M. Recovery of Returning Halley-type Comet 12P/Pons-Brooks with the Lowell Discovery Telescope. *Res. Notes Am. Astron. Soc.* **2020**, *4*, 101. [CrossRef]
263. Ardeberg, A.; Andersen, T. VLT Design Implications of the Nordic Optical Telescope. In *Very Large Telescopes and their Instrumentation, Volume 2*; European Southern Observatory Conference and Workshop Proceedings; European Southern Observatory: München, Germany, 1988; Volume 30, p. 183.
264. Ardeberg, A.; Andersen, T. Low turbulence–high performance. In *Advanced Technology Optical Telescopes IV*; Barr, L.D., Ed.; Society of Photo-Optical Instrumentation Engineers (SPIE) Conference Series; SPIE Press: Bellingham, DC, USA, 1990; Volume 1236, pp. 543–558. [CrossRef]
265. Andersen, T.; Larsen, O.B.; Owner-Petersen, M.; Steenberg, K. Active Optics on the Nordic Optical Telescope. In *European Southern Observatory Conference and Workshop Proceedings*; European Southern Observatory: München, Germany, 1992; Volume 42, p. 311.
266. Djupvik, A.A.; Andersen, J. The Nordic Optical Telescope. In *Highlights of Spanish Astrophysics V*; Astrophysics and Space Science Proceedings; Springer Science+Business Media: Berlin/Heidelberg, Germany, 2010; Volume 14, p. 211. [CrossRef]
267. Vernet, J.; Dekker, H.; D'Odorico, S.; Kaper, L.; Kjaergaard, P.; Hammer, F.; Randich, S.; Zerbi, F.; Groot, P.J.; Hjorth, J.; et al. X-shooter, the new wide band intermediate resolution spectrograph at the ESO Very Large Telescope. *Astron. Astrophys.* **2011**, *536*, A105. [CrossRef]
268. Appenzeller, I.; Fricke, K.; Fürtig, W.; Gässler, W.; Häfner, R.; Harke, R.; Hess, H.J.; Hummel, W.; Jürgens, P.; Kudritzki, R.P.; et al. Successful commissioning of FORS1—The first optical instrument on the VLT. *Messenger* **1998**, *94*, 1–6.
269. Rhodes, L.; van der Horst, A.J.; Fender, R.; Monageng, I.M.; Anderson, G.E.; Antoniadis, J.; Bietenholz, M.F.; Böttcher, M.; Bright, J.S.; Green, D.A.; et al. Radio afterglows of very high-energy gamma-ray bursts 190829A and 180720B. *Mon. Not. R. Astron. Soc.* **2020**, *496*, 3326–3335. [CrossRef]
270. De Colle, F.; Kumar, P.; Aguilera-Dena, D.R. Radio Emission from the Cocoon of a GRB Jet: Implications for Relativistic Supernovae and Off-axis GRB Emission. *Astrophys. J.* **2018**, *863*, 32. [CrossRef]

271. Laskar, T.; Alexander, K.D.; Gill, R.; Granot, J.; Berger, E.; Mundell, C.G.; Barniol Duran, R.; Bolmer, J.; Duffell, P.; van Eerten, H.; et al. ALMA Detection of a Linearly Polarized Reverse Shock in GRB 190114C. *Astrophys. J. Lett.* **2019**, *878*, L26. [CrossRef]
272. Chandra, P. Gamma-Ray Bursts: A Radio Perspective. *Adv. Astron.* **2016**, *2016*, 296781. [CrossRef]
273. Hancock, P.J.; Gaensler, B.M.; Murphy, T. Two Populations of Gamma-Ray Burst Radio Afterglows. *Astrophys. J.* **2013**, *776*, 106. [CrossRef]
274. Lloyd-Ronning, N.M.; Fryer, C.L. On the lack of a radio afterglow from some gamma-ray bursts - insight into their progenitors? *Mon. Not. R. Astron. Soc.* **2017**, *467*, 3413–3423. [CrossRef]
275. Lloyd-Ronning, N.M.; Gompertz, B.; Pe'er, A.; Dainotti, M.; Fruchter, A. A Comparison between Radio Loud and Quiet Gamma-Ray Bursts, and Evidence for a Potential Correlation between Intrinsic Duration and Redshift in the Radio Loud Population. *Astrophys. J.* **2019**, *871*, 118. [CrossRef]
276. Eichler, D.; Waxman, E. The Efficiency of Electron Acceleration in Collisionless Shocks and Gamma-Ray Burst Energetics. *Astrophys. J.* **2005**, *627*, 861–867. [CrossRef]
277. Giannios, D.; Spitkovsky, A. Signatures of a Maxwellian component in shock-accelerated electrons in GRBs. *Mon. Not. R. Astron. Soc.* **2009**, *400*, 330–336. [CrossRef]
278. Ressler, S.M.; Laskar, T. Thermal Electrons in Gamma-Ray Burst Afterglows. *Astrophys. J.* **2017**, *845*, 150. [CrossRef]
279. Warren, D.C.; Barkov, M.V.; Ito, H.; Nagataki, S.; Laskar, T. Synchrotron self-absorption in GRB afterglows: The effects of a thermal electron population. *Mon. Not. R. Astron. Soc.* **2018**, *480*, 4060–4068. [CrossRef]
280. Kangas, T.; Fruchter, A.S.; Cenko, S.B.; Corsi, A.; de Ugarte Postigo, A.; Pe'er, A.; Vogel, S.N.; Cucchiara, A.; Gompertz, B.; Graham, J.; et al. The Late-time Afterglow Evolution of Long Gamma-Ray Bursts GRB 160625B and GRB 160509A. *Astrophys. J.* **2020**, *894*, 43. [CrossRef]
281. Frail, D.A.; Metzger, B.D.; Berger, E.; Kulkarni, S.R.; Yost, S.A. A Late-Time Flattening of Afterglow Light Curves. *Astrophys. J.* **2004**, *600*, 828–833. [CrossRef]
282. Berger, E.; Kulkarni, S.R.; Pooley, G.; Frail, D.A.; McIntyre, V.; Wark, R.M.; Sari, R.; Soderberg, A.M.; Fox, D.W.; Yost, S.; et al. A common origin for cosmic explosions inferred from calorimetry of GRB030329. *Nature* **2003**, *426*, 154–157. [CrossRef]
283. Peng, F.; Königl, A.; Granot, J. Two-Component Jet Models of Gamma-Ray Burst Sources. *Astrophys. J.* **2005**, *626*, 966–977. [CrossRef]
284. Lazzati, D.; Begelman, M.C. Universal GRB Jets from Jet-Cocoon Interaction in Massive Stars. *Astrophys. J.* **2005**, *629*, 903–907. [CrossRef]
285. Panaitescu, A.; Kumar, P. The slow decay of some radio afterglows—A puzzle for the simplest γ-ray burst fireball model. *Mon. Not. R. Astron. Soc.* **2004**, *350*, 213–231. [CrossRef]
286. Zwart, J.T.L.; Barker, R.W.; Biddulph, P.; Bly, D.; Boysen, R.C.; Brown, A.R.; Clementson, C.; Crofts, M.; Culverhouse, T.L.; Czeres, J.; et al. The Arcminute Microkelvin Imager. *Mon. Not. R. Astron. Soc.* **2008**, *391*, 1545–1558. [CrossRef]
287. Perley, R.A.; Chandler, C.J.; Butler, B.J.; Wrobel, J.M. The Expanded Very Large Array: A New Telescope for New Science. *Astrophys. J. Lett.* **2011**, *739*, L1. [CrossRef]
288. Hotan, A.W.; Bunton, J.D.; Chippendale, A.P.; Whiting, M.; Tuthill, J.; Moss, V.A.; McConnell, D.; Amy, S.W.; Huynh, M.T.; Allison, J.R.; et al. Australian square kilometre array pathfinder: I. System description. *Publ. Astron. Soc. Aust.* **2021**, *38*, e009. [CrossRef]
289. van Haarlem, M.P.; Wise, M.W.; Gunst, A.W.; Heald, G.; McKean, J.P.; Hessels, J.W.T.; de Bruyn, A.G.; Nijboer, R.; Swinbank, J.; Fallows, R.; et al. LOFAR: The LOw-Frequency ARray. *Astron. Astrophys.* **2013**, *556*, A2. [CrossRef]
290. Camilo, F.; Scholz, P.; Serylak, M.; Buchner, S.; Merryfield, M.; Kaspi, V.M.; Archibald, R.F.; Bailes, M.; Jameson, A.; van Straten, W.; et al. Revival of the Magnetar PSR J1622-4950: Observations with MeerKAT, Parkes, XMM-Newton, Swift, Chandra, and NuSTAR. *Astrophys. J.* **2018**, *856*, 180. [CrossRef]
291. Muxlow, T.W.B.; Thomson, A.P.; Radcliffe, J.F.; Wrigley, N.H.; Beswick, R.J.; Smail, I.; McHardy, I.M.; Garrington, S.T.; Ivison, R.J.; Jarvis, M.J.; et al. The e-MERGE Survey (e-MERLIN Galaxy Evolution Survey): Overview and survey description. *Mon. Not. R. Astron. Soc.* **2020**, *495*, 1188–1208. [CrossRef]
292. Tingay, S.; Goeke, R.; Hewitt, J.N.; Morgan, E.; Remillard, R.A.; Williams, C.L.; Bowman, J.D.; Emrich, E.; Ord, S.M.; Booler, T.; et al. Realisation of a low frequency SKA Precursor: The Murchison Widefield Array. In *Resolving the Sky—Radio Interferometry: Past, Present and Future*; Sissa Medialab: Trieste, Italy, 2012; p. 36.
293. Frater, R.H.; Brooks, J.W.; Whiteoak, J.B. The Australia Telescope—Overview. *J. Electr. Electron. Eng. Aust.* **1992**, *12*, 103–112.
294. Wilson, W.E.; Ferris, R.H.; Axtens, P.; Brown, A.; Davis, E.; Hampson, G.; Leach, M.; Roberts, P.; Saunders, S.; Koribalski, B.S.; et al. The Australia Telescope Compact Array Broad-band Backend: Description and first results. *Mon. Not. R. Astron. Soc.* **2011**, *416*, 832–856. [CrossRef]
295. Sari, R.; Esin, A.A. On the Synchrotron Self-Compton Emission from Relativistic Shocks and Its Implications for Gamma-Ray Burst Afterglows. *Astrophys. J.* **2001**, *548*, 787–799. [CrossRef]
296. Kumar, P.; Barniol Duran, R. On the generation of high-energy photons detected by the Fermi Satellite from gamma-ray bursts. *Mon. Not. R. Astron. Soc.* **2009**, *400*, L75–L79. [CrossRef]
297. Ghisellini, G.; Ghirlanda, G.; Nava, L.; Celotti, A. GeV emission from gamma-ray bursts: A radiative fireball? *Mon. Not. R. Astron. Soc.* **2010**, *403*, 926–937. [CrossRef]
298. Wang, X.Y.; He, H.N.; Li, Z.; Wu, X.F.; Dai, Z.G. Klein-Nishina Effects on the High-energy Afterglow Emission of Gamma-ray Bursts. *Astrophys. J.* **2010**, *712*, 1232–1240. [CrossRef]

299. Ajello, M.; Baldini, L.; Barbiellini, G.; Bastieri, D.; Bellazzini, R.; Bissaldi, E.; Blandford, R.D.; Bonino, R.; Bottacini, E.; Bregeon, J.; et al. Investigating the Nature of Late-time High-energy GRB Emission through Joint Fermi/Swift Observations. *Astrophys. J.* **2018**, *863*, 138. [CrossRef]
300. Razzaque, S.; Dermer, C.D.; Finke, J.D. Synchrotron Radiation from Ultra-High Energy Protons and the Fermi Observations of GRB 080916C. *Open Astron. J.* **2010**, *3*, 150–155. [CrossRef]
301. Kumar, P.; Zhang, B. The physics of gamma-ray bursts & relativistic jets. *Phys. Rep.* **2015**, *561*, 1–109. [CrossRef]
302. Waxman, E. Gamma-Ray–Burst Afterglow: Supporting the Cosmological Fireball Model, Constraining Parameters, and Making Predictions. *Astrophys. J. Lett.* **1997**, *485*, L5–L8. [CrossRef]
303. Zhang, B.; Mészáros, P. High-Energy Spectral Components in Gamma-Ray Burst Afterglows. *Astrophys. J.* **2001**, *559*, 110–122. [CrossRef]
304. Derishev, E.; Piran, T. The Physical Conditions of the Afterglow Implied by MAGIC's Sub-TeV Observations of GRB 190114C. *Astrophys. J. Lett.* **2019**, *880*, L27. [CrossRef]
305. Wang, X.Y.; Liu, R.Y.; Zhang, H.M.; Xi, S.Q.; Zhang, B. Synchrotron Self-Compton Emission from External Shocks as the Origin of the Sub-TeV Emission in GRB 180720B and GRB 190114C. *Astrophys. J.* **2019**, *884*, 117. [CrossRef]
306. Abdalla, H.; Adam, R.; Aharonian, F.; Ait Benkhali, F.; Angüner, E.O.; Arakawa, M.; Arcaro, C.; Armand, C.; Ashkar, H.; Backes, M.; et al. A very-high-energy component deep in the γ-ray burst afterglow. *Nature* **2019**, *575*, 464–467. [CrossRef]
307. Salafia, O.S.; Berti, A.; Covino, S.; D'Elia, V.; Miceli, D.; Nava, L.; Patricelli, B.; Righi, C.; Inoue, S.; Antonelli, L.A.; et al. Follow-up observations of GW170817 with the MAGIC telescopes. In Proceedings of the 37th International Cosmic Ray Conference, Berlin, Germany, 12–23 July 2021; p. 944.
308. Abdalla, H.; Abramowski, A.; Aharonian, F.; Ait Benkhali, F.; Angüner, E.O.; Arakawa, M.; Arrieta, M.; Aubert, P.; Backes, M.; Balzer, A.; et al. TeV Gamma-Ray Observations of the Binary Neutron Star Merger GW170817 with H.E.S.S. *Astrophys. J. Lett.* **2017**, *850*, L22. [CrossRef]
309. Acciari, V.A.; Ansoldi, S.; Antonelli, L.A.; Arbet Engels, A.; Asano, K.; Baack, D.; Babić, A.; Baquero, A.; Barres de Almeida, U.; Barrio, J.A.; et al. MAGIC Observations of the Nearby Short Gamma-Ray Burst GRB 160821B. *Astrophys. J.* **2021**, *908*, 90. [CrossRef]
310. Aleksić, J.; Ansoldi, S.; Antonelli, L.A.; Antoranz, P.; Babic, A.; Bangale, P.; Barceló, M.; Barrio, J.A.; Becerra González, J.; Bednarek, W.; et al. The major upgrade of the MAGIC telescopes, Part II: A performance study using observations of the Crab Nebula. *Astropart. Phys.* **2016**, *72*, 76–94. [CrossRef]
311. Holder, J.; Atkins, R.W.; Badran, H.M.; Blaylock, G.; Bradbury, S.M.; Buckley, J.H.; Byrum, K.L.; Carter-Lewis, D.A.; Celik, O.; Chow, Y.C.K.; et al. The first VERITAS telescope. *Astropart. Phys.* **2006**, *25*, 391–401. [CrossRef]
312. Hinton, J.A.; HESS Collaboration. The status of the HESS project. *New Astron. Rev.* **2004**, *48*, 331–337. [CrossRef]
313. Abeysekara, A.U.; Aguilar, J.A.; Aguilar, S.; Alfaro, R.; Almaraz, E.; Álvarez, C.; Álvarez-Romero, J.d.D.; Álvarez, M.; Arceo, R.; Arteaga-Velázquez, J.C.; et al. On the sensitivity of the HAWC observatory to gamma-ray bursts. *Astropart. Phys.* **2012**, *35*, 641–650. [CrossRef]
314. Albert, A.; Alfaro, R.; Ashkar, H.; Alvarez, C.; Álvarez, J.; Arteaga-Velázquez, J.C.; Ayala Solares, H.A.; Arceo, R.; Bellido, J.A.; BenZvi, S.; et al. Science Case for a Wide Field-of-View Very-High-Energy Gamma-Ray Observatory in the Southern Hemisphere. *arXiv* **2019**, arXiv:1902.08429.
315. León Vargas, H. Highlights from HAWC. *Eur. Phys. J. Web Conf.* **2019**, *208*, 14001. [CrossRef]
316. Casanova, S. First year results from the HAWC observatory. *Eur. Phys. J. Web Conf.* **2017**, *136*, 03005. [CrossRef]
317. Ajello, M.; Atwood, W.B.; Axelsson, M.; Bagagli, R.; Bagni, M.; Baldini, L.; Bastieri, D.; Bellardi, F.; Bellazzini, R.; Bissaldi, E.; et al. Fermi Large Area Telescope Performance after 10 Years of Operation. *Astrophys. J. Suppl.* **2021**, *256*, 12. [CrossRef]
318. IceCube Collaboration; Aartsen, M.G.; Ackermann, M.; Adams, J.; Aguilar, J.A.; Ahlers, M.; Ahrens, M.; Al Samarai, I.; Altmann, D.; Andeen, K.; et al. Multimessenger observations of a flaring blazar coincident with high-energy neutrino IceCube-170922A. *Science* **2018**, *361*, eaat1378. [CrossRef]
319. MAGIC Collaboration; Acciari, V.A.; Ansoldi, S.; Antonelli, L.A.; Engels, A.A.; Baack, D.; Babić, A.; Banerjee, B.; Barres de Almeida, U.; Barrio, J.A.; et al. Observation of inverse Compton emission from a long γ-ray burst. *Nature* **2019**, *575*, 459–463. [CrossRef]
320. MAGIC Collaboration; Acciari, V.A.; Ansoldi, S.; Antonelli, L.A.; Arbet Engels, A.; Baack, D.; Babić, A.; Banerjee, B.; Barres de Almeida, U.; Barrio, J.A.; et al. Teraelectronvolt emission from the γ-ray burst GRB 190114C. *Nature* **2019**, *575*, 455–458. [CrossRef]
321. Sagiv, I.; Gal-Yam, A.; Ofek, E.O.; Waxman, E.; Aharonson, O.; Kulkarni, S.R.; Nakar, E.; Maoz, D.; Trakhtenbrot, B.; Phinney, E.S.; et al. Science with a Wide-field UV Transient Explorer. *Astron. J.* **2014**, *147*, 79; Erratum in *Astron. J.* **2014**, *148*, 138. [CrossRef]
322. Atteia, J.L.; Cordier, B.; Wei, J. The SVOM mission. *Int. J. Mod. Phys. D* **2022**, *31*, 2230008. [CrossRef]
323. Yuan, W.; Zhang, C.; Feng, H.; Zhang, S.N.; Ling, Z.X.; Zhao, D.; Deng, J.; Qiu, Y.; Osborne, J.P.; O'Brien, P.; et al. Einstein Probe - a small mission to monitor and explore the dynamic X-ray Universe. *arXiv* **2015**, arXiv:1506.07735.
324. Yuan, W.; Zhang, C.; Ling, Z.; Zhao, D.; Wang, W.; Chen, Y.; Lu, F.; Zhang, S.N.; Cui, W. Einstein Probe: A lobster-eye telescope for monitoring the x-ray sky. In *Space Telescopes and Instrumentation 2018: Ultraviolet to Gamma Ray*; den Herder, J.W.A., Nikzad, S., Nakazawa, K., Eds.; Society of Photo-Optical Instrumentation Engineers (SPIE) Conference Series; SPIE Press: Bellingham, DC, USA, 2018, Volume 10699, p. 1069925. [CrossRef]

325. Amati, L.; O'Brien, P.T.; Götz, D.; Bozzo, E.; Santangelo, A.; Tanvir, N.; Frontera, F.; Mereghetti, S.; Osborne, J.P.; Blain, A.; et al. The THESEUS space mission: Science goals, requirements and mission concept. *Exp. Astron.* **2021**, *52*, 183–218. [CrossRef]
326. Ghirlanda, G.; Salvaterra, R.; Toffano, M.; Ronchini, S.; Guidorzi, C.; Oganesyan, G.; Ascenzi, S.; Bernardini, M.G.; Camisasca, A.E.; Mereghetti, S.; et al. Gamma ray burst studies with THESEUS. *Exp. Astron.* **2021**, *52*, 277–308. [CrossRef]
327. Nandra, K.; Barret, D.; Barcons, X.; Fabian, A.; den Herder, J.W.; Piro, L.; Watson, M.; Adami, C.; Aird, J.; Afonso, J.M.; et al. The Hot and Energetic Universe: A White Paper presenting the science theme motivating the Athena+ mission. *arXiv* **2013**, arXiv:1306.2307.
328. Neichel, B.; Mouillet, D.; Gendron, E.; Correia, C.; Sauvage, J.F.; Fusco, T. Overview of the European Extremely Large Telescope and its instrument suite. In Proceedings of the SF2A-2018: Proceedings of the Annual meeting of the French Society of Astronomy and Astrophysics, Bordeaux, France, 3–6 July 2018.
329. Burlon, D.; Ghirlanda, G.; van der Horst, A.; Murphy, T.; Wijers, R.A.M.J.; Gaensler, B.; Ghisellini, G.; Prandoni, I. The SKA View of Gamma-Ray Bursts. In Proceedings of the Advancing Astrophysics with the Square Kilometre Array (AASKA14), Giardini Naxos, Italy, 9–13 June 2015; p. 52.
330. Barres de Almeida, U.; CTA Consortium. Science with the Cherenkov Telescope Array. *Bol. Asoc. Argent. Astron. Plata Argent.* **2020**, *61C*, 19–21.
331. Inoue, S.; Granot, J.; O'Brien, P.T.; Asano, K.; Bouvier, A.; Carosi, A.; Connaughton, V.; Garczarczyk, M.; Gilmore, R.; Hinton, J.; et al. Gamma-ray burst science in the era of the Cherenkov Telescope Array. *Astropart. Phys.* **2013**, *43*, 252–275. [CrossRef]
332. Abbott, B.P.; Abbott, R.; Abbott, T.D.; Abraham, S.; Acernese, F.; Ackley, K.; Adams, C.; Adya, V.B.; Affeldt, C.; Agathos, M.; et al. Prospects for observing and localizing gravitational-wave transients with Advanced LIGO, Advanced Virgo and KAGRA. *Living Rev. Relativ.* **2020**, *23*, 3. [CrossRef]
333. Maggiore, M.; Van Den Broeck, C.; Bartolo, N.; Belgacem, E.; Bertacca, D.; Bizouard, M.A.; Branchesi, M.; Clesse, S.; Foffa, S.; García-Bellido, J.; et al. Science case for the Einstein telescope. *J. Cosmol. Astropart. Phys.* **2020**, *2020*, 050. [CrossRef]
334. Evans, M.; Adhikari, R.X.; Afle, C.; Ballmer, S.W.; Biscoveanu, S.; Borhanian, S.; Brown, D.A.; Chen, Y.; Eisenstein, R.; Gruson, A.; et al. A Horizon Study for Cosmic Explorer: Science, Observatories, and Community. *arXiv* **2021**, arXiv:2109.09882.
335. Amaro-Seoane, P.; Audley, H.; Babak, S.; Baker, J.; Barausse, E.; Bender, P.; Berti, E.; Binetruy, P.; Born, M.; Bortoluzzi, D.; et al. Laser Interferometer Space Antenna. *arXiv* **2017**, arXiv:1702.00786.
336. Adrián-Martínez, S.; Ageron, M.; Aharonian, F.; Aiello, S.; Albert, A.; Ameli, F.; Anassontzis, E.; Andre, M.; Androulakis, G.; Anghinolfi, M.; et al. Letter of intent for KM3NeT 2.0. *J. Phys. Nucl. Phys.* **2016**, *43*, 084001. [CrossRef]
337. Aartsen, M.G.; Abbasi, R.; Ackermann, M.; Adams, J.; Aguilar, J.A.; Ahlers, M.; Ahrens, M.; Alispach, C.; Allison, P.; Amin, N.M.; et al. IceCube-Gen2: The window to the extreme Universe. *J. Phys. G Nucl. Phys.* **2021**, *48*, 060501. [CrossRef]
338. McEnery, J.; van der Horst, A.; Dominguez, A.; Moiseev, A.; Marcowith, A.; Harding, A.; Lien, A.; Giuliani, A.; Inglis, A.; Ansoldi, S.; et al. All-sky Medium Energy Gamma-ray Observatory: Exploring the Extreme Multimessenger Universe. *Bull. Am. Astron. Soc.* **2019**, *51*, 245.
339. Grindlay, J.; Gehrels, N.; Harrison, F.; Blandford, R.; Fishman, G.; Kouveliotou, C.; Hartmann, D.H.; Woosley, S.; Craig, W.; Hong, J. Proposed Next Generation GRB Mission: EXIST. In *Gamma-Ray Burst and Afterglow Astronomy 2001: A Workshop Celebrating the First Year of the HETE Mission*; Ricker, G.R., Vanderspek, R.K., Eds.; American Institute of Physics Conference Series; American Institute of Physics: College Park, MA, USA, 2003; Volume 662, pp. 477–480. [CrossRef]
340. Yonetoku, D.; Mihara, T.; Sawano, T.; Ikeda, H.; Harayama, A.; Takata, S.; Yoshida, K.; Seta, H.; Toyanago, A.; Kagawa, Y.; et al. High-z gamma-ray bursts for unraveling the dark ages mission HiZ-GUNDAM. In *Space Telescopes and Instrumentation 2014: Ultraviolet to Gamma Ray*; Takahashi, T., den Herder, J.W.A., Bautz, M., Eds.; Society of Photo-Optical Instrumentation Engineers (SPIE) Conference Series; SPIE Press: Bellingham, DC, USA, 2014; Volume 9144, pp. 840–851. [CrossRef]
341. Camp, J.; Abel, J.; Barthelmy, S.; Bautz, M.; Behar, E.; Berger, E.; Spolaor, S.; Cenko, S.B.; Cornish, N.; Dal Canton, T.; et al. Transient Astrophysics Probe. In *Bulletin of the American Astronomical Society*; American Astronomical Society: Washington, DC, USA, 2019; Volume 51, p. 85.
342. White, N.E.; Bauer, F.E.; Baumgartner, W.; Bautz, M.; Berger, E.; Cenko, B.; Chang, T.C.; Falcone, A.; Fausey, H.; Feldman, C.; et al. *The Gamow Explorer: A Gamma-Ray Burst Observatory to Study the High Redshift Universe and Enable Multi-Messenger Astrophysics*; Society of Photo-Optical Instrumentation Engineers (SPIE) Conference Series; SPIE Press: Bellingham, DC, USA, 2021; Volume 11821, pp. 87–100. [CrossRef]
343. Toma, K.; Sakamoto, T.; Zhang, B.; Hill, J.E.; McConnell, M.L.; Bloser, P.F.; Yamazaki, R.; Ioka, K.; Nakamura, T. Statistical Properties of Gamma-Ray Burst Polarization. *Astrophys. J.* **2009**, *698*, 1042–1053. [CrossRef]
344. Gill, R.; Granot, J.; Kumar, P. Linear polarization in gamma-ray burst prompt emission. *Mon. Not. R. Astron. Soc.* **2020**, *491*, 3343–3373. [CrossRef]
345. in't Zand, J.J.M.; Bozzo, E.; Qu, J.; Li, X.D.; Amati, L.; Chen, Y.; Donnarumma, I.; Doroshenko, V.; Drake, S.A.; Hernanz, M.; et al. Observatory science with eXTP. *Sci. China Phys. Mech. Astron.* **2019**, *62*, 29506. [CrossRef]
346. Hulsman, J. *POLAR-2: A Large Scale Gamma-Ray Polarimeter for GRBs*; Society of Photo-Optical Instrumentation Engineers (SPIE) Conference Series; SPIE Press: Bellingham, DC, USA, 2020; Volume 11444, pp. 474–488. [CrossRef]